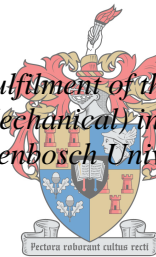


Transient Flow, Flow Pattern Characterisation and Performance Evaluation of a Two-Phase Natural Circulation Heat Transfer Loop

by
Paul Tudieji Senda

Thesis presented in partial fulfilment of the requirements for the degree of Master of Engineering (Mechanical) in the Faculty of Engineering at Stellenbosch University



UNIVERSITEIT
iYUNIVESITHI
STELLENBOSCH
UNIVERSITY

100
1918 · 2018

Supervisor: Mr Robert T Dobson

March 2018

DECLARATION

By submitting this thesis electronically, I declare that the entirety of the work contained therein is my own, original work, that I am the sole author thereof (save to the extent explicitly otherwise stated), that reproduction and publication thereof by Stellenbosch University will not infringe any third party rights and that I have not previously in its entirety or in part submitted it for obtaining any qualification.

Date:March 2018.....

SUMMARY

This thesis project focusses on the experimental and theoretical analysis of the transient behaviour of a single and two-phase flow natural circulation heat transfer loop using water as the working fluid. The background theory provided by a literature survey shows that natural thermosyphon loops offer attractive solutions for passive cooling and heat transfer, and safety systems; especially in the nuclear and process industries. In particular the thesis considers a passive reactor cavity cooling system (RCCS) for next generation high temperature nuclear reactors such as “the pebble bed modular reactor (PBMR)”.

A time-dependent mathematical computer simulation program of a 7 m high by 8 m wide, 32 mm inside diameter vertically orientated rectangular natural circulation loop was developed. The major assumption was that the flow is quasi-static; implying that although the mass flow rate might be changing with time, that at any instant in time that the mass flow rate is constant at axial position along the loop. To theoretically simulate the loop the working fluid was discretised into a series of one dimensional control volumes. By applying the conservation of mass, momentum and energy and suitable property functions to each control volume as series of time dependent partial differential equations were generated and then solved using an explicit finite difference method.

The one vertical side of the loop was heated by a series of electrical heating elements and the other vertical side cooled using a series of water-cooling jackets. Transparent pipe lengths were inserted in the loop to observe the two-phase flow patterns. The loop was supplied with an expansion tank and operated in single and two-phase modes with water as the working fluid at a mass flow rate determined using an orifice-plate flow meter. A reasonable correlation between the experimental and theoretical simulations was found using a separated two-phase flow with frictional multipliers and vapour-liquid void fraction correlations, similar to those originally suggested by Martinelli.

It was concluded that the as developed theoretical model adequately captured the actual transient and dynamic flow and heat transfer behaviour of the loop. It is thus recommended that a series of such loops could be used with confidence for a RCCS.

OPSOMMING

Hierdie studie het gefokus op die eksperimentele en teoretiese ontleding van die oorgangsgedrag van 'n natuurlikesirkulasie-hitteoordraglus in enkel en tweefasevloei deur water as die werkvloeistof te gebruik. Die agtergrondse teorie wat deur die literatuuroorsig verskaf word, toon dat natuurlike termosifonlusse aanloklike oplossings vir passiewe verkoeling en hitteoordrag asook veiligheidstelsels bied, veral in die kern- en prosesbedrywe. Die studie het spesifiek 'n passiewe reaktorholte-verkoelingstelsel (RHVS) ondersoek vir volgendegenerasie-hoëtemperatuur-kernreaktors soos die spoelkliplaag- modulêre reaktor.

'n Tydafhanklike wiskundige rekenaarsimulasieprogram van 'n vertikaal georiënteerde reghoekige natuurlike sirkulasielus, 7 m hoog, 8 m breed, met 'n binnedeursnee van 32 mm, is ontwikkel. Die vernaamste aanname was dat die vloei kwasi-stadies is, wat impliseer dat alhoewel die massavloeikoers wel moontlik met verloop van tyd verander, dit by 'n aksiale posisie in die lus in enige tydsoomblik konstant sal wees. Ten einde die lus teoreties te simuleer, is die werkvloeistof in 'n reeks eendimensionele beheervolumes verdeel. Deur die behoud van massa, momentum en energie en geskikte eienskapsfunksies op elke beheervolume toe te pas, is 'n reeks tyd-afhanklike gedeeltelike differensiaalvergelykings gegenereer en met behulp van 'n eksplisiete eindigeverskil-metode opgelos.

Die een vertikale kant van die lus is deur 'n reeks elektriese verhitingsselemente verhit en die ander kant met 'n reeks waterverkoelende mantels verkoel. Deursigtige pypstukke is in die lus geplaas om die tweefase-vloeipatrone waar te neem. Die lus is met 'n uitsittentk toegerus. Die massavloeikoers is met behulp van 'n gaatjiesplaatvloeiometer bepaal. Die lus is in enkelfase- en tweefasebedryfsmodus in werking gestel. 'n Redelike korrelasie tussen die eksperimentele en teoretiese simulasies is gevind met behulp van 'n geskeide tweefasevloei met wrywingvermenigvuldigers en dampvloeistof-leegtebreukkorrelasies, soortgelyk aan dié wat oorspronklik deur Martinelli voorgestel is.

Die gevolgtrekking was dat die ontwikkelde teoretiese model die werklike oorgangs- en dinamiese vloei en hitteoordrag-gedrag van die lus genoegsaam vasgelê het. Die aanbeveling word dus gemaak dat 'n reeks van hierdie lusse met gerustheid vir 'n RHVS gebruik kan word.

ACKNOWLEDGEMENTS

I would like to acknowledge with very great appreciation all the people who assisted and supported me to complete this thesis.

Special thanks to the Almighty God for his grace.

Mr Dobson, special thanks to you for your unlimited support, guidance and assistance for the duration of this thesis.

Sylvie and Sarah thank you. Your love, sacrifices and support throughout the time of my study was my strength.

My family, thank you for always be there for me with much love and support.

Mr Zietsman and all the technicians, thank you for the time, support and assistance during the experimental work.

DEDICATION

To my family

TABLE OF CONTENTS

DECLARATION	i
PLAGIAATVERKLARING / PLAGIARISM DECLARATION	Error!
Bookmark not defined.	
SUMMARY	ii
OPSOMMING	iii
ACKNOWLEDGEMENTS	iv
DEDICATION	v
TABLE OF CONTENTS	vi
LIST OF TABLES	ix
LIST OF FIGURES	x
NOMENCLATURE	xiii
1 INTRODUCTION	1-1
1.1 Background	1-3
1.2 Objectives	1-4
1.3 Thesis layout	1-5
2 LITERATURE STUDY	2-1
2.1 Nuclear reactors	2-1
2.2 Passive safety systems	2-3
2.2.1 Categorisation of passive systems	2-4
2.2.2 Passive system implementation in advanced reactor designs	2-5
2.2.3 Passive cooling	2-5
2.3 Natural circulation loops	2-5
2.3.1 Introduction	2-5
2.3.2 Thermosyphon configurations	2-6
2.3.3 Two-phase flow simulation of a natural circulation loop	2-7
2.3.4 Flow instabilities	2-8
2.3.5 Flow pattern characterisation	2-13
2.3.6 Pressure drop	2-15
2.3.7 Homogeneous flow model for two-phase flow	2-17

2.3.8	Separated flow model for two-phase flow	2-18
2.4	Mathematical modelling.....	2-19
2.4.1	Heat transfer correlations	2-19
3	MATHEMATICAL MODELLING	3-1
3.1	Simplifying assumptions	3-2
3.2	Conservation equations	3-4
3.2.1	Conservation of mass	3-5
3.2.2	Conservation of energy	3-6
3.2.3	Conservation of momentum.....	3-10
3.3	Numerical simulation model	3-11
3.4	Property functions	3-12
3.5	Solution procedure	3-12
4	EXPERIMENTAL SETUP	4-1
4.1	Thermosyphon loop characteristics.....	4-1
4.2	Experimental setup.....	4-2
4.3	Loop re-commissioning and instrumentation.....	4-3
4.4	Experimental procedure	4-3
5	RESULTS.....	5-1
5.1	Experimental results.....	5-1
5.1.1	Single phase operating mode test.....	5-1
5.1.2	Single to two-phase experimental operating mode	5-7
5.2	Theoretical results	5-14
5.3	Comparison results.....	5-18
6	DISCUSSION AND CONCLUSION	6-1
7	RECOMMENDATIONS	7-1
7.1	Loop materials.....	7-1
7.2	Mathematical model.....	7-1
8	REFERENCES	8-1
APPENDIX A THERMOPHYSICAL PROPERTIES OF MATERIALS ...		A-1
A.1	Properties of water	A-1
A.2	Properties of loop's structure materials	A-2

A.3 Property functions.....	A-3
APPENDIX B CONSERVATION OF THERMAL ENERGY EQUATION	B-1
APPENDIX C NUMERICAL SIMULATION ALGORITHM	C-1
APPENDIX D CALIBRATION OF EXPERIMENTAL MEASURING INSTRUMENTS AND ERROR ANALYSIS.....	D-1
D.1 Calibration of thermocouples.....	D-1
D.2 Orifice plate calibration.....	D-4
D.3 Calibration of Endress and Hauser pressure sensor	D-6
D.4 Test-runs 1c and 3b results sample	D-7
APPENDIX E SAFETY PROCEDURES	E-1
E.1 Background	E-1
E.2 Safety Instructions.....	E-1
E.3 User guide	E-3
E.3.1 Normal operating conditions.....	E-3
E.3.2 Accident and malfunction conditions	E-3

LIST OF TABLES

Table 5-1	Test-run 1 electrical power input.....	5-2
Table 5-2	Test-run 1a electrical power input.....	5-4
Table 5-3	Error assessment of the flow parameters.....	5-5
Table 5-4	Heating plate electrical power input for test run 3	5-7
Table 5-5	Heating plate electrical power input for test-run 4.....	5-10
Table 5-6	Heating plate electrical power input for test-run 3a.....	5-13
Table A-1	Saturated liquid specific internal energy u_f as a function of pressure	A-3
Table A-2	Saturated vapour specific internal energy u_g as a function of pressure	A-4
Table A-3	Saturated liquid density ρ_f as function of pressure	A-4
Table A-4	Saturated vapour density ρ_g as function of pressure.....	A-4
Table A-5	Saturated temperature T_{sat} as a function of pressure	A-5
Table A-6	Subcooled liquid density ρ as function of specific internal energy and pressure	A-5
Table A-7	Subcooled temperature T as a function of specific internal energy and pressure	A-6
Table A-8	Superheated temperature T as a function of specific internal energy and pressure	A-6
Table A-9	Liquid viscosity μ_l as a function of temperature	A-6
Table A-10	Vapour dynamic viscosity μ_v as a function of temperature.....	A-7
Table A-11	Saturated pressure P_{sat} as a function of temperature	A-7
Table A-12	Saturated temperature T_{sat} as a function of saturated specific internal energy.....	A-7
Table A-13	Surface tension σ as a function of temperature	A-8
Table D-1	Working fluid k-type thermocouples calibration	D-1
Table D-2	Heating plates k-type thermocouples calibration	D-1
Table D-3	Cooling fluid k-type thermocouples calibration.....	D-3
Table E-1	Safety procedure instructions for closed loop thermosyphon (Sittmann, 2010)	E-1

LIST OF FIGURES

Figure 1-1	Natural circulation loop diagrammatic representation.....	1-2
Figure 1-2	Proposed RCCS representation, Dobson (2006).....	1-4
Figure 2-1	Nuclear energy generation systems: program overview” (US-DOE, 2011)	2-2
Figure 2-2	Simple concept drawing of a High temperature reactor (HTR) illustrating a NC loop (WNA, 2017).....	2-3
Figure 2-3	Thermosyphon loops, integrated (a), separated (b), closed (c), heat pipe type (d) respectively and a surface tension capillary structure or wicked heat pipe (e) (Dobson, 2015).....	2-7
Figure 2-4	(a) Typical low power and high power unstable zones for two-phase natural circulation flow; (b) typical stability map for two-phase density wave instability (Vijayan & Nayak, 2010).....	2-10
Figure 2-5	Qualitative representation of the pressure difference ΔP across the flow meter and the power supplied to the heating section as a function of time (adapted from Vijayan & Nayak, 2010)	2-11
Figure 2-6	Experimentally determined water flow rate dependence on air flow rate at different submergence ratios h/L (a) for a simple water-air lift pump; (b) volumetric characteristics (Stenning & Martin, 1968).....	2-12
Figure 2-7	Two-phase flow patterns, (a) bubbly, (b) and (c) bubbly, small plugs and plug, (d) churn, (e) annular, wispy-annular (Whalley, 1986) ..	2-14
Figure 2-8	Reynolds, Bond and Morton numbers for single rising bubbles (Whalley, 1987)	2-14
Figure 2-9	One-dimensional control volume for a fluid flowing in a pipe (Dobson, 2015)	2-17
Figure 2-10	One-dimensional separated flow conservation of momentum control volumes for two-phase fluid flow in a pipe	2-18
Figure 3-1	Open loop natural circulation thermosyphon.....	3-1
Figure 3-2	Discretisation schematic of the natural circulation theoretical thermosyphon loop.....	3-4
Figure 3-3	Conservation of (a) mass, (b) momentum and (c) energy as applied to a representative control volume (Dobson, 2015).....	3-5
Figure 3-4	Pressure-specific internal energy diagram showing a sub-cooled liquid 1, a two-phase vapour plus liquid 2 and a vapour 3 state point (Dobson, 2015)	3-8
Figure 3-5	Computer algorithm flow chart.....	3-13
Figure 4-1	Experimental thermosyphon loop diagrammatic representation.....	4-1
Figure 4-1	Experimental setup in laboratory (Sittmann, 2010).....	4-2

Figure 5-1	Experimental single phase operating mode with power gradually input (a) heating plate temperatures, (b) working fluid temperatures, (c) system pressure difference, (d) electrical power input (e) working fluid mass flow rate measured with HBM pressure sensor and (f) working fluid mass flow rate measured using E&H pressure sensor	5-3
Figure 5-2	Repeated test (single phase) at low cooling water mass flow rate with electrical power gradually input measured with (a) HBM pressure sensor and (b) E&H pressure sensor.....	5-4
Figure 5-3	Experimental single phase operating mode at full power from start-up to switch off (a) plate temperatures, (b) working fluid temperatures, (c) system pressure difference ΔP (d) mass flow rate \dot{m} measured with HBM and (e) mass flow rate \dot{m} measured with E&H pressure sensor for test-run 2.....	5-6
Figure 5-4	Experimental single to two-phase operating mode with gradually input, (a) fin temperatures, (b) working fluid temperatures, (c) system pressure difference ΔP (d) power input, (e) mass flow rate \dot{m} measured with E&H pressure sensor and (f) mass flow rate \dot{m} measured with HBM pressure sensor for test-run 3.....	5-8
Figure 5-5	Experimental single to two-phase operating mode with increased cooling rate, (a) fin temperatures, (b) working fluid temperatures, (c) system pressure difference ΔP (d) power input, (e) mass flow rate \dot{m} measured with HBM pressure sensor and (f) mass flow rate \dot{m} measured with E&H pressure sensor	5-11
Figure 5-6	Experimental single to two-phase operating mode at full power (9400 W) (a) average fin temperatures, (b) working fluid temperatures, (c) system pressure difference ΔP and (d) mass flow rate \dot{m} (using the E&H).....	5-12
Figure 5-7	Two-phase working fluid mass flow rate repeatability comparison with power gradually input measured with (a) HBM test run 3, (b) E&H test run 3, (c) HBM test run 3a and (d) E&H test run 3a	5-13
Figure 5-8	Hand drawing depictions of two-phase flow patterns adjacent to the two-phase photographic images [poor photographic images due to semi-transparent observation windows]	5-14
Figure 5-9	Theoretical single to two-phase operating mode (a) working fluid temperatures, (b) system pressure difference $\Delta P = \rho g h_{\text{tank}}$ and (c) mass flow rate \dot{m} , with a cooling water mass flow rate at 0.038 g/s	5-16
Figure 5-10	Theoretical single to two-phase operating mode with low cooling water mass flow rate (a) working fluid temperatures, (b) system	

pressure difference $\Delta P = \rho g h_{\text{tank}}$ and (c) Mass flow rate m , with a cooling water mass flow rate of 0.024 g/s	5-17
Figure 5-11 Experimental mass flow rate m_{exp} as given in figure 5.4(f) vs theoretical mass flow rate m_{th} as given in figure 5.9(c) function of time.	5-19
Figure 5-12 Experimental mass flow rate m_{exp} measured with E&H pressure sensor vs theoretical mass flow rate m_{th} , as a function of time ...	5-19
Figure 5-13 Experimental (test-run 3) vs theoretical pressure difference, as a function of time	5-20
Figure 5-14 Working fluid temperatures: theoretical vs experimental (a) experimental working fluid temperatures, (b) theoretical working fluid temperatures	5-21
Figure 6-1 Polycarbonate sight glass located on the (a) top of the evaporator section, (b) bottom pipe and (c) top of condenser	6-2
Figure D-1 HBM pressure transducer calibration positive flow.....	D-4
Figure D-2 HBM pressure transducer calibration reverse flow.....	D-5
Figure D-3 E&H pressure transducer calibration positive flow	D-6
Figure D-4 E&H pressure transducer calibration	D-7
Figure D-5 Experimental single and two-phase operating modes (a) working fluid temperatures test-run 1c, (b) working fluid mass flow rate test-run 1c, (c) working fluid temperatures test-run 2b, (d) working fluid mas flow rate test-run 2b	D-8
Figure D-6 Certificate of calibration	D-10 - D-11

NOMENCLATURE

a	acceleration, m/s^2
A	area, m^2
A_x	cross sectional area, m^2
A_z	heat transfer area, m^2
Bo	Bond number $Bo = gL^2(\rho_l - \rho_g)/\sigma$
c	specific heat, (c_p, c_v) J/kgK
C_f	coefficient of friction
d	diameter, m
D	diameter, m
f	Darcy friction factor, two-phase flow friction factor
Fr	Froude number, $Fr = v/\sqrt{gl}$
g	acceleration due to gravity, m/s^2 , saturated gas
G	force due to gravity, N ; mass flux, kg/s/m^2 , mass velocity, $\text{kg/m}^2\text{s}$
Gr	Grashof number, $Gr = (g\beta\Delta T/(\mu/\rho)^2)L^3$
h	height, head, m
h	specific enthalpy, J/kg
h_{fg}	latent heat of vaporisation, J/kg
k	thermal conductivity, W/mK
K	minor loss coefficient
l	length, m
L	length, m
m	mass, kg
\dot{m}	mass flow rate, kg/s
M	Morton number $Mo = g\mu^4(\rho_l - \rho_v)/(\rho_l^2\sigma^3)$
N	Number
n	Number
Nu	Nusselt number, $Nu = hd/k$
P	pressure, Pa
\wp	perimeter, m
Pr	Prandtl number, $Pr = \mu c_p/k$

Q	energy, J
\dot{Q}	heat flow rate, W
\dot{Q}'''	heat transfer rate per unit volume, W/m ³
R	thermal resistance, K/W
Ra	Rayleigh number, $Ra = GrPr$
Re	Reynolds' number $Re = \rho v d / \mu$
Rho	density, kg/m ³
S	slip factor; Suppression factor
T	temperature, K, °C; period, s
t	time, s
u	specific internal energy, J/kg
U	total internal energy, J; overall heat transfer coefficient, W/m ² K
v	velocity, m/s
V	volume, m ³
x	mass fraction, $m_{\text{vapour}} / (m_{\text{vapour}} + m_{\text{liquid}})$; thermodynamic quality; displacement, m
X	Martinelli parameter
z	distance, m
z_{minor}	minor losses

Greek symbols

α	void fraction, $V_{\text{vapour}} / (V_{\text{vapour}} + V_{\text{liquid}})$
β	thermal expansion coefficient, K ⁻¹
ε	emissivity
θ	inclination angle, rad
λ	thermal conductivity, W/mK
μ	dynamic viscosity, Ns/m ²
ν	kinematic viscosity, m ² /s
ρ	density, kg/m ³
σ	surface tension N/m, stefan-Boltzmann constant, W/m ² K ⁴
τ	shear stress, N/m ²
ϕ^2	two-phase frictional multiplier

Superscript

t	time
Δt	time step

Subscripts

a	air, ambient
atm	atmospheric
$bottom$	bottom of the loop
D	diameter
e	electrical; equivalent
f	saturated liquid; friction
F	wall friction
g	gas
G	gravity
h	hydraulic; wetted perimeter; homogeneous
he	heat exchanger
hp	heat pipe
i	i^{th} control volume or element
in	inlet
ins	insulation
l	liquid
L	length
lo	liquid only
$loss$	loss
M	momentum
$minor$	minor losses
o	only; outside
out	outlet
q	constant heat flux
r	reference
sat	saturated

<i>T</i>	constant temperature
<i>tank</i>	tank
<i>tot</i>	total
<i>v</i>	vapour
<i>w</i>	water, wall
<i>x</i>	at a particular point along the surface
<i>z</i>	heat transfer

Abbreviations

<i>AGR</i>	Advanced Gas-cooled Reactor
<i>BL</i>	Bottom Left
<i>BR</i>	Bottom Right
<i>BWR</i>	Boiling Water Reactor
<i>CANDU</i>	Canada Deuterium Uranium
<i>CV</i>	Control Volume
<i>ESKOM</i>	Electricity Supply Commission
<i>F</i>	Friction
<i>G</i>	Gravity
<i>H</i>	Heater, Heating element
<i>HE</i>	Heat Exchanger
<i>HTGR</i>	High Temperature Gas Reactor
<i>HTR</i>	High Temperature Reactor
<i>IAEA</i>	International Atomic Energy Agency
<i>ID</i>	Inner Diameter
<i>IHTP</i>	Inverse Heat Transfer Problems
<i>LHS</i>	Left Hand Side
<i>LOCA</i>	Loss-of-coolant Accident
<i>M</i>	Mass
<i>MF</i>	Momentum Flux
<i>MHTGR</i>	Modular High Temperature Gas Reactor
<i>NC</i>	Natural Circulation
<i>OD</i>	Outer Diameter

<i>P</i>	Pressure
<i>PBMR</i>	Pebble Bed Modular Reactor
<i>PRT</i>	Platinum Resistance Thermometer
<i>PWR</i>	Pressure Water Reactor
<i>RBMK</i>	Reaktor Bolshoy Moshchnosti Kanalnyy
<i>RCCS</i>	Reactor Cavity Cooling System
<i>RHS</i>	Right Hand Side
<i>RPV</i>	Reactor Pressure Vessel
<i>SF</i>	Slip Factor
<i>TL</i>	Top Left
<i>TR</i>	Top Right

1 INTRODUCTION

In this thesis the theory needed to simulate the transient behaviour of a natural circulation loop using the separated two-phase model will be presented and validated experimentally using an existing loop that has been re-commissioned and more extensively instrumented.

A natural circulation loop is a closed thermosyphon loop that transfers energy from a heat source to a detached heat sink over a distance without the help of any mechanically moving devices. This process, also called passive system does not require the use of active components such as pumps, or uses them in a limited way to circulate the fluid. The process is also self-controlling as the temperature difference increases, so too do the heat transfer rate and flow rate (Grief, 1988; Bieliński & Mikielewicz, 2011; IAEA, 2005).

Thermosyphon loops have many applications and can be used in solar heaters, air conditioning and ventilation, nuclear reactors and thermal management of electrical and electronic devices. In the nuclear industry this thermosyphonic flow process is considered a passive system, hence also inherently safe, making it particularly suitable for use in this industry; where reliability and safety are vital. For instance, they may be used in high temperature reactors in the reactor cavity cooling system (RCCS) (Bieliński & Mikielewicz, 2011). The objective of the RCCS designs being the transfer of heat from the reactor cavity to an outside environment (“heat sink”), and thereby ensuring thermal reliability of the fuel, core vessel and critical equipment within the reactor cavity concrete containment structures for the entire spectrum of postulated accident sequences (IAEA, 2000).

The natural circulation, or thermosyphonic flow process, may also be explained in terms of simple fundamental principles considering a small package of fluid or control volume. An upwards force acts on it due to the hydrostatic pressure difference between the bottom and the top. A downwards force acts on the particle due to gravity. Depending on the resultant of these two forces the particle will either moves upwards or downwards. As a result the fluid in the simple vertically orientated loop, as shown in Figure 1.1, flows with a mass flow rate \dot{m} in a clockwise direction provided the left hand section is heated and the right hand section is cooled.

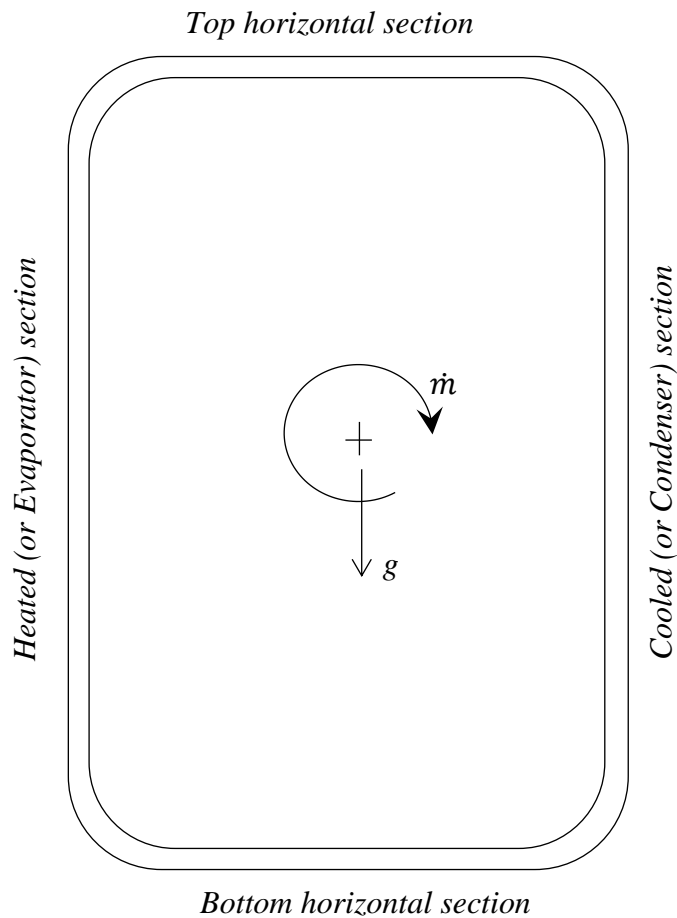


Figure 1-1 Natural circulation loop diagrammatic representation

The force imbalance in the loop is created by a temperature induced change in density for a single component fluid or by a change in the liquid to vapour fraction. Normally the fluid in a natural circulation loop is initially a liquid but as more heat is added vapour is formed in the liquid and a two-phase flow is initiated. Boiling will occur when the saturated pressure corresponding to the liquid temperature is higher than the local pressure in the liquid. If it ("boiling") has not yet occurred in the heated portion, the liquid is considered sub-cooled or compressed liquid. However the subcooled liquid can also start to boil as it rises and the local pressure decreases as soon as the saturated pressure corresponding with the liquid temperature is higher than the local pressure; this is often called flashing (Kolev, 2011; Petelin & Bostjan, 1998).

Two boiling cases may be identified, either when the saturated pressure corresponding with the liquid temperature is higher than local pressure (normally called boiling) and in the case where the pressure corresponding to temperature of the liquid is greater than the local pressure that is called *flashing*.

Depending on the visually observed shape of the bubbles, the two-phase flow may be characterised as bubble, plug, churn, or annular flow. In horizontal and inclined pipes, if the flow rate is low enough, the liquid tends to flow in the bottom of the pipe and the less dense vapour in the top of the tube; this is termed stratified flow.

1.1 Background

Thirty countries worldwide operate 438 nuclear reactors for electricity generation as of July 2015 and 67 new nuclear plants are under construction in 15 countries. In 2012 nuclear provided 10.9 per cent of world's electricity (NEI, 2015). As such, nuclear power must be regarded not only as a proven technology and commercially viable power industry, but in an age when global warming and pollution is becoming of universal concern, it must also be regarded as a potentially environmentally friendly source of energy (Buzz, 2009). However, as a result of the widely publicised Three Mile Island, Chernobyl and Fukushima accidents, nuclear energy's public acceptance has been somewhat tarnished (Bromet, 2014). In an attempt to make nuclear energy a more acceptable alternative to fossil fuel sources for the generation of electrical power and process heat it thus appears justified to investigate nuclear power and heat solutions with the potential of a more convincing safety philosophy that also includes the use of passive safety systems (NEA, 2002).

Passive safety systems, such as thermosyphon loops, are integrated into the nuclear reactors in order to improve reliability and safety and are also used as a means for heat transfer from a heated to a cooled section through thermally induced density gradients resulting in natural circulation (IAEA, 2009). Thermosyphons are often found in situations where energy efficiency and low cost and low maintenance are a concern. They are also used in nuclear energy as cooling systems for the reactor core and surrounding structures (IAEA, 2009).

In 2000, Eskom planned to increase nuclear power production in South Africa as part of its integrated electricity plans, thus formed a partnership with the PBMR company (www.eskom.co.za). In order to facilitate future development of nuclear, one of the programs launched by the PBMR and South African universities was to investigate on a suitable passive reactor cavity cooling systems (RCCS) (Van Staden, 2001, www.pbmr.com).

In 2006 Dobson proposed a RCCS concept for the PBMR as shown in Figure 1.2. His concept included a number of closed natural circulation loops with the heated section in the hot air cavity and the cooled in the heat sink. These loops are spaced around the periphery of the reactor cavity at a pitch angle θ .

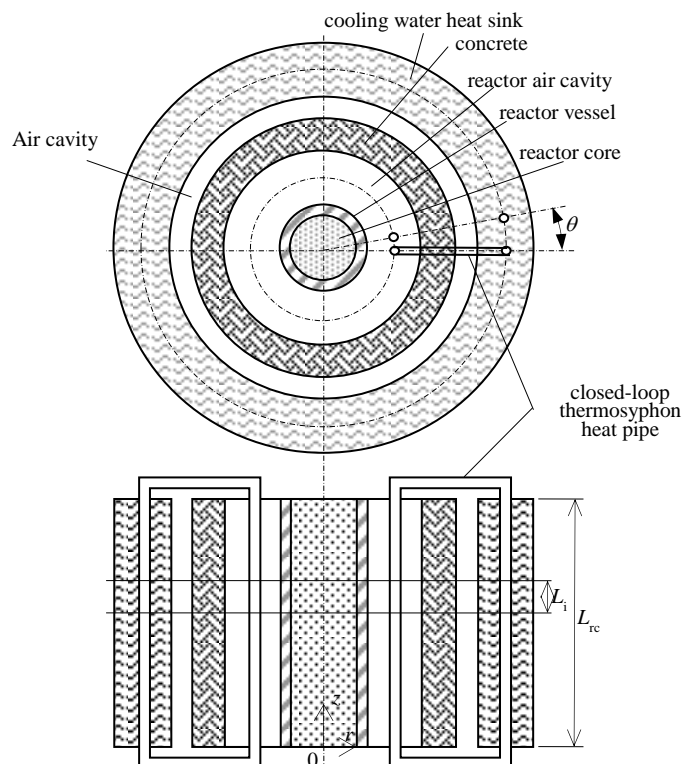


Figure 1-2 Proposed RCCS representation, Dobson (2006)

Two types of thermosiphon can be identified; the open loop thermosyphon and the closed loop thermosyphon (Chen, *et al.*, 1987). In both types three operating *modes* may be identified. The single phase mode where the fluid flows in liquid phase from start to finish; the single to two-phase mode, in this mode the fluid initially single phase boils and two-phase flow occurs with liquid being forced into an expansion tank (Haider, *et al.*, 2002), and the heat pipe mode where the experiment starts off with a loop partially filled with saturated liquid and its vapour (Dobson, 1993; Tuma, 2006; Yeo *et al.*, 2014).

For experimental purposes an old heat transfer loop built by Sittmann (2010) was re-commissioned. This loop had been used at that time to investigate natural circulation in a RCCS.

1.2 Objectives

Five objectives were identified for this project as follow.

- 1) Present a literature survey of thermosyphon loops and the natural circulation simulation theory with specific reference to the nuclear industry.

- 2) Theoretically model and simulate the thermal-hydraulic behaviour of a natural circulation cooling loop suitable as a coolant heat removal loop of an inherently safe nuclear passive system.
- 3) Develop a computer program to numerically solve the theoretically derived mathematical simulation model.
- 4) Re-commission and instrument an existing loop and experimentally evaluate the transient heat transfer behaviour of the loop for different power inputs and cooling temperatures.
- 5) Validate the theoretical simulation model experimentally for single phase and two-phase operating modes using a separated two-phase flow model.

1.3 Thesis layout

A literature survey was first conducted to identify the theories of nuclear reactors, passive systems, thermosyphon loops, single phase and two-phase natural circulation loops. This is presented in Chapter 2 of this thesis. Chapter 3 deals with the mathematical modelling of the loop for the theoretical simulations of the natural circulation loop as schematically depicted in Figure 3.1 using the separated two-phase flow model. Chapter 4 of this project describes the experimental setup of the thermosyphon loop re-commissioned and instrumented in order to obtain the experimental data. The results obtained from the collected data are presented in Chapter 5. Chapter 5 also provides theoretical results and a comparison between the two results is given to validate the theoretical simulations. Chapter 6 presents a discussion and a conclusion to the project, as related to the original objectives and Chapter 7 offers recommendations for future work.

2 LITERATURE STUDY

Recently, South Africa has shown the need for more electricity generation capacity to ease both the industrial and local demand (DTI, 2014). In 2015, country-wide load-shedding was implemented to meet this demand which adversely affected the manufacturing industry and the South African economy in general (loadshedding.eskom.co.za). In an attempt to ameliorate this adverse situation, different and more sustainable means of energy generation are being investigated; these include nuclear, renewables and new fossil-fuelled plants (DOE, 2015). This literature study however focusses on the passive natural circulation cooling of nuclear power plants; passive systems being regarded as inherently safe and more reliable than active systems (IAEA, 1993).

In particular, this literature study considers passive natural circulation safety systems for core decay heat removal and containment cooling systems of nuclear reactors. The application of these systems to the reactors of Generation III+ and IV and Innovative reactor designs is emphasised and investigated under the following subsections: nuclear reactors in general, passive safety, passive cooling systems and natural circulation thermosyphons (IAEA, 2009).

2.1 Nuclear reactors

Energy is produced from splitting the atoms of certain elements in nuclear reactors. This energy is used to make steam to drive a turbine which in turn drives an electrical producing generator.

According to the world nuclear organisation (WNO, 2017), the first nuclear reactors operated manually in rich uranium deposits about two billion years ago to develop into today's reactors. These reactors derived from designs originally developed for propelling submarines and large naval ships generate about 85% of the world's nuclear electricity. Globally, two water reactors are common in nuclear plants; the pressurised water reactor (PWR) representing 65% of the reactors operating now and the boiling water reactors (BWR) representing 15% (CAN, 2017).

From many different proposed reactor systems six (i.e. Magnox, AGR, PWR, BWR, CANDU and RBMK) have emerged for commercial electricity production in the world (IEE, 2005). Further the IAEA categorized nuclear reactors in generation I, II, III, III+ and IV (IAEA, 2009). Gen I, II and III derived from designs originally developed for naval use beginning in the late 1940s and is referred to the launching of civil nuclear power, while Gen II refers to a class of commercial, economical and reliable reactors and Gen III are essentially an improved Gen II (IAEA, 2009). These reactors are still operating worldwide today

(Goldberg et al., 2011). Figure 2.1 shows an overview of the United States of America's history of reactor generations and a program of generation IV, a key factor of nuclear development (US-DOE, 2011).

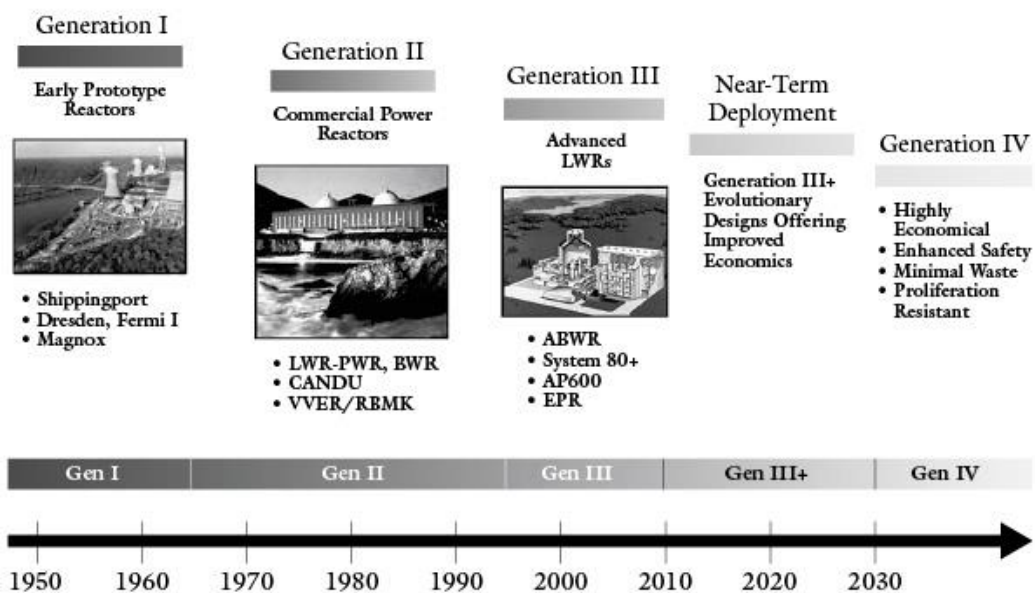


Figure 2-1 Nuclear energy generation systems: program overview” (US-DOE, 2011))

Gen III+ and VI reactors are important in the nuclear industry and a viable long term option with the first being an evolutionary of Gen III and the later (Gen IV) still two to four decades away, although some designs could be available within a decade (Goldberg *et al.*, 2011).

A fast growth in installed nuclear power capacity (up to 300 GW) was observed in the early 1980s, however its development was hit by anti-nuclear sentiment because of the 1986 Chernobyl's accident causing a different perception with fear of possible nuclear radiation and also because of the risk of nuclear material being used for terrorist activities (NEA, 2002). The transport and storage of nuclear waste are also a contentious issue and the rising costs when compared to fossil fuels causing a setback in investment for new nuclear power stations (Ruppersberg, 2008).

In South Africa, Eskom planned to reach 82 GW by 2015, of which 20 GW would come from nuclear power plants (Eskom, 2004); therefore investments were directed in research for high temperature gas reactor technologies such as the pebble bed modular reactor (PBMR) and projects were fully supported by the government. Due to potential failure of demonstrations and the costs involved the funding on the PMBR projects was stopped (Senda, 2012). This development

does not impact this research, as the work done for this study is applicable to other high temperature reactor technology.

The PBMR is a reincarnation of the ‘high temperature gas reactor’ or HTGR in a modular version, known as the MHTGR (Makhijani, 2001). The PBMR is a variant of the HTGR; helium cooled graphite moderated High Temperature Reactor (HTR). Figure 2.2 illustrate a concept of a HTR (WNA, 2017). It is a very high efficiency nuclear reactor and attractive economics are possible without compromising the high levels of passive safety expected of advanced nuclear designs (PBMR, 2017).

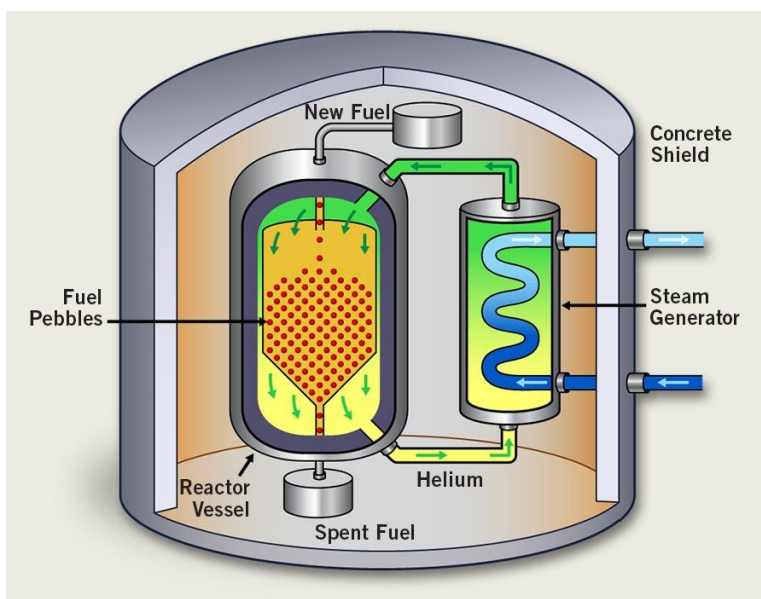


Figure 2-2 Simple concept drawing of a High temperature reactor (HTR) illustrating a NC loop (WNA, 2017)

Passive safety systems are integrated in Gen IV nuclear reactor concepts, with high temperature and high pressure, whether as a primary coolant, decay heat removal, containment cooling and loss-of-coolant-accident (LOCA) or an emergency core cooling system (Vijayan, *et al.*, 2013). A wide range of literature on nuclear reactors’ generation (Sherry, *et al.*, 2010; Piro, *et al.*, 2016); thus they will not be discussed in this work.

2.2 Passive safety systems

This section looks at some aspects of the safety mechanisms implemented in HTRs such as the RCCS for the core decay heat removal and reactor containment cooling. The International Atomic Energy Agency (IAEA) (IAEA, 1991) gives definitions for safety related terms as applied to advanced reactors of generation III+ and IV, where the concept of passive safety system is defined and compared

to the active safety systems (Senru, 1988). A passive safety system includes only passive components and structures or uses active components in a very limited way to activate the ("passive") operation (IAEA, 2009) and possible failure because of the lack of human action or a power failure would not happen in these systems (IAEA, 1991).

2.2.1 Categorisation of passive systems

Based on the four characteristics given below that the system does not make use of, the IAEA classifies the degree of passive safety of components four categories from A to D (IAEA, 1991).

1. no signal inputs of intelligence;
2. no moving mechanical parts;
3. no moving working fluid; and
4. no external power input or force.

- Category A

Category A is characterised by the combination of all four (1+2+3+4) considerations. This group represents barriers against the release of fission products; therefore they must always be closed if they are not at the reprocessing plant.

- Category B

Category B (1+2+4) represents the surge line that controls the pressure in the primary loop of a PWR using moving working fluid when the safety function is activated (IAEA, 1991; Burgazzi, 2012).

- Category C

In category C (1+4) the fluid moves as in category B (IAEA, 1991). For a PWR, category C can be represented by accumulator (Ravnik, 1991).

- Category D

Category D (4) represents the transition between active and passive where an external signal is necessary to activate the passive process and is referred as "passive execution/active initiation" (IAEA, 1991).

It is important to know that passivity is not synonymous with reliability, availability or adequacy of the safety features (IAEA, 1991).

2.2.2 Passive system implementation in advanced reactor designs

The extensive use of passive systems and their reliability in new and advanced nuclear power plants is now subjects to intense discussions (NEA, 2002). Passive systems are therefore widely considered in innovative or advanced nuclear designs and are adopted for coping with critical safety functions for removing the decay heat from the core after a reactor scram. For generation III+ and VI reactor designs, the following passive safety systems have major function for the core decay heat removal and reactor containment (IAEA, 2009).

- Pre-pressurized core flooding tanks (accumulators);
- Elevated tank natural circulation loops (core make-up tanks);
- Gravity drain tanks;
- Passively cooled steam generator natural circulation;
- Passive residual heat removal heat exchangers;
- Passively cooled core isolation condensers; and
- Sump natural circulation.

There are many published papers and information on these different types of passive safety systems (IWGATWCR, 1989; IAEA, 2009), therefore they will not be detailed in this literature survey.

2.2.3 Passive cooling

A passive cooling system uses natural processes for heating or cooling to attain internal equilibrium and energy flows by natural means such as radiation, conduction or convection without the use of mechanical or electrical device (Kamal, 2012). However there is a very important issue with the driving force depending on whether the flow is sustained by a density difference in the fluid (natural circulation) or by a pump (forced convection). If the system is represented by a loop, the interior balanced conditions permit fluid to flow freely in the system as natural circulation.

2.3 Natural circulation loops

2.3.1 Introduction

A natural circulation loop is also called a loop thermosyphon. It is a thermo-fluid design that works with temperature induced density gradients to create the natural circulation of the working fluid in the system. The thermosyphon loop operates as the natural convection of the liquid when heat added to the liquid; it gives rise to a temperature difference from one side of the loop to the other where the warmer fluid is less dense and thus more buoyant than the cooler fluid on the other side of the loop (Ruppersburg & Dobson, 2007). With the assist of gravity, the liquid will move from the denser section (the condenser section) to the less dense section (the

evaporator section). Here the liquid will be heated and pushed again toward the condenser. This back and forth phenomenon will allow the fluid to circulate in the loop without the help of any mechanical device.

Natural circulation loops have an extensive range of applications in chemical process industry (Arneth, 2001; Chexal & Bergles, 1986), large scale nuclear reactors and medium-scale chemical reactors (Sinha & Kakodkar, 2006; Sutharshan, 2011 and Haide *et al.*, 2002), solar water heaters (Cheng, *et al.*, 1982), waste heat recovery (Yilmaz, 1991), closed loop pulsating heat pipes (Dobson & Harms, 1999; Sardeshpande & Ranade, 2013), electronics industry (Khodabandeh, 2002), and in the nuclear industry (Hsu, 1988; IAEA, 2000; Sha, 2004).

2.3.2 Thermosyphon configurations

Thermosyphon configurations are usually classified into closed loop and open loop (Greif, 1988). The open loop has one or more heating or cooling legs drawing fluid from one thermal reservoir to a second reservoir while closed loop continuously circulates the fluid through a closed path with periodic heating or cooling sections (Gebhart, *et al.*, 1988; Greif, 1988; Torrance, 1979). The majority of the literature focused on how to create thermal balance between the heating and cooling sections while ensuring that the net heat addition is balanced by the heat removal (Greif, 1988).

Many geometric configurations of open and closed loop thermosyphon have been studied; however there are two most common configurations: toroidal and rectangular loops (Bau & Torrance, 1981; Damerell & Schoenhals, 1979; Creveling, *et al.*, 1975; Nayak, *et al.*, 1995). A toroidal loop that is symmetrically heated from below and cooled from above has been found to be unstable at some heating rates (Greif, *et al.*, 1979), although the stability was found to improve when the toroid was rotated such that the heating was not symmetric (Damerell & Schoenhals, 1979). Natural circulation loops, in so far as they relate to reactor core heat removal systems, may be termed integrated, separated, or heat pipe (Dobson, 2006; Dobson, 2015; Bhattacharyya, 2012). A natural circulation system may be said to be integrated when the circulation takes place entirely within a single containment vessel. For example, the hot reactor core coolant flows upward inside riser in a riser and downward on the outside, where it cooled by the secondary flow through the heat exchanger positioned between the riser and the reactor vessel; as shown schematically by in Figure 2.3

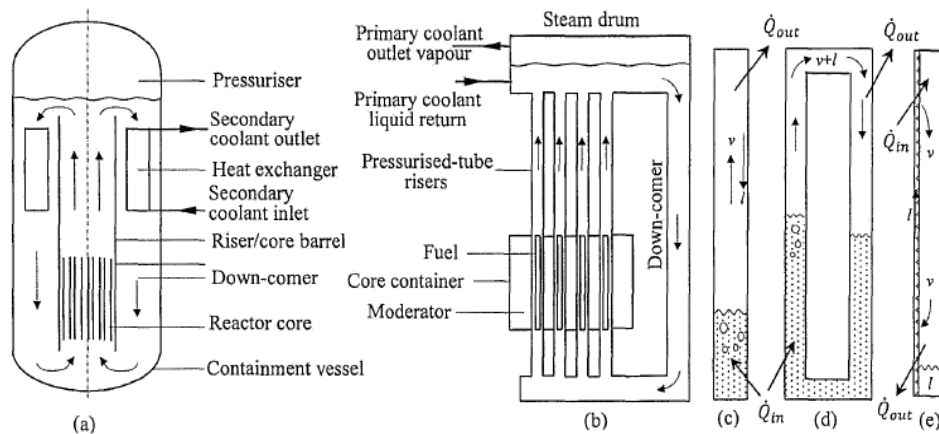


Figure 2-3 Thermosyphon loops, integrated (a), separated (b), closed (c), heat pipe type (d) respectively and a surface tension capillary structure or wicked heat pipe (e) (Dobson, 2015)

A relatively large amount of published literature is available relating to a rectangular loop thermosyphons with the lower horizontal portion heated and the upper horizontal portion cooled (Basaran & Kucuka, 2003; Durig & Shadday, 1986; Bieliński & Mikielewicz, 2011). This configuration is significant in the emergency cooling of many pressurised water reactors but the flow is prone to bifurcation. There are also stability problems as the flow in the thermosyphon heated in this way has an equal chance of flowing either clockwise or counter clockwise (Dobson, 1993; Knaai and Zvirin, 1993; Grief, 1998). This case will however not be considered here as this should be avoided by making sure that the heating and subsequent cooling portions are positioned in such a way so to ensure that the desired flow direction is guaranteed; by heating the lower portion of one vertical side and cooling the top portion of the other vertical side.

Both single phase and two-phase natural circulation systems have been widely investigated and assumptions made (Dobson, 1993; Grief, 1988; Welander, 1967). Knaai and Zvirin (1990) show that the single phase loop theory may be extended to a two-phase loop by specifying suitable equations for the friction factor, two-phase frictional multiplier, heat transfer coefficient and the void and mass fractions. Capturing the transient performance of a two-phase flow loop has shown to be more complex and requiring a large amount of differential equations (Dobson, 1993; Vincent & Kok, 1992).

2.3.3 Two-phase flow simulation of a natural circulation loop

The basic approach in theoretical simulations of the single and two-phase flow is to discretise the loop into a series of parallel one-dimensional axially symmetrical parallel control volumes, in which the two phases are treated as two separate fluids, and applying the equations of change (mass, momentum and energy) to each control volumes, thus resulting in six separate equations for each control

volume (Ruppersberg, 2008). These equations are then used with simplified assumptions to generate computational codes in different numerical computer programs that may sometimes be very complex; however, they can be used to simulate a wide range of geometrical configurations and a large variety of thermal-hydraulic problems (Manera, 2003).

Simpler approaches are possible, the simplest being the homogeneous equilibrium model (HEM). In this model the two-phase flow is imagined as a single fluid in which both phases are well-mixed and cannot be distinguished from each other. The phases travel at the same velocity and have a density ρ , given in terms of the mass fraction x as $\rho = (x/\rho_v + (1 - x)/\rho_l)^{-1}$ (Whalley, 1990; Guo *et al.*, 2015). A homogeneous model is able to predict the occurrence of flashing. Once boiling commences a void fraction α , defined as the fraction of the volume of gas to the total volume of the control volume. It may also be defined as cross-sectional area of the vapour divided of the cross-sectional area of a uniformly flowing control volume (i.e. cross-sectional void fraction) $A_v/(A_v + A_l)$. It is needed to predict the buoyancy term in two-phase flow (Thome, 2011). In this case the vapour and liquid are considered to flow as two separately flowing fluids, and is called a *separated* two-phase flow model, and assumes that both phases are in thermal equilibrium with each other at any cross-sectional position in the loop. In this case the density is given as $\rho = \alpha\rho_v + (1 - \alpha)\rho_l$ and the void fraction as $\alpha = \left(1 + \frac{v_v}{v_l} \frac{1-x}{x} \frac{\rho_v}{\rho_l}\right)^{-1}$ where v_v/v_l is given by an experimentally determined correlation (Carey, 1992).

Another one-dimensional approach is to use a drift flux model in the conservation of momentum equation together with a void fraction and two-phase frictional multiplier to simulate density wave oscillations (Guanghai *et al.*, 2002). This model is relatively difficult to understand but the separated model appears to be more popular and, according to Manera (2003), the separated flow model is a good compromise taking into account complexity and its relative simplicity.

2.3.4 Flow instabilities

In most of the two-phase flow and heat transfer solutions equations of conservation of mass, momentum and energy are used. Although correct conservation equations can be determine, the degree of complexity for simulation and modelling, and the large amount of material required in simulation, restrict their use in practical applications (Yadigaroglu & Lahey, 1975). Thus it is necessary to use simplified forms of the conservation equations for problems of practical significance. Further, a review of the published literature will reveal that it is unlikely that any two author's solution procedures of any two ostensible similar problems are precisely the same. Rather than establish a systematic review and appraisal of all versions of the published mathematical formulations and solution procedures, and their mathematical formulations, the simulation model as used in this thesis is given in Chapter 3 (Mathematical modelling). It is essentially

a separated flow model and according to Manera (2003), includes sufficient complexity to fully take into account the essential physical phenomena encountered during both single and/or flashing conditions. Moreover because of the number of empirical correlations (the two-phase frictional multiplier and the void fraction correlations), cause-effect relationships can more readily be assessed.

A comprehensive review of advancements over the last two decades in two-phase natural circulation loops has been undertaken by Bhattacharyya, *et al.* (2012). It is clear from this review that the single most important research activity revolves around what is termed "instabilities"; an important concept in so far as the perception of what constitutes the safe and reliable operation of nuclear reactors is concerned. In this regard instabilities are universally classified as either a static or a dynamic instability. A static instability being defined as when the operating conditions are changed by a small step from the original, it is not possible to regain a steady state close to the previous one. Vijayan and Nayak (2010) in their course notes on an introduction to instabilities in natural circulation systems further classify instabilities as depending on the:

- Analysis method (or the governing equations of change used). Different sets of governing equations are used for different instabilities based on the prediction of instability threshold. Based on the governing equations Boure, *et al.* (1973) classified instabilities into four basic types including pure static and dynamic instabilities and compound static and dynamic instabilities.
- Propagation method. Here two instabilities are considered, density waves instability, and acoustic instabilities (Vijayan & Nayak, 2010). Density wave instabilities occur when there is a time varying density around the loop due to the change in density (due to change in temperature and the consequent change in density due to thermal expansion of the liquid in single phase flows and/or in two-phase flow the change in void fraction) around a loop (Yadigaroglu & Lahey, 1975). The frequency of these instabilities is proportional to the time it takes for a particle or small package of fluid to flow around the loop and wherein in its transit around the loop its density also changes with time and at different axial positions around the loop (Vijayan & Nayak, 2010). Acoustic instability, on the other hand, has been suggested as being a visually observable movement of a small package of fluid that is due to perturbations moving at the speed of sound in the fluid (Nayak & Vijayan, 2008). For example, consider a 10 m circumferential loop; a density wave travelling at 5 m/s will have a time period $T = 10 \text{ m} / 2 \text{ m/s} = 5 \text{ s}$ or 0.2 Hz. On the other hand, changes in flow rate as manifested by the rate of change of pressure difference across a flow meter are said to be acoustic instabilities if their time period is in the order of $10 \text{ m} / 1000 \text{ m/s} = 0.01 \text{ s}$ or 100 Hz. This is assuming that the average speed of sound in the fluid as being somewhere that of water and air of about 1500 m/s and 350 m/s, respectively or $(1500 + 350)/2 \approx 1000 \text{ m/s}$ (Mills & Ganesan, 2009).

- Nature and or number of unstable zones. Depending on operating conditions and natural frequency of the fluid supporting pipes and structures the oscillations may be periodic or chaotic. In the density wave in two-phase flow natural circulation, there are low and high power unstable zones (see Figure 2.4(a)) (Vijayan & Nayak, 2010). Fukuda and Kobori (1979) found that gravitational pressure drop is a key factor for type I instability in the unheated section and frictional drop in type II. Generally if the stability map encloses a stable zone, then it has two unstable zones (Vijayan & Nayak, 2010). This stability map can be seen in Figure 2.4(b).

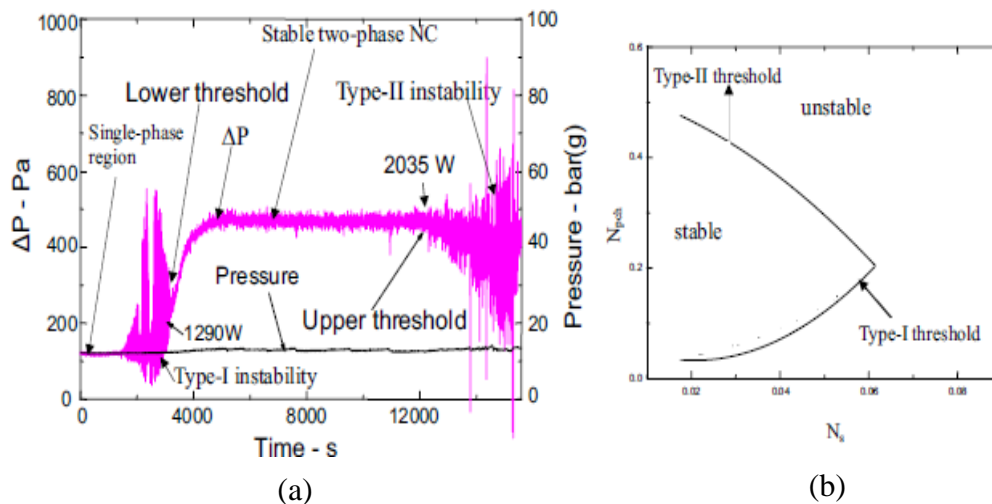


Figure 2-4 (a) Typical low power and high power unstable zones for two-phase natural circulation flow; (b) typical stability map for two-phase density wave instability (Vijayan & Nayak, 2010)

- Loop geometry. For example, symmetrically heated and cooled loops tend to be unstable
- Disturbances. Such as boiling inception, flashing, flow pattern transitions, laminar to turbulent transitions, slip-stick that is the friction factor tends to infinity as the velocity tends to zero; in accordance with the concept of static and dynamic friction between solids.

Vijayan and Nayak (2010) found that it is convenient to consider the single-phase, boiling inception and two-phase natural circulation instabilities separately. The transition to two-phase flow passes through boiling inception, therefore the two-phase natural circulation instabilities are observed right from boiling inception.

Detectable fluctuation in particle speed in a natural circulation loop is said to be an acoustic instability and is thought to be caused by the resonance of pressure waves. Vijayan and Nayak (2010) observed acoustic oscillations during *blowdown* (pressure relieving) experiments with pressurized hot-water systems in subcooled

boiling, bulk boiling and film boiling. They characterised them by high frequencies of the order of 10–100 Hz related to the pressure wave propagation time.

Vijayan and Nayak (2010) give an experimentally determined, stability map, as shown in Figure 2.4(a), for a $\phi 9.1$ diameter pipe as adapted from Vijayan and Nayak (2010) in Figure 2.5. Note that the pressure difference is across a flow meter and hence indicative of the volumetric flow rate in the loop. Note also that the heating method is by means of an electrical resistance heating element which at a given power is essentially a constant heat flux heating load.

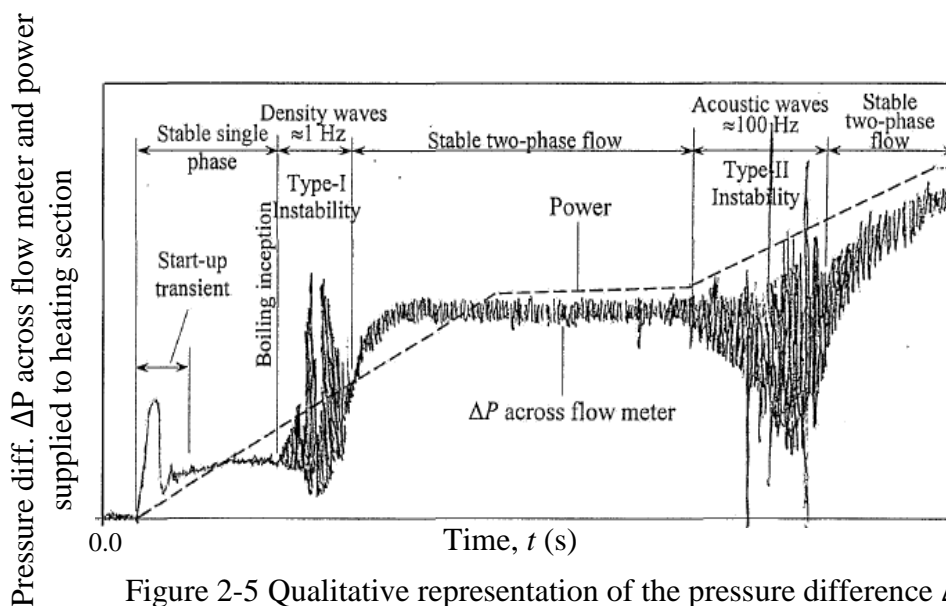


Figure 2-5 Qualitative representation of the pressure difference ΔP across the flow meter and the power supplied to the heating section as a function of time (adapted from Vijayan & Nayak, 2010)

To develop a better appreciation of density or buoyancy driven flow, consider a simple small-diameter airlift water pump operating at different submergence h/L ratios, as shown in Figure 2.6. As the air flow rate increases so too does the water flow rate, and, in this case, at an air flow rate of about $5 \text{ m}^3/\text{hour}$ the water flow reaches a maximum at the different submergence ratios. At this air flow rate, the flow pattern is essentially plug flow as depicted in Figure 2.6(a) and consists of relatively large bullet-shaped bubbles flowing at a relatively low frequency. As the bubbles rise, water is displaced upwards intermittently in pulses corresponding more-or-less to the flow rate of the bubbles. Up until this point, the flow is said to be buoyancy driven or gravity dominated. If the flow rate is measured using an electronic flow metering device and plotted graphically as a function of time, it is seen to flow in an oscillatory wave-like manner at a frequency of about 1 Hz; this region is thus also called the density wave (or type-I instability) region. As the air flow rate increases yet further the water flow rate decreases; in this operating region of the air-lift pump the flow is said to be friction dominated.

Referring back to Figure 2.4(a) and Figure 2.5, for example a wall heat flux driven flow as the heat flux is relatively slowly increased and the flow rate exhibits a single phase start-up transient. In this example the flow rate increases slowly up to a maximum before falling down and after a number of smaller oscillations settles down and increases proportional to the slowly increasing heat flux. As the temperature slowly increases in the heating section vapour bubbles start to form and the flow rate enters a single to two-phase transition (shown in Figure 2.4(a) and Figure 2.5 as the density wave region) but on further increase in power the amplitude of the oscillations tend to reduce and up to a certain power the flow is relatively stable with only small oscillations. However, at a certain higher power level the flow is again oscillatory, the flow tends to decrease but the amplitude of the oscillations increase dramatically; the frequency of the oscillations in this region are in the order of about 100 Hz which also corresponds with the natural frequency of sound waves of the fluid flow, hence they may be termed acoustic waves. On increasing the heat flux further the amplitude of the oscillations tend to decrease but the flow rate now increases again; this region is termed the stable two-phase flow region. The flow at these high heat fluxes tends to become separated with a thin liquid film around the inside periphery of the pipe and a relatively high speed vapour flowing in the core of the pipe.

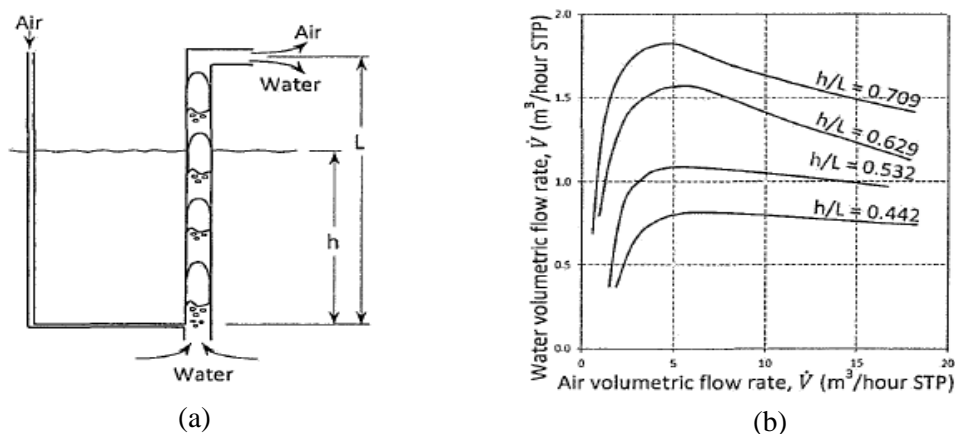


Figure 2-6 Experimentally determined water flow rate dependence on air flow rate at different submergence ratios defined as h/L (a) for a simple water-air lift pump; (b) volumetric characteristics (Stenning & Martin, 1968)

The pipe diameters of the loops that Vijayan and Nayak (2010) tested varied from 6 to 40 mm. It has however been suggested that for larger diameter pipes, say from $\phi 200$ mm upwards, the two-phase flow and instability behaviour cannot be extrapolated. Very little published literature is available for larger diameter (> 70 mm) tubes, especially with water and steam.

2.3.5 Flow pattern characterisation

Flow patterns in small diameter pipes (that is if the Bond number $Bo = (g(\rho_l - \rho_v)L^2)/\sigma$ is less than 40 or about 70 mm for water) are typically characterised in terms of so-called bubbly, plug (or slug), churn and annular flow patterns (Whalley, 1987) as shown in Figure 2.7 by way of sample photographs (a) and stylised sketches (b). For spherical bubbles Whalley (1987) derives an equation (by equating the buoyancy and drag forces acting on the bubble) for the terminal rising velocity, for low Reynolds numbers of less than one, as

$$u_b = \frac{a_b^2 g(\rho_l - \rho_v)}{12\mu_l}$$

Larger bubbles are however not spherical, nor do they obey Stokes' law; Whalley (1987) gives a chart a useful formulation (from Clift *et al.* 1978) for the characterisation of bubble type flow in what he calls intermediate sized diameter pipes in terms of the Bond (or Eotvos) Bo , Reynolds Re and Morton M numbers, respectively (and as given in Figure 2.8) as

$$Bo = (g(\rho_l - \rho_v)L^2)/\sigma \quad (2.1)$$

$$Re = (\rho_l v d_e)/\mu_l \quad (2.2)$$

$$M = \frac{g\mu_l^4(\rho_l - \rho_v)}{\rho_l^2 \sigma^3} \quad (2.3)$$

Where in this case d_e is the equivalent diameter in m and is the diameter the bubble would have if it was spherical, and the surface tension σ is in N/m. The rising velocity of the bubble can therefore be found by

- i) calculating the Bond number from equation 2.1,
- ii) calculating the Morton number from equation 2.3,
- iii) looking up the Reynolds number from figure 2.8, and then
- iv) the rising velocity can then be found from equation 3.4.

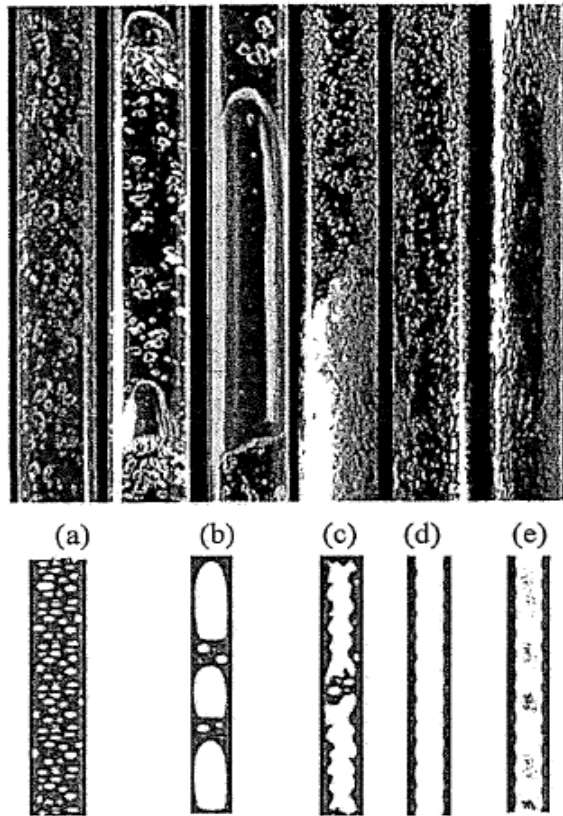


Figure 2-7 Two-phase flow patterns, (a) bubbly, (b) and (c) bubbly, small plugs and plug , (d) churn, (e) annular, wispy-annular (Whalley, 1987)

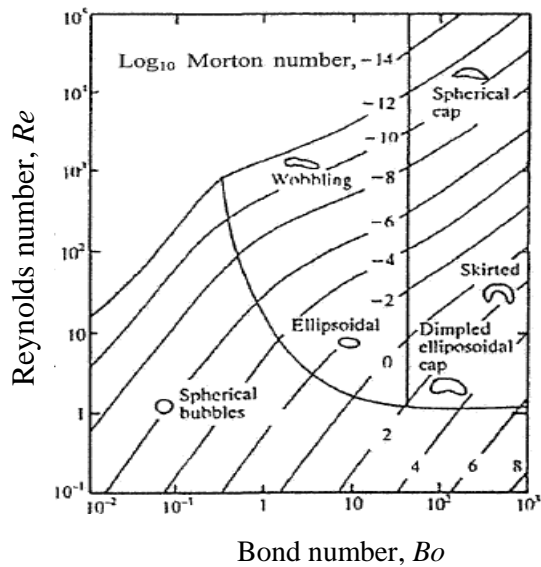


Figure 2-8 Reynolds, Bond and Morton numbers for single rising bubbles (Whalley, 1987)

2.3.6 Pressure drop

Pressure drop can be caused by resistance to flow, changes in elevation, density, flow area and flow direction (Kroger, 1998). In natural circulation systems it has a urge impact in their steady state, transient and stability performance (Vincent & Kok, 1992).

Mills and Ganesan (2009) showed that the pressure drop very difficult due to uncertainty and complexity of the flow behaviour in two-phase flow. Much research has been done on this, with only partial success (Cioncolin & Thome, 2017; Autee & Giri, 2016; Hernandez-perez, *et al.*, 2010; Hewitt, 1982).

Hernandez-perez *et al.* (2010) found that the pressure drop in vertical two-phase flow is less (frictional) as a function of pipe diameter mainly for gas at velocities higher than 2 m/s. Autee and Giri (2016) tried to measure and predict the pressure drop across tubes and bends, important for the enhancement of the performance and safety of the heat exchanger and flow transmitting devices. Their research revealed that the predicted values of pressure drop using a comparative study of some of the available two-phase flow correlations may differ by large amounts.

Accurate prediction is empirical and limited in range of applicability (Mills & Ganesan, 2009). For simplicity, the calculation of the pressure drop is based on the homogeneous model of two-phase flow that ignores detail of the flow patterns. The pressure gradient in a straight tube can be found as shown in equation 2.4

$$\frac{dP}{dz} = \left(\frac{dP}{dz}\right)_F + \left(\frac{dP}{dz}\right)_G + \left(\frac{dP}{dz}\right)_M \quad (2.4)$$

Where subscripts F, G and M refer to pressure gradient due to wall friction, gravity and momentum changes, respectively and they are calculated as shown in equations 2.5, 2.9 and 2.10 respectively. The homogeneous model of two-phase flow assumes that the velocity of each phase is the same.

$$\left(\frac{dP}{dz}\right)_F = -\frac{f}{D} \frac{G^2}{2\rho} \quad (2.5)$$

Where f is the two-phase flow frictional factor, G the mass velocities and D the pipe diameter. The simplest method for evaluating the two-phase flow frictional factor is to assume that pure liquid is flowing at the mixture mass velocity that is at a Reynolds number $Re = GD/\mu_l$. This friction factor will generally be too low at qualities below about 70%, and too high at qualities above 70% and the limiting value for pure vapour $x = 1$ (Mills & Ganesan, 2009). To overcome this, the simple reference viscosity given by equation 2.6 should be used (Mills & Ganesan, 2009).

$$\frac{1}{\mu_r} = \frac{x}{\mu_v} + \frac{1-x}{\mu_l} \quad (2.6)$$

Which mass-weights the inverse of viscosity and has the limits

$$x = 0: \mu_r = \mu_l$$

$$x = 1: \mu_r = \mu_v$$

The mass velocity is calculated from

$$G = G_v + G_l; \quad G_v = \frac{\dot{m}_v}{A_x}; \quad G_l = \frac{\dot{m}_l}{A_x} \quad (2.7)$$

where A_x is the tube-cross section

The mass flow rates in terms of mass velocities and quality are calculated by way of equation 2.8 (Mills & Ganesan, 2009).

$$\dot{m}_v = GA_x x; \quad \dot{m}_l = GA_x(1 - x) \quad (2.8)$$

The pressure gradient due to gravity is calculated from

$$\left(\frac{dP}{dz}\right)_G = -\rho g \sin \theta \quad (2.9)$$

Where θ is the angle measured from the horizontal.

The pressure gradient due to momentum change is found from

$$\left(\frac{dP}{dz}\right)_M = -\frac{d}{dz} \left(\frac{G^2}{\rho}\right) \quad (2.10)$$

Since G is constant along the tube

$$\left(\frac{dP}{dz}\right)_M = -G^2 \frac{d}{dz} \left(\frac{1}{\rho}\right) = \left(\frac{G}{\rho}\right)^2 \frac{d\rho}{dz} \quad (2.11)$$

Literature relating to purely experimental observations and demonstrations are also considered in Chapter 5. Welander (1966) considered the fluid to be driven by the pressure difference and a buoyancy force, and is retarded by a frictional force. The assumptions made included.

- The Boussinesq approximation,
- The tangential friction force on the fluid is proportional to the average flow rate $v = \dot{m}/\rho A$, and
- Quasi-equilibrium one-dimensional flow that is the speed of sound in the fluid is much greater than the particle velocity of the fluid.

2.3.7 Homogeneous flow model for two-phase flow

In order to apply the homogeneous flow model, it is assumed that the two-phase flow is replaced by a special single-phase incompressible fluid in which both phases are well mixed and are travelling at the same velocities ($v_g = v_l = v$) and with a homogeneous density ρ_h and void fraction α_h (Faghri & Zhang, 2006). Figure 2.9 presents a 1-dimensional control volume of a fluid flowing at a steady state in a pipe with the conservation of mass, momentum and energy applied (Dobson, 2015).

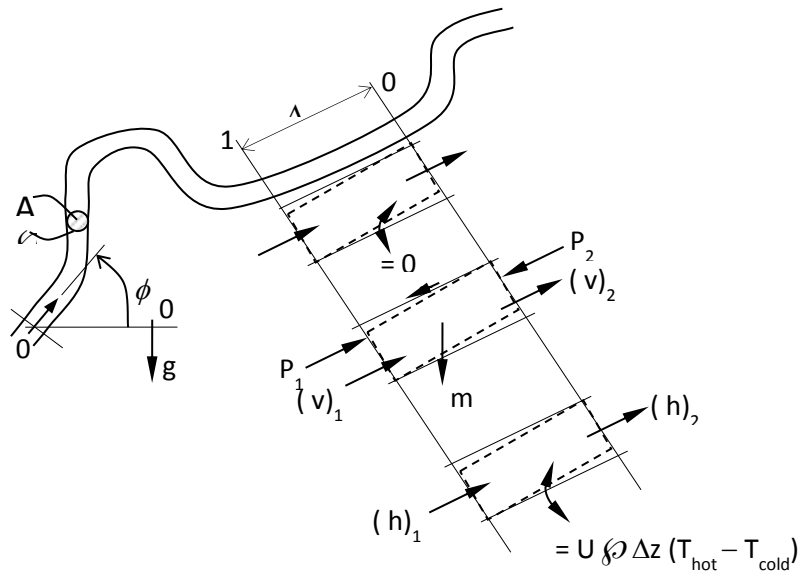


Figure 2-9 One-dimensional control volume for a fluid flowing in a pipe (Dobson, 2015)

The density and void fraction for the homogeneous flow model are given by equation 2.12 and 2.13 respectively (Carey, 1992).

$$\rho_h = \rho_g \alpha_h + \rho_l (1 - \alpha_h) \quad (2.12)$$

$$\alpha_h = \frac{1}{1 + \frac{1-x}{x} \frac{\rho_g v_g}{\rho_l v_l}} \quad (2.13)$$

Note that by substituting for α_h the homogeneous density can also be given as

$$\rho_h = \frac{1}{\frac{x}{\rho_g} + \frac{1-x}{\rho_l}} \quad (2.14)$$

This allows a homogeneous viscosity to be (arbitrarily) defined as in equation 2.6.

All other parameters are determined as shown in Chapter 3 of this thesis.

2.3.8 Separated flow model for two-phase flow

In the separated flow model, gas and liquid flow are considered separately as shown in Figure 2.10 (Dobson, 2015). Applying the conservation of momentum to the gas control volume, the pressure difference can be expressed as being made up of an acceleration, a gravitational and a frictional pressure difference as given in equation 2.15 (Carey, 1992).

$$\Delta P = -\frac{\dot{m}^2}{A^2} \Delta \left[\frac{x^2}{\rho_g \alpha} + \frac{(1-x)^2}{\rho_l (1-\alpha)} \right] - [\alpha \bar{\rho}_g + (1-\alpha) \bar{\rho}_l] \Delta z \sin \phi - \left(C_{f_{lo}} \bar{\rho}_l \frac{u_{lo}^2 \phi_w}{2} \frac{\phi_w}{A} \right) \phi_{lo}^2 \quad (2.15)$$

Where $C_{f_{lo}} = 0.078 \text{Re}^{-0.25}$ and knowing the mass flow rate \dot{m} and the mass fraction x the various terms in equations 2.15 may be determined provided that there is a correlation for the void fraction α and the frictional pressure difference multiplier ϕ_{lo}^2 (Carey, 1992).

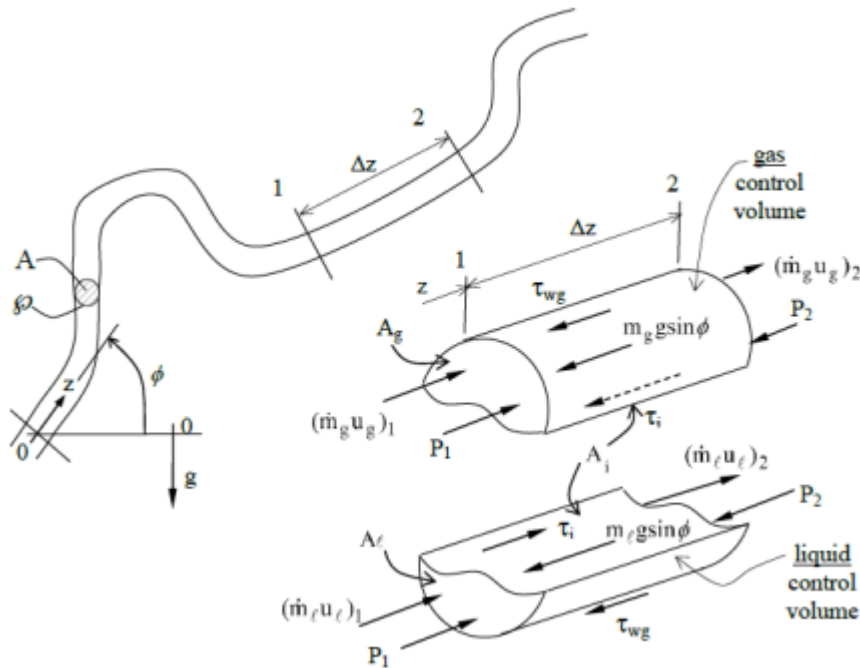


Figure 2-10 One-dimensional separated flow conservation of momentum control volumes for two-phase fluid flow in a pipe (Dobson, 2015)

2.4 Mathematical modelling

Mathematical modelling of the natural circulation loop is an important tool to predict the dynamic of the flow behaviour and heat transfer in both single phase and two-phase flow thermosyphon loops (Yilmaz, 1991; Guo *et al.*, 2015). This is however a matter complicated by the fact that there are instabilities involved in the process and the dependence of heat transfer on the fluid velocity (Nayak *et al.*, 1995; Vijayan *et al.*, 2013; Vijayan & Nayak, 2010). In the case of the two-phase flow, additional mathematical correlations such as the friction factor, the heat transfer coefficient, the void fraction and the two-phase multiplier are used to complete the mathematical model (Stephan & Abdelsalam, 1980; Dobson 2006).

Two methods, namely lumped and sectorial, are considered for numerical simulation. In the lumped method the two-phase region is considered as a single body and a single correlation is used to analyse the forced convective boiling taking place, and the sectorial method divides the two-phase region into smaller regions characterized by definite flow patterns (Lee & Rhi, 2000). This requires more than one correlation related to each flow pattern and is even more complicated for the transition regions between the flow patterns. The lumped method is therefore the easier to program but cannot analyse the flow in as much detail as the sectorial method.

2.4.1 Heat transfer correlations

Prediction of the heat coefficient is still a difficult matter and to-date there exists no comprehensive theory allowing their application in natural convection boiling (Stephan & Abdelsalam, 1980). The issue of simultaneously determining the heat transfer coefficient on the cooling and heating liquid is ranked among inverse heat transfer problems (IHTP) (Beck *et al.*, 1985).

In order to establish correlations with wide application, different approaches were investigated. Stephan & Abdelsalam (1980) proposed a method of regression for natural convection boiling heat transfer. They found that one equation may valid for multiple purposes, but the accuracy would be less than if used individual correlations.

Kew and Cornwell (1997) related their work to boiling small-diameter tubes as part of a study of compact two-phase heat exchangers. They showed that correlations for heat transfer coefficients predict reasonably well for large than small tubes.

Chen *et al.* (1987) developed a correlation for annular flow condensation in vertical tubes based on analytical and theoretical results from the literature. This correlation uses the Nusselt number and takes the form of equation 2.16:

$$Nu_x = \left[\left(0.31 * Re_x^{-1.32} + \frac{Re_x^{2.4} Pr_l^{3.9}}{2.37 \times 10^{14}} \right)^{1/3} \right]^{1/2} + \frac{A_D Pr_l^{1.3}}{771.6} (Re_r - Re_x)^{1.4} Re_x^{0.4} \quad (2.16)$$

where A_D , Pr_l , Re_x and Re_r represent the heat transfer area, Prandtl number and Reynolds's numbers respectively and can the form of equations 2.17 to 2.20.

$$A_z = \frac{0.252 \mu_l^{1.177} \mu_v^{0.156}}{D^2 g^{2/3} \rho_l^{0.553} \rho_v^{0.78}} \quad (2.17)$$

$$Pr_l = \frac{h v_l^{2/3}}{k_l g^{1/3}} \quad (2.18)$$

$$Re_r = \frac{G(1-x)D}{\mu_l} \quad (2.19)$$

$$Re_x = \frac{GD}{\mu_l} \quad (2.20)$$

The mathematical model generated for the circulation loop of this project uses different correlations for the heat transfer in both the single phase and the two-phase flow modes. For single phase flow the Fanning friction factor is used, while in two-phase mode the Martenelli correlations for friction factor and void fraction are used (see section 3.1).

For single phase natural circulation, free convection takes place and there is slow moving fluid near surfaces, but is rarely significant in turbulent flow. Thus, it is necessary to check and compensate for free convection only in laminar flow problems using the Collier correlation (Collier & Thome, 1994) to calculate the heat transfer coefficient, as given in equation 2.21.

$$Nu_D = 0.17 Re_D^{0.33} Pr^{0.43} \left(\frac{Pr}{Pr_w} \right)^{0.25} Gr^{0.1} \quad Re_D \leq 2000 \quad (2.21)$$

Where Gr is the Grashof number used to assess the impact of natural convection and Pr the Prandtl number calculated by equations 2.22 and 2.23 respectively (Mills & Ganesan, 2009).

$$Gr = \frac{L^3 \rho g \beta \Delta T}{\mu^2} \quad (2.22)$$

where L is the control volume length in the direction of the flow.

$$Pr = \frac{c_p \mu_l}{k_l} \quad (2.23)$$

For single phase forced flow turbulent convection the Gnielinski correlation heat transfer coefficient is used as given by equation 2.24 (Mills & Ganesan, 2009).

$$Nu_D = \frac{(f/8)(Re_D - 1000)Pr}{1 + 12.7(f/8)^{1/2}(Pr^{2/3} - 1)}; \quad 3000 < Re_D < 10^6 \quad (2.24)$$

In order to take into account the effects of natural convection present in natural circulation, a Rayleigh number correction factor is introduced (Yang *et al.*, 2006).

$$Nu_D = Nu_D Ra^{-0.011} \quad (2.25)$$

Other correlations are based on hydrodynamic considerations. The heat transfer during the flow of a particular fluid in pipelines or tubes is determined by the nature of the flow, i.e. laminar, transitional or turbulent. Furthermore, the flow may be fully developed hydrodynamically and thermally or it may be developing in one form or another. Numerous analytical and numerical solutions have been found for the heat transfer coefficient in laminar flow, however in the region of transitional and turbulent flow, correlations based experimental measurements are employed to predict the heat transfer rates (Kroger, 1998).

According to Kays (1955), the mean Nusselt number for hydrodynamically fully developed laminar flow in a round tube at a constant wall temperature is

$$Nu_T = 3.66 + \frac{0.0668 Re Pr d/L}{1 + 0.04(Re Pr d/L)^{0.667}} \quad (2.26)$$

Schlunder (1972) proposes the following correlation for these conditions:

$$Nu_T = (3.66^3 + 4.2 Re Pr d/L)^{0.333} \quad (2.27)$$

When the inlet velocity distribution to the tube is uniform, Kays (1955) recommends the following equation:

$$Nu_T = 3.66 + \frac{0.104 Re Pr d/L}{1 + 0.0016 (Re Pr d/L)^{0.8}} \quad (2.28)$$

Under certain operating conditions the heat flux between the tube wall and the fluid may be constant. When this is the case and the velocity distribution is fully developed, the mean Nusselt number according to Shah (1975) is.

$$Nu_q = 4.364 + 0.0722 Re Pr d/L \quad \text{for } L/(Re Pr d) > 0.03 \quad (2.29)$$

$$Nu_q = 1.953(Re Pr d/L)^{0.333} \quad \text{for } L/(Re Pr d) \leq 0.03 \quad (2.30)$$

3 MATHEMATICAL MODELLING

This section describes the theoretical simulation of the NC loop as schematically represented in Figures 3.1 and 3.2; Figure 3.2 is essentially a schematic drawing showing the discretisation into discrete control volumes representing the arrangement of different parts of the natural circulation nuclear reactor cooling system loop that is given in Chapter 4 and shown in Figure 4.1.

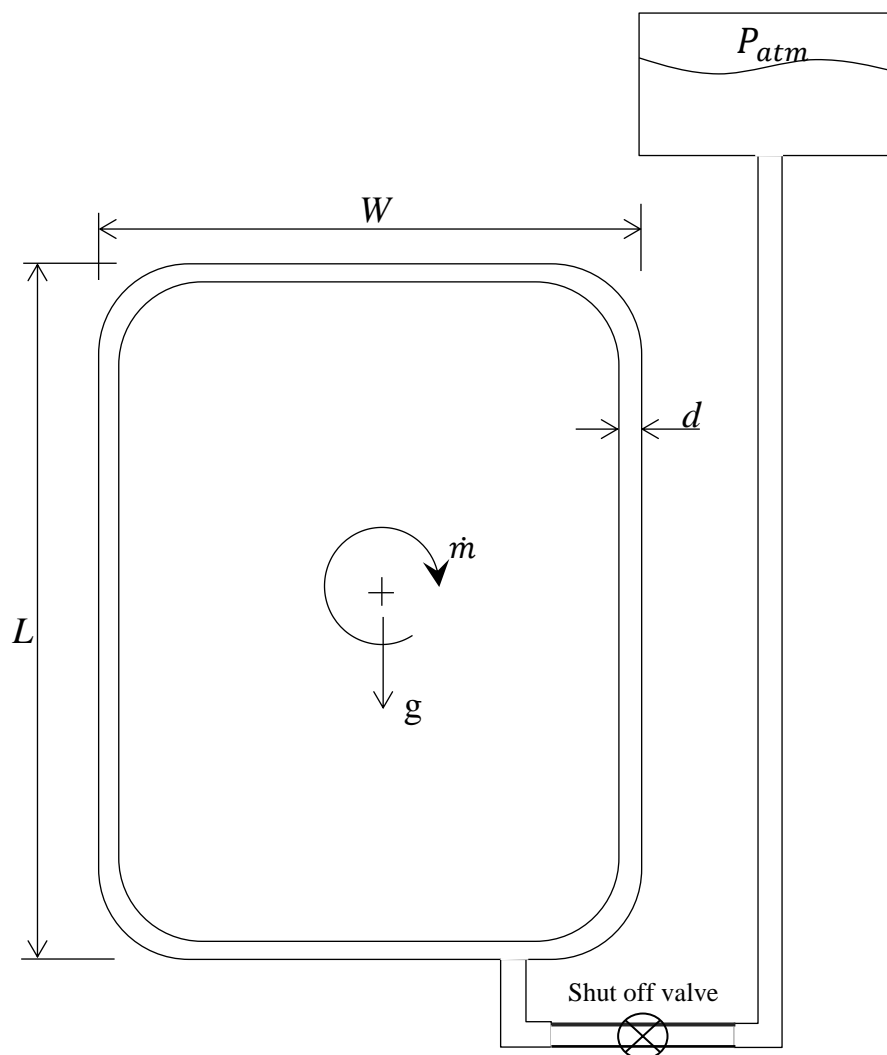


Figure 3-1 Open loop natural circulation thermosyphon

3.1 Simplifying assumptions

In this study several assumptions have to be made to simplify the mathematical model of the thermosyphon loop depicted in Figure 3.1 that can be discretised into a number of cylindrical-shaped control volumes as shown in Figure 3.2. Figure 3.3 shows schematically the application of the conservation of mass, momentum and energy to the i^{th} control volume. The assumptions made are as follow.

- i) The cylindrically-shaped control volumes are one-dimensional; that is at any cross-section area along the axis of the flow $\dot{m} = \int_0^R \rho v 2\pi dr = \rho v A$, where $A = \pi R^2$ (Shih, 2009).
- ii) The mass flow rate is independent of its position in the loop at any instant in time; this implies that at any instant in time that $\frac{\partial \dot{m}}{\partial z} = 0$ but $\frac{\partial \dot{m}}{\partial t} \neq 0$. This condition is often called quasi-static or quasi-equilibrium (Mills & Ganesan, 2009). For this assumption to be valid the fluid particle velocity is much slower than the speed of sound in the fluid; this implies that at any instant in time the fluid, (both the liquid and vapour), is essentially incompressible and that as steam forms in the control volume liquid is displaced instantaneously out of the control volume (White, 2006). This displaced liquid, and its internal energy is then assumed to find itself instantaneous and directly into the upper horizontal pipe of the loop on top of liquid without affecting the energy of the control volumes between the control volume in which it was formed and the upper horizontal pipe (Cengel & Cimbala, 2014).
- iii) At any cross-section both the compressible and incompressible streams are in thermodynamic equilibrium with each other (Cengel & Boles, 2008).
- iv) A so-called *separated two-phase flow model* (Carey, 1992) may be used to represent the properties and behaviour of the control volumes containing both the liquid and steam. Such a two-phase model requires for a control volume that $m = m_v + m_l$, $\dot{m} = \dot{m}_v + \dot{m}_l$, $\dot{m}_v = \rho_v v_v A_v$ and $\dot{m}_l = \rho_l v_l A_l$, a mass fraction $x = \frac{m_v}{m_v + m_l} = \frac{\dot{m}_v}{\dot{m}_v + \dot{m}_l}$, and a density $\rho = \alpha \rho_v + (1 - \alpha) \rho_l$ where the *void fraction* α is defined by $\alpha = \frac{V_v}{V_v + V_l} = \frac{\dot{V}_v}{\dot{V}_v + \dot{V}_l} = \frac{A_v}{A_v + A_l}$. The void fraction may also be expressed as $\alpha = \left(1 + \frac{v_v}{v_l} \frac{1-x}{x} \frac{\rho_v}{\rho_l}\right)^{-1}$. The ratio v_v/v_l is termed *slip factor* and needs to be given as an experimentally correlated expression. One such correlation (Chisholm, 1983) for the void fraction for a two-phase water system is given by the Lockart-Martinelli correlation as $\alpha = (1 + 0.28X)^{-1}$ where X , the so-called Martinelli parameter, is given as $X = 1 + \left(\frac{\rho_v}{\rho_l}\right)^{0.5} \left(\frac{\mu_l}{\mu_v}\right)^{0.5} \left(\frac{1-x}{x}\right)^{0.875}$. Further, an experimentally determined correlation for a so-called frictional multiplier ϕ is needed (Thome, 2011). One such correlation, the *Lockart-Martinelli liquid only two-phase frictional multiplier* is given as

$\phi_{lo}^2 = \left(1 + \frac{20}{x} + \frac{1}{x^2}\right) (1 - x)^{1.75}$ and in this case it implies that there is a *liquid only* velocity defined as $v_{lo} = \frac{\dot{m}_v + \dot{m}_l}{\rho_l(A_v + A_l)}$ and with a *liquid only* Reynolds number given as $Re_{lo} = \rho_l \left(\frac{\dot{m}_v + \dot{m}_l}{\rho_l(A_v + A_l)}\right) d_h / \mu_l = \dot{m}'' d_h / \mu_l$ where $d_h = 4A / \wp \Delta z$, \wp being the wetted perimeter and $\dot{m}'' = \dot{m} / A$ is the mass flux (Carey, 1992). These definitions allow the shear stress to be expressed in terms of a *liquid-only shear stress* τ_{lo} and a *two-phase liquid-only frictional multiplier* ϕ_{lo}^2 as $\tau = \tau_{lo} \phi_{lo}^2$ where $\tau_{lo} = C_{f_{lo}} \frac{\dot{m}^2}{2\rho_l A^2}$ (Chisholm, 1967; Zhang *et al.*, 2010). Assuming a Blasius-type *liquid-only* coefficient of friction (for a smooth tube) as $C_{f_{lo}} = 0.079 Re_{lo}^{-0.25}$ for turbulent flow and $C_{f_{lo}} = 16 / Re_{lo}$ for laminar flow, and to ensure non-division, by zero if $Re_{lo} < 1$ as, say $C_{f_{lo}} = 16$ (Cengel & Cimbala, 2014). Note that taking the Reynolds number as 1181 for the transition from turbulent to laminar flow, and visa versa, ensures that the coefficient of friction $C_{f_{lo}}$ is a continuous of Re_{lo} , if deemed appropriate (Kerswell, 2005). Maybe one would want to build in some “extra complexity” into the simulation model by introducing some sort of hysteresis, assuming for example, that laminar flow becomes turbulent at $Re = 2300$ and that turbulent flow changes to laminar flow at $Re = 1800$ (William *et al.*, 2005).

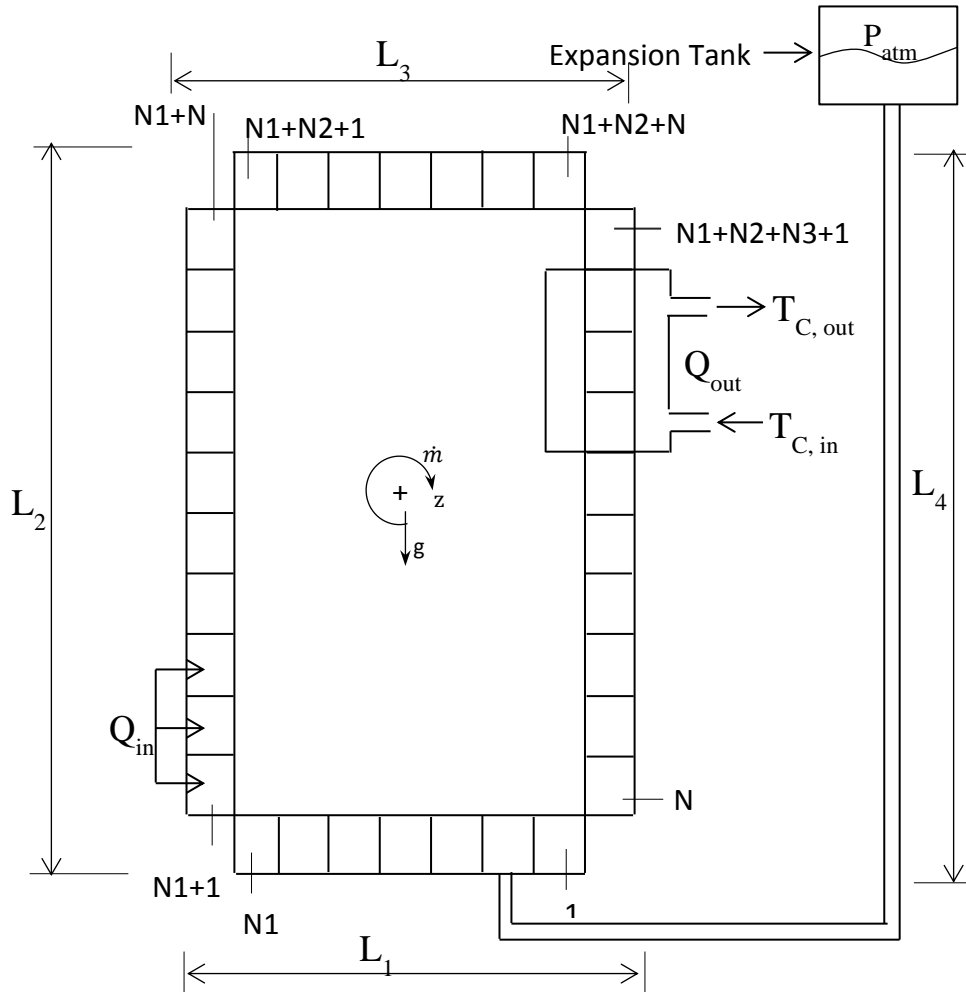


Figure 3-2 Discretisation schematic of the natural circulation theoretical thermosyphon loop

3.2 Conservation equations

This section deals with the equation of change obtained by applying the general statements of the conservation of mass, momentum and energy to each control volume of the discretised system, in order to develop differential equations for theoretical algorithm computer simulation.

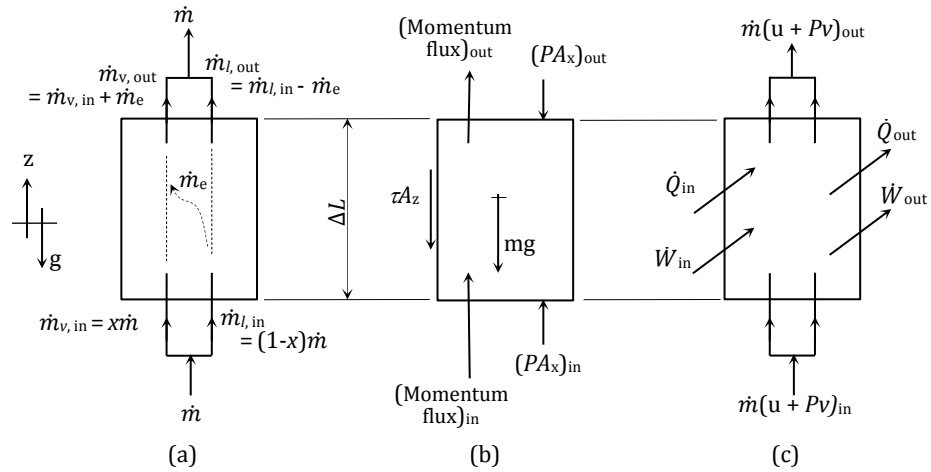


Figure 3-3 Conservation of (a) mass, (b) momentum and (c) energy as applied to a representative control volume (Dobson, 2015)

3.2.1 Conservation of mass

In order to know how much mass is transferred to or from the expansion tank, the conservation of mass is applied to the control volume given in figure 3.2(a)

$$\frac{\Delta m}{\Delta t} = \dot{m}_{in} - \dot{m}_{out} \quad [kg/s] \quad (3.1)$$

Equation 3.1 can also be represented in an explicit form as

$$m_i^{t+\Delta t} = m_i^t + \Delta t(\dot{m}_{in} - \dot{m}_{out})_i^t \quad (3.2)$$

where

$$m = \rho A_x \Delta z \quad (3.3)$$

And

$$\dot{m} = \rho v A_x = \rho G \quad (3.4)$$

Since $v = G/A_x$ and $A_x = \pi d^2/4$

For the control volume (i) the density is determined knowing the volume of the control volume.

$$\rho_i^{t+\Delta t} = m_i^{t+\Delta t}/V_i \quad (3.5)$$

Equation 3.2 introduces the new mixture mass, therefore the new phase masses will be given function of the mass fraction x , and the new volume function of the void fraction α as follow (Whalley, 1987).

$$m_v = xm \quad (3.6)$$

$$m_l = (1 - x)m \quad (3.7)$$

$$V_v = \alpha V \quad (3.8)$$

$$V_l = (1 - \alpha)V \quad (3.9)$$

For a two-phase control volume and in terms of the mass fraction x and void fraction α , by

$$\dot{m} = \dot{m}_v + \dot{m}_l = x\dot{m} + (1 - x)\dot{m} \quad (3.10)$$

$$V = V_v + V_l = \alpha V + (1 - \alpha)V \quad (3.11)$$

$$\rho = \rho_v + \rho_l = \alpha\rho + (1 - \alpha)\rho \quad (3.12)$$

3.2.2 Conservation of energy

Applying the conservation of energy, in terms of the so-called *thermal energy* equation, as formally derived from the more commonly used *total energy* equation (Appendix B), to the control volume in Figure 3.2(c) to get equation 3.13.

$$\frac{\Delta}{\Delta t}(\dot{m}u) = (\dot{m}u)_{in} - (\dot{m}u)_{out} + \dot{Q}_{in} - \dot{Q}_{out} + (PAv)_{in} - (PAv)_{out} - \tau_w A_z v [W] \quad (3.13)$$

Equation 3.13 can be written explicitly as

$$u_i^{t+\Delta t} = [(\dot{m}u)_i^t + \Delta t \sum \dot{E}_i^t] / m_i^{t+\Delta t} \quad (3.14)$$

where

$$\sum \dot{E}_i^t = \left[(\dot{m}u)_{in} - (\dot{m}u)_{out} + \dot{Q}_{in} - \dot{Q}_{out} + (PAv)_{in} - (PAv)_{out} - \tau_w A_z v \right]_i^t \quad (3.15)$$

All thermodynamic properties will then be a represented function of internal energy $u_i^{t+\Delta t}$ and the density $\rho_i^{t+\Delta t}$; $f(u_i^{t+\Delta t}, \rho_i^{t+\Delta t})$.

For the solution algorithm computer program given in Appendix C, the following are used in the selected procedure.

$$m_i^{t+\Delta t} = m_i^t + \Delta t \left(\frac{\Delta m}{\Delta t} \right)_i^{t-\Delta t/2} \quad (3.16)$$

where

$$m_i^{t+\Delta t} = \left(\frac{\Delta m}{\Delta t} \right)_i^{t-\Delta t/2} = \frac{m_i^t - m_i^{t-1}}{\Delta t}$$

And

$$P_i^{t+\Delta t} = P_i^t + \Delta t \left(\frac{\Delta P}{\Delta t} \right)_i^{t-\Delta t/2} \quad (3.17)$$

where

$$\left(\frac{\Delta P}{\Delta t} \right)_i^{t-\Delta t/2} = \frac{P_i^t - P_i^{t-1}}{\Delta t}$$

Having now determined $u_i^{t+\Delta t}$ using equation 3.14 with $m_i^{t+\Delta t}$ as given by equation 3.16 then the remaining thermodynamic properties may be determined as function of $u_i^{t+\Delta t}$ and $P_i^{t+\Delta t}$, that is $T_i^{t+\Delta t} = f(u_i^{t+\Delta t}, P_i^{t+\Delta t})$ and $\rho_i^{t+\Delta t} = f(u_i^{t+\Delta t}, P_i^{t+\Delta t})$, for a so-called sub-cooled or superheated single phase control

volume (see Figure 3.4). Using equations 3.14 and 3.16, the mass fraction for a two-phase liquid-vapour control volume is given as

$$x_i^{t+\Delta t} = (u_i^{t+\Delta t} - u_{f,i}^{t+\Delta t}) / (u_{g,i}^{t+\Delta t} - u_{f,i}^{t+\Delta t}) \quad (3.18)$$

where

$u_{f,i}^{t+\Delta t} = f(P_{sat,i}^{t+\Delta t})$ and $u_{g,i}^{t+\Delta t} = f(P_{sat,i}^{t+\Delta t})$, and the volume or void fraction $\alpha = V_l/V_v$ is given by

$$\alpha_i^{t+\Delta t} = \left(1 + SF \frac{\rho_{g,i}^{t+\Delta t} (1-x_i^{t+\Delta t})}{\rho_{f,i}^{t+\Delta t} x_i^{t+\Delta t}}\right)^{-1} \quad (3.19)$$

Where SF is the so-called slip factor, being the ratio of the vapour to liquid velocities v_v/v_l and given by an experimentally determined correlation in terms of the vapour and liquid densities and dynamic viscosities and the mass fraction and surface tension (Premoli *et al*, 1970; Mills & Ganesan 2009). Another correlation of the void fraction is given in terms of the so-called Martinelli parameter X (Carey, 1992), as

$$\alpha = (1 + 0.28X^{0.71})^{-1} \quad (3.20)$$

where

$$X = \left(\frac{\rho_v}{\rho_l}\right)^{0.5} \left(\frac{\mu_l}{\mu_v}\right)^{0.5} \left(\frac{1-x}{x}\right)^{0.875} \quad (3.21)$$

Having now the mass and void fractions x and α the density and temperature at $t + \Delta t$, the remaining thermodynamic properties are then necessarily given by

$$\rho_i^{t+\Delta t} = \alpha_i^{t+\Delta t} \rho_{g,i}^{t+\Delta t} + (1 - \alpha_i^{t+\Delta t}) \rho_{f,i}^{t+\Delta t} \quad (3.22)$$

and

$$T_i^{t+\Delta t} = f(P_{sat,i}^{t+\Delta t}) \quad (3.23)$$

Equation (3.13) contains even though neglected, the axial conduction in the fluid as an additional heat transfer rate terms and is given by (Mills et al, 2009)

$$\dot{Q}_{cond,in} = (T_{i-1} - T_i) / \left[(\Delta z_{i-1} + \Delta z_i) / 2kA \right] \quad (3.24)$$

and

$$\dot{Q}_{cond,out} = (T_i - T_{i+1}) / \left[(\Delta z_i + \Delta z_{i+1}) / 2kA \right] \quad (3.25)$$

where A is the smaller of A_{i-1} and A_i or A_i and A_{i+1} , respectively.

The term $[(PAv)_{in} - (PAv)_{out}]$ is the reversible rate of work done on the fluid and is positive if the fluid in the control volume is being compressed and negative if the fluid in the control volume is expanding. The term $[-\tau_w A_z v]$ is the work done against friction. It is irreversible and thus necessarily always positive and thus always manifests itself as an increase in the temperature of the fluid.

bends, outlets or expansions, etc. Typical values for these losses, for an inlet, outlet and elbow may be taken as $18d$, $30d$ and $52d$, respectively (Batty & Folkman, 1983). The average velocity, to keep it simple, may be taken as $v = \frac{\dot{m}}{((A\rho)_{in}+(A\rho)_{out})/2}$ where $\rho = \alpha\rho_v + (1 - \alpha)\rho_l$. The term ϕ_{lo}^2 is experimentally-established and is termed the *liquid only multiplier* (Thome, 2011). The friction coefficient C_{flo} is, conveniently, given by $C_{flo} = 0.079Re_{lo}^{-0.25}$ for turbulent flow and $C_{flo} = 16/Re$ for laminar flow (Kerswell, 2005). Note that if the simulation of the fluid movement is started from standstill the Reynolds number is infinitely large and hence so too is the friction coefficient and there will be no flow (Tsukahara *et al.*, 2014). The so-called slip-stick theory describing this phenomenon is complex but for the sake of simplicity may be arbitrarily determined by assuming for instance that if $Re < 1$ then, say, $C_{flo} = 16$ (Cengel & Cimbala, 2014). Further, the transition flow (between laminar and turbulent) may be taken as $Re = 1181$; at this Reynolds number the laminar and turbulent coefficients of friction as given by the two equal preceding equations for coefficient of friction are equal to each other (William *et al.*, 2005). Another facet of this transition as is that there is definite degree of hysteresis associated with transition (Mills & Ganesan, 2009). Texts normally quote that the transition takes place when the Reynolds number is between 1800 and 2300 (Cengel & Cimbala, 2014). However, if the flow is laminar then as the velocity increases there is a rather sudden transition to turbulent flow at a Reynolds number closer to the upper limit (Cengel & Cimbala, 2014; Mills & Ganesan, 2009).. However, if the flow is turbulent and the velocity is decreased a similarly-sudden transition to laminar flow occurs but at a Reynolds number closer to the lower of the two limits (Mills & Ganesan, 2009; William *et al.*, 2005).

In the homogeneous two-phase flow, the frictional multiplier as given in equation 3.29 is used to estimate the pressure drop.

$$\phi_{lo}^2 = \frac{C_{fh} \rho_l}{C_{flo} \rho_v} \quad (3.29)$$

Assuming that $C_{fh} = C_{flo}$, the multiplier equation becomes (Whalley, 1990)

$$\phi_{lo}^2 \approx \rho_l / \rho_v \quad (3.30)$$

Considering the Martinelli-Nelson correlation for water (Brennen, 2005)

$$\phi_{lo}^2 = (1 - x)^{1.75} \phi_l^2 \quad (3.31)$$

Where ϕ_l^2 refers the Lockhart-Martinelli correlation for two-phase multiplier for liquid phase friction and is given by (Carey, 1992)

$$\phi_l^2 = \left(1 + \frac{20}{X} + \frac{1}{X^2}\right)^{0.5} \quad (3.32)$$

where X is the Martinelli parameter and given by equation 3.21

3.2.3 Conservation of momentum

Apply the conservation of momentum to the control volume depicted in Figure 3.2(b) to get

$$\frac{\Delta}{\Delta t} (mv) = (\dot{m}v)_{in} - (\dot{m}v)_{out} + (PA)_{in} - (PA)_{out} - m_i g \sin \theta - \tau A_z \quad (3.33)$$

For a single phase flow model; or using $v = \dot{m}/\rho A$ and dividing throughout by the cross sectional area A, as

$$\frac{\Delta}{\Delta t} \left(\frac{m\dot{m}}{A\rho} \right) = \left(\frac{\dot{m}^2}{A\rho} \right)_{in,i} - (\dot{m}v)_{out,i} + (PA)_{in,i} - (PA)_{out,i} - m_i g \sin \theta_i - \tau A_z \quad (3.34)$$

For a separated two-phase flow model, after dividing throughout by the cross sectional area A of the control volume and making use of the identities of equations 3.4 and 3.12, the momentum equation may be expressed in terms of the mass, mass flow rate, void fraction and mass fraction as

$$\frac{\Delta}{\Delta t} \left[\frac{m\dot{m}}{A^2} \left(\frac{x^2}{\alpha\rho_v} + \frac{(1-x)^2}{(1-\alpha)\rho_l} \right) \right]_i = \frac{\dot{m}^2}{A_i} \left[\left(\frac{x^2}{\alpha\rho_v} + \frac{(1-x)^2}{(1-\alpha)\rho_l} \right)_{in} - \left(\frac{x^2}{\alpha\rho_v} + \frac{(1-x)^2}{(1-\alpha)\rho_l} \right)_{out} \right] + P_{in,i} - P_{out,i} - [(\alpha\rho_v + (1-\alpha)\rho_l)g \sin \theta \Delta z]_i - \left[\frac{\tau_{lo}\phi_{lo}^2 A_z}{A} \right]_i \quad (3.35)$$

where $m = (\alpha\rho_v + (1-\alpha)\rho_l)A\Delta z$

In accordance with the concept of upwind differencing for the momentum flux term (the first term on the right hand side of equation 3.35 $in = i - 1$ if $\dot{m} \geq 0$ and $in = i + 1$ if $\dot{m} < 0$ and “out” always equals “in”, irrespective of the flow direction.

The mass flow rate of the fluid in and around the loop, at any instance in time, is then given by summing all the control volumes around the loop from 1 to N_{tot} and noting that the pressure terms all cancel out.

$$\frac{\Delta}{\Delta t} (\dot{m}M) = \dot{m}^2 MF - G - F \quad (3.36)$$

Equation 3.36 is also explicitly given by

$$\dot{m}^{t+\Delta t} = [\dot{m}^t M^t + \Delta t (\dot{m}^2 MF - G - F)^t] / M^{t+\Delta t} \quad (3.37)$$

where

$$M_i^t = \sum_{i=1}^{N_{tot}} \left[m_i^t / A_i^2 \left(\left(\frac{x^2}{\alpha\rho_v} \right)_i^t + \left(\frac{(1-x)^2}{(1-\alpha)\rho_l} \right)_i^t \right) \right] \quad (3.38)$$

$$M_i^{t+\Delta t} = \sum_{i=1}^{N_{tot}} \left[m_i^{t+\Delta t} / A_i^2 \left(\left(\frac{x^2}{\alpha\rho_v} \right)_i^{t+\Delta t} + \left(\frac{(1-x)^2}{(1-\alpha)\rho_l} \right)_i^{t+\Delta t} \right) \right] \quad (3.39)$$

$$MF = \sum_{i=1}^{N_{tot}} \left[\frac{1}{A_i} \left(\left(\frac{x^2}{\alpha A \rho_v} + \frac{(1-x)^2}{(1-\alpha) A \rho_l} \right)_{in} - \left(\frac{x^2}{\alpha A \rho_v} + \frac{(1-x)^2}{(1-\alpha) A \rho_l} \right)_{out} \right) \right]_i \quad (3.40)$$

$$G = \sum_{i=1}^{N_{tot}} [(\alpha \rho_v + (1-\alpha) \rho_l) g \sin \theta \Delta Z]_i \quad (3.41)$$

and

$$F = \sum_{i=1}^{N_{tot}} [\tau_{lo} \phi_{lo}^2 \wp (\Delta Z + \Delta Z_{minor}) / A]_i \quad (3.42)$$

where ΔZ_{minor} is the equivalent length of pipe of the same diameter and represents the minor losses or the irreversible work done on the fluid, as a result of there being inlets or contractions, bends, outlets or expansions etc.

Having now determined the mass flow rate at any instant in time $t + \Delta t$, the control volume pressure may now be determined at the so-to-say new-time $t + \Delta t$ using equation 3.33 and re-arranged as

$$\begin{aligned} P_{out,i} = P_{in,i} + \frac{\dot{m}^2}{A_i} \left[\left(\frac{x^2}{\alpha A \rho_v} + \frac{(1-x)^2}{(1-\alpha) A \rho_l} \right)_{in,i} - \left(\frac{x^2}{\alpha A \rho_v} + \frac{(1-x)^2}{(1-\alpha) A \rho_l} \right)_{out,i} \right] \\ - [(\alpha \rho_v + (1-\alpha) \rho_l) g \sin \theta \Delta Z]_i - \left[\frac{\tau_{lo} \phi_{lo}^2 \wp (\Delta Z + \Delta Z_{minor})}{A} \right]_i \\ - \frac{\Delta}{\Delta t} \left[\frac{m \dot{m}}{A^2} \left(\frac{x^2}{\alpha \rho_v} + \frac{(1-x)^2}{(1-\alpha) \rho_l} \right) \right]_i^{t-\Delta t/2} \end{aligned} \quad (3.43)$$

3.3 Numerical simulation model

An explicit numerical solution method is used to solve the set of time dependent temperature coupled partial differential equations constituting the theoretical simulation model of the thermosyphon loop of the project. Figure 3.2 shows a discretised model into a series of control volumes of the natural circulation loop and Figure 3.3 gives the applicable i^{th} control volume after applying the conservation equations described in section 3.2 and the assumptions stipulated in section 3.1. The solution algorithm in step-wise is shown in the flow chart in Figure 3.5 is detailed in Appendix C. The explicit scheme solution is used so that each equation has one unknown which is the function of calculated variables at the previous time step. Each equation is solved consecutively rather than simultaneously, as in the implicit scheme. However, this method has limitations on some parameters, such as the control volume length and the time step size in order to avoid numerical instability. For instance, the control volume and time step are set so that a particle traveling through the circulation loop does not travel through more than one control volume at any given time step.

The initial conditions were set to correspond to the system in thermal equilibrium with the surroundings. As such the initial mass flow rate was taken as 0 g/s as there were no temperature difference induced density gradient. The expansion

tank was exposed to the atmospheric pressure which for Stellenbosch is approximately 98 kPa.

3.4 Property functions

The property functions as used in the computer algorithm given in Appendix C and in the computer algorithm flow chart in Figure 3.5 are given in Appendix A. These properties are classified into three regions; the subcooled liquid region, the two-phase region and the superheated region. The property functions with respect to each region are as follow.

Subcooled liquid region, that is $x \leq 0$ and $\alpha \leq 0$ where x is defined as $x = \frac{u-u_f}{u_g-u_f}$ and α is given by $\alpha = \frac{A_v}{A_v+A_l}$

$$u = f(T), T = f(u, P), \rho = f(u, P)$$

Two-phase region, that is $0 < x < 1$ and $0 < \alpha < 1$

$$u_f = f(P), u_g = f(P), T_{sat} = f(P), \rho_f = f(P), \rho_g = f(P)$$

Superheated region, that is $x \geq 1$ and $\alpha \geq 1$

$$T = f(u, P), \rho = f(u, P)$$

Sundry property functions

$$\sigma = f(T), \mu = f(T)$$

3.5 Solution procedure

The solution procedure is given by a computer program written using QBasic 64 and results were imported to Microsoft Excel to draw the graphs.

The solution procedure proceeds is as follows:

1. Define the geometry that is the physical dimensions of the loop and the number and length of the control volumes.
2. Define constant and material properties.
3. Define the problem-specific constants and stability criteria.
4. Apply initial conditions of all thermo-physic parameters used. These include temperature, volume, density, pressure, mass, mass flow rate, mass fraction, void fraction and heat flow to each control volume.
5. Estimate the new mass and new pressure using equations 3.16 and 3.17.

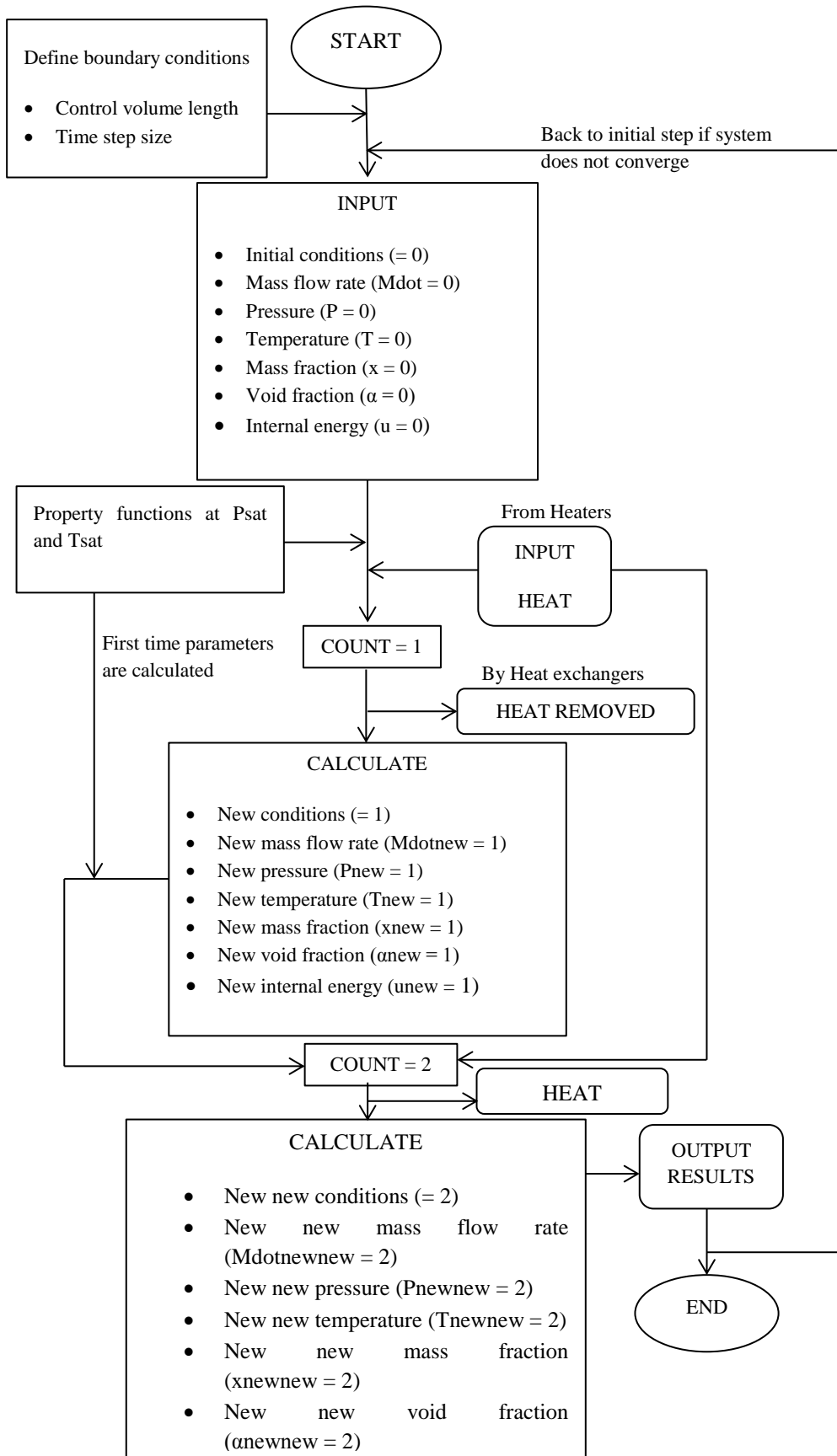


Figure 3-5 Computer algorithm flow

6. Calculate the total heat which is evaluated by combining the heat losses to the environment, the heat removed by heat exchanger, the change in internal energy through convection, the reversible and irreversible work and the internal energy.
7. Estimate the new mass flow rate using equation 3.10.
8. Compute the new temperature for each control volume using equation 3.22.
9. Calculate the new density, new mass fraction and new void fraction for the mixture using the new temperature.
10. Estimate the new internal energy with equation 3.18.
11. Compute the two-phase multiplier using defined correlations.
12. Evaluate the new heat loss through each control volume of the condenser.
13. Calculate the heat transfer rate per control volume.
14. Calculate all the variables of the momentum equation given in equation 3.35. These terms include the sum of momentum terms, the sum of momentum flux terms and the sum of friction terms.
15. Calculate the pressure drop and use it to find the new pressures for the control volumes, the interface pressure and the new tank pressure.
16. Calculate the saturation temperature given as function of new pressure.
17. Use the mass conservation equation to compute the amount of mass transferred to or from the expansion tank.
18. Calculate the sum of heat added or removed to or from the loop.
19. Record the output data to text file.
20. Steps 4 to 19 are repeated until final result is obtained.

4 EXPERIMENTAL SETUP

This chapter presents the re-commissioning of the Sittmann's (2010) experimental loop and the re-instrumentation of the loop. It also includes the experimental procedures and operating instructions.

4.1 Thermosyphon loop characteristics

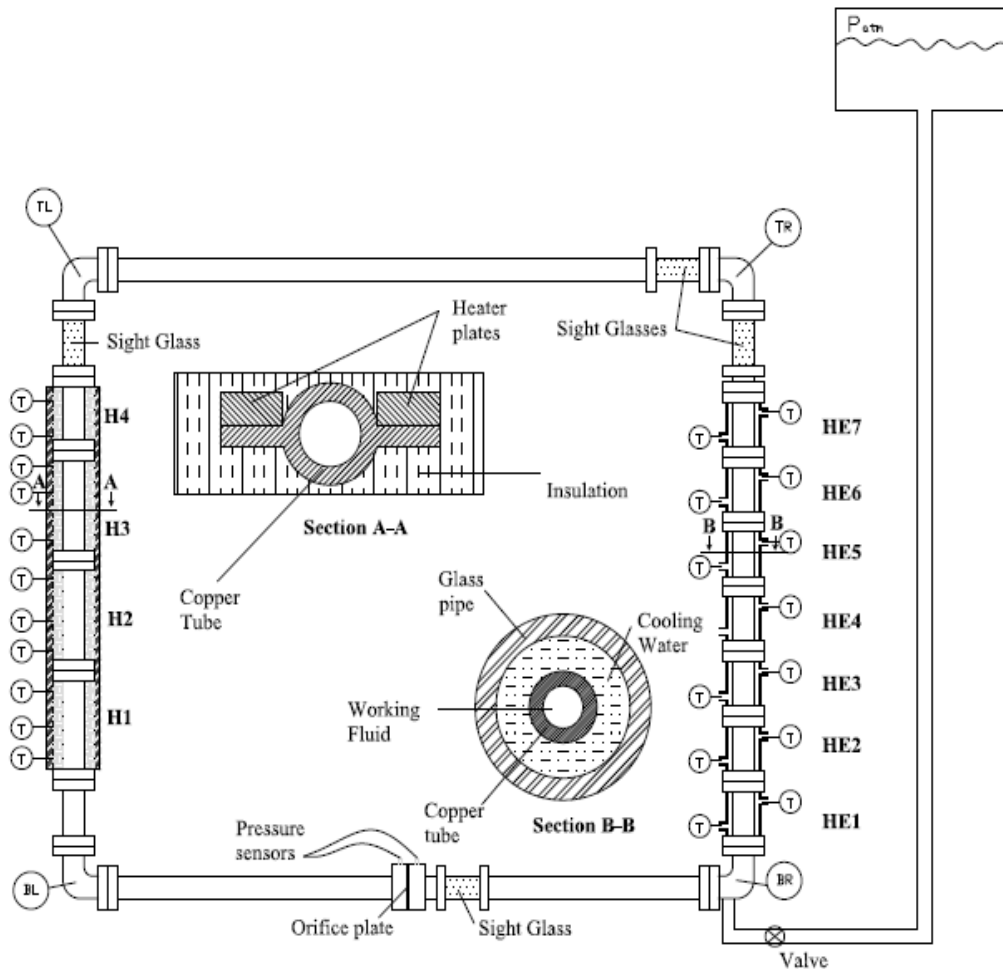


Figure 4-1 Experimental thermosyphon loop diagrammatic representation

Figure 4.1 shows the diagrammatic representation of the RCCS thermosyphon loop designed and constructed by Sittmann (2010) from 35 mm OD, 32 mm ID copper tubes and is 8 m wide and 7 m height. Copper is used due to its high thermal conductivity thereby making its thermal resistance very small compared with the inside and outside heat transfer coefficient and can therefore be

neglected. Four transparent polycarbonate sight glasses are incorporated in the loop positioned as shown in Figure 4.1 for viewing the working fluid (water) flow in the loop. To establish natural circulation one vertical leg of the loop is heated using four installed heating plate elements (H1, H2, H3 and H4) and the other leg is cooled with the cooling water passing through one or all of the seven pipe-in-pipe heat exchangers (HE1, HE2, HE3, HE4, HE5, HE6 and HE7). The loop is connected to an expansion tank located 12 m height above the horizontal pipe at the bottom of the loop and is located on the roof of the building.

4.2 Experimental setup

The experimental setup (as shown in Figures 4.1 and 4.2) was used to measure temperatures of heating plates, cooling water and working fluid, and mass flow rate of both the working fluid and cooling water in order to validate with the theoretically calculated values. This section will give details about the experimental setup and procedures followed to obtain results.

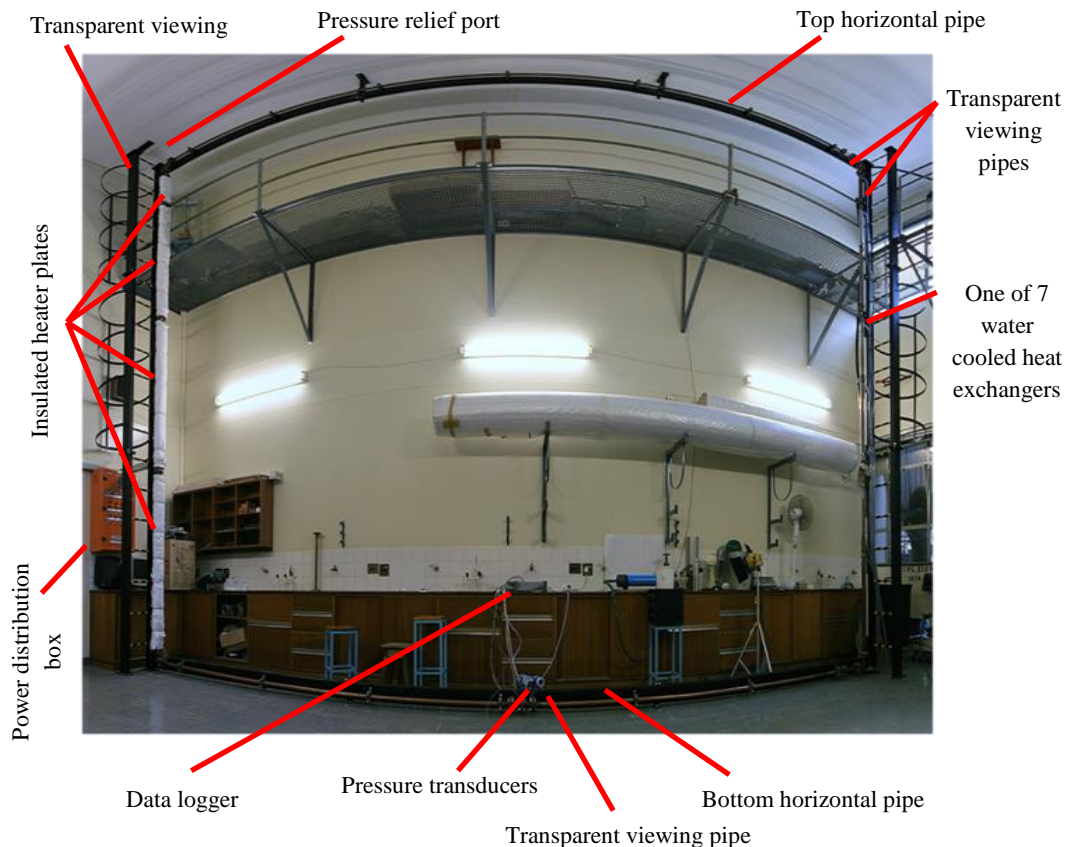


Figure 4-2 Experimental setup in laboratory (Sittmann, 2010)

4.3 Loop re-commissioning and instrumentation

The loop not having been used these past eight years needed to be re-commissioned. New instruments were installed including two different differential pressure transducers in order to better evaluate the mass flow rate, as well as one static pressure transducer. Damaged thermocouples were replaced and all the thermocouples were recalibrated.

Before starting the loop was emptied and refilled five times in order to clean the inside and to check for leaks. Two K-type thermocouples were found on the two top corners (TL and TR) of the loop. Two other K-type thermocouples were then installed in the two bottom corners (BL and BR). These four thermocouples used to measure the working fluid's temperature and eight more of the same type (K-type) used to measure the cooling water's temperatures were calibrated against a calibrated (Rapid Instrumentation cc certificate number RAP38810, 26 April 2017) Platinum Resistance Thermometer (PRT), as shown in appendix D. Eleven high temperature clad K-type thermocouples used to measure the temperature of the heating plate elements were also calibrated.

The mass flow rate was measured using an orifice plate and two calibrated differential pressure transducers (see Appendix D); a Hottinger Baldwin Messtechnik type PD1 (HBM-PD1) No 12068 with a full scale differential pressure of 0.1 bar and an allowable nominal operating pressure of 50 bars, and a Deltabar M Endress & Hauser (E&H) IP66/IP67 PMD75 model pressure transducer No S/N A806930109D and the pressure in the loop was measured using a calibrated Deltabar E&H IP66/IP67 PMC7 model static pressure transducer No S/N A808780109C. The pressure transducers were calibrated using a van Essen BETZ type 5000 having a measuring range of -10 to 5000 Pa (gauge pressure) and an accuracy of ± 0.2 Pa.

The thermocouples were directly connected to a 34970A Agilent data acquisition, serial number MY44045582 while the pressure transducers for the mass flow rate and pressure measuring were connected to the same data logger, but through the 24V/1A DC amplifiers. The data logger had two cards of 20 channels each and S/N 34901A and S/N 34901B. Thermocouples were arranged in the channels of the cards for the entire period of the experiments. The data logger was set to collect data every 10 ms intervals, but recorded an averaged value every 1.445 s.

4.4 Experimental procedure

The first step was to fill the loop with working fluid from the expansion tank until water escape via the air purge valve on top of the loop. This is very important as if the air is not removed it may influence the mass flow rate or collect as an insulating layer on the condenser walls thereby affecting the convective heat transfer coefficient and consequently also the heat transfer rate. Air in solution

was released by boiling the water, in the loop, a number of times until no more air escaped from the purge valve.

Before each experimental test run air purging was initiated as explained in the previous paragraph and all connections were water tight. The water level in the expansion tank was checked, the room temperature and air pressure were measured, the cooling water turned on and its mass flow rate determined using a measuring cylinder and stopwatch, and the power switched on. (Detailed experimental procedures are given in Appendix E.) The electrical heating element voltage was regulated manually at the power distribution box.

Measurements were taken as function of time at power input level of 30%, 50%, 70% and 100% of the full power of 9.4 kW. A typical test run is shown by way of figure 5.1. Similar tests were done at three to four days intervals, allowing the working fluid to cool down, and attained thermal equilibrium with its surroundings.

5 RESULTS

Results achieved for a number of test-run data sets with the experimental setup given in Chapter 4 are presented in this Chapter. The theoretical results generated by the mathematical model described in Chapter 3 are also given. The theoretical and experimental results are then compared.

5.1 Experimental results

Ten test-runs of at least 4 hours each were completed with averaged data recorded every 1.445 seconds. This delivered a vast number of information (data) to more accurately represent the results. This section shows the experimental results for both the single and two-phase flow modes of the loop.

5.1.1 Single phase operating mode test

Five test-runs named test-run 1, test-run 1a, test-run 1b, test-run 2 and test-run 2a were conducted for the single phase operating mode in which test-run 1a was a repeat of test-run 1 and test-run 2a a repeat of test-run 2. Test-run 1b results are shown in Appendix D. During these tests all four heating elements (H1, H2, H3 and H4) and all seven pipe-in-pipe heat exchangers (HE1, HE2, HE3, HE4, HE5, HE6 and HE7) were operational. These test-runs were operated in single phase mode and up to 100 per cent of the available input power of 9.4 kW was used. Boiling did not occur as all the cooling water heat exchangers were operated.

Results for the single phase operating mode are presented in this section. Figures 5.1 and 5.2 present the results for test-run 1 and test-run 2 while Figures 5.3 and 5.4 give comparisons between these tests and their repeated tests. In test-run 1 electrical heating power was increased in steps of 30 to 100 per cent of full power as shown in table 5-1. In test-run 2 the full power was used from start-up to shut down and with a cooling water mass flow rate greater than in test-run 1. Repeatability tests are named test-run 1a and test-run 2a representing the repeated test for test-run 1 and test-run 2.

Test-run 1

The experimental results for test-run 1 with the heating plate electrical input powers as a function of time as shown in table 5-1 are reflected in figure 5.1. They show a single phase operating mode with low cooling water mass flow rate per heat exchanger of 0.031 g/s, 0.03 g/s, 0.031 g/s, 0.032 g/s, 0.031 g/s, 0.032 g/s and 0.03 g/s for HE1, HE2, HE3, HE4, HE5, HE6 and HE7 respectively.

Table 5-1 Test-run 1 electrical power input

Power (%)	Time (s)	Heating plate 1 (W)	Heating plate 2 (W)	Heating plate 3 (W)	Heating plate 4 (W)	Total (W)
30	0	439.18	439.18	229.58	114.63	1222.57
50	1210	1148.18	1064.70	1064.70	449.54	3727.12
70	8300	2041.20	2041.20	2022.34	960.26	7065.50
100	11520	2790.80	2704.70	2704.70	1173.06	9373.26
0	14210	0.00	0.00	0.00	0.00	0.00

Figure 5.1(a) shows the heating plate temperatures; while Figure 5.1(b) shows the temperature of the working fluid measured with the thermocouples installed at the four corners of the loop, T_{TL} , T_{TR} , T_{BL} and T_{BR} . Figure 5.1(c) shows the pressure difference $\Delta P = \rho g h_{tank}$ from the water level in the expansion tank to a specific point in the loop and Figure 5.1(d) shows the electrical power input levels. Figures 5.1(e) and 5.1(f) show the working fluid mass flow rate as function of time measured using both the HBM and E&H pressure sensors.

Figure 5.1(b) shows that the four measured temperatures of working fluid stayed almost constant for the first 900 s with a very small average temperature increase of about 0.41°C . This indicates that with 30% of the full electrical power input into the system, there is little effect on the working fluid temperatures; instead the fact that little power is input in the system allows thermal equilibrium in the loop. From 1210 s, the input power was increased to 50 % of full power (i.e. 3.732 kW). The working fluid temperatures then increased sharply with the temperature at the top of the heated (evaporator) section T_{TL} reaching the highest point of 87.4°C at 5400 s. At the top section of the condenser (cooled section) the temperature T_{TR} was slightly less (86.5°C) due to heat loss through natural convection between the copper pipe of the loop and the air inside the laboratory. At this instant the temperature at the bottom loop's corner T_{BL} reached a peak of 72.27°C . Although the cooling water mass flow rate was extremely small per heat exchanger, the temperature difference over the length of the cooled section, given by $\Delta T_c = T_{TR} - T_{BR}$ (i.e. 14.23°C), removed a significant amount of heat from the system ($\dot{Q}_{out} = \dot{m}_{cooling} x c_p x \Delta T_c$), i.e. 12.93 W. After 7634 s all four working fluid measured temperatures decreased for about 600 s and when the power was increased to 70%, they increased slightly with T_{TL} reaching the highest peak of 90.83°C while T_{TL} reached the lowest peak at 76.6°C after 10042 s. When the full power was used, all temperatures increased to their highest peak of 91.72°C , 90.67°C , 78.02°C and 77.2°C respectively for T_{TL} , T_{TR} , T_{BL} , and T_{BR} . At 14210 s the power was switched off and the working fluid was allowed to cool down for 3281 seconds before stopping the test run. Boiling could not occur as the highest peak temperature of the working fluid measured at the top left of the evaporator section (i.e. 91.72°C) was significantly less than the saturation

temperature (i.e. 107 °C) corresponding to the local pressure of 102.3 kPa at ambient conditions.

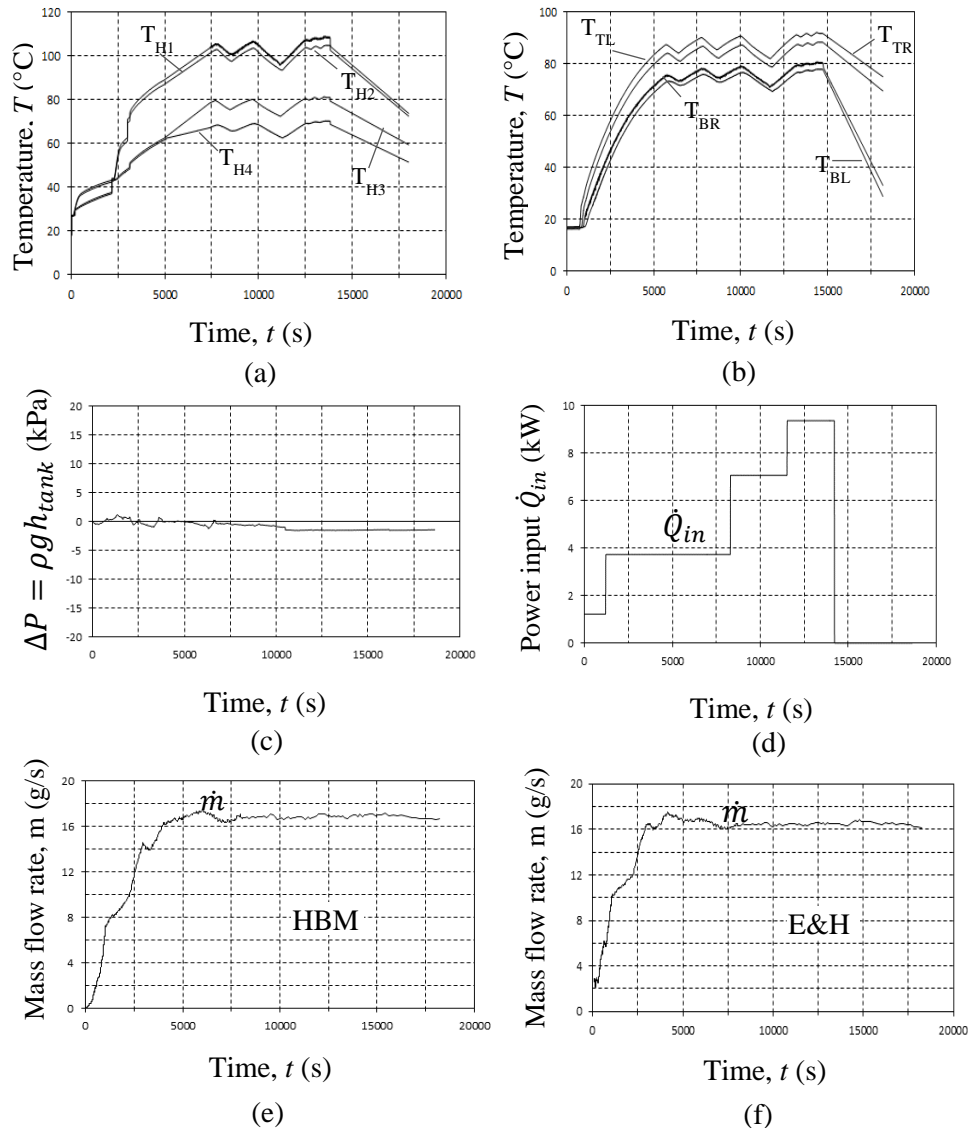


Figure 5-1 Experimental single phase operating mode with power gradually input (a) heating plate temperatures, (b) working fluid temperatures, (c) system pressure difference, (d) electrical power input (e) working fluid mass flow rate measured with HBM pressure sensor and (f) working fluid mass flow rate measured using E&H pressure sensor.

Figure 5.1(c) shows the static pressure difference as a function of time. At the atmospheric pressure of 102.3 kPa (on the day of test-run 1) the pressure at the bottom of the loop ($P = P_{atm} + \rho g h_{tank}$) was at 200.4 kPa.

Figures 5.1(e) and (f) show the working fluid mass flow rate as measured by the pressure drop over the orifice plate with the HBM and E&H pressure sensors respectively. The two sensors gave similar results, thereby adding confidence in the validity of the mass flow rate measurement. The flow rate started from rest where the working fluid was stationary or at 0 (zero) g/s. As more heat was supplied to the system, it increased the driving force between the lighter (heated) and denser (cooled) fluid therefore increasing the mass flow rate after 150 s. As the temperature continued rising, the mass flow rate increased even further to reach a peak of 17.16 g/s for the HBM and 17.56 g/s for the E&H sensors at about 5869 s. After reaching the peak, both mass flow rates showed a slight decrease before they showed a characteristic small amplitude oscillatory behaviour.

Test-run 1a

Table 5-2 Test-run 1a electrical power input

Power (%)	Time (s)	Heating plate 1 (W)	Heating plate 2 (W)	Heating plate 3 (W)	Heating plate 4 (W)	Total (W)
30	0	439.18	439.18	229.60	114.62	1222.58
50	1210	1148.18	1064.68	1064.68	449.55	3727.09
70	8300	2041.19	2041.19	2022.34	960.26	7065.48
100	11520	2790.79	2704.72	2704.72	1173.05	9373.28
0	14210	0.00	0.00	0.00	0.00	0.00

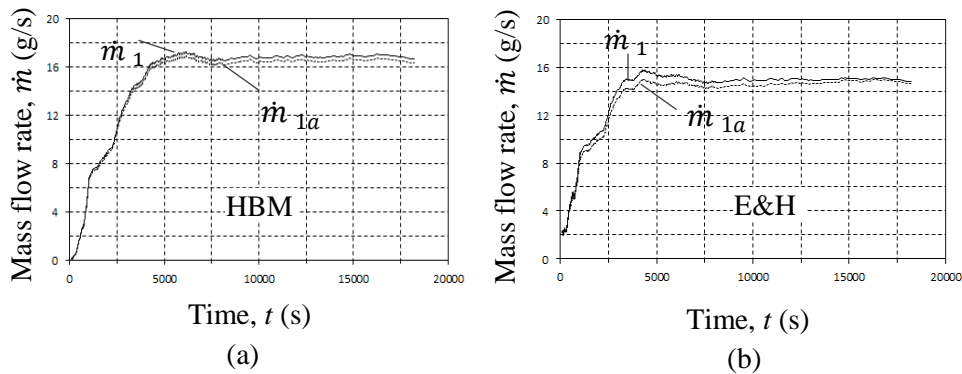


Figure 5-2 Repeated test (single phase) at low cooling water mass flow rate with electrical power gradually input measured with (a) HBM pressure sensor and (b) E&H pressure sensor

Test-run 1a was run four days after test-run 1 with the same water cooling rate and electrical power time steps. Figure 5.2 shows a comparison of the working fluid mass flow rate as a function of time between test-run 1 and test-run 1a with both the HDM and E&H pressure sensors. Their profiles are similar however a small deviation is observed in both readings with the HBM reaching a new peak

of 17.13 g/s and the E&H a peak of 17.50 g/s (at about the same time as test-run 1 or 5869 s) due to the change in power ratings as shown in table 5.2 and the error (random and systematic) that may have occurred during the test. A summary of the error assessment presented in Appendix D is given in Table 5-3. This summary is based on systematic error on the reading of the mass flow rate, pressure and temperature.

Table 5-3 error assessment of the flow parameters

Flow parameter	Error (%)	Actual value
E&H differential pressure	0.2	$P_{actual} = P_{reading} \pm \frac{0.2}{100} P_{reading} \text{mbar}$
E&H static pressure	0.2	$P_{actual} = P_{reading} \pm \frac{0.2}{100} P_{reading} \text{mbar}$
Cooling water temperature	0.35	$T_{actual} = T_{reading} \pm \frac{0.35}{100} T_{reading} \text{ K}$
Heating plate temperature	0.18	$T_{actual} = T_{reading} \pm \frac{0.18}{100} T_{reading} \text{ K}$
Working fluid temperature	0.45	$T_{actual} = T_{reading} \pm \frac{0.45}{100} T_{reading} \text{ K}$

Test-run 2

Test-run 2, as shown in Figure 5.3, is essentially a repetition of test-run 1 (and test-run 1a) but with the full power from start-up to switch off at 14000 s and a relatively higher cooling mass flow rate. Figure 5.3(a) gives the temperatures of the heating plates as a function of time. Figure 5.3(b) presents the working fluid's temperatures measured at the four designated points of the loop. Figure 5.3(c) shows the pressure difference $\Delta P = \rho g h_{tank}$ in the loop.

The working fluid temperatures measured, as in test-run 1 are shown in Figure 5.3(b) where all four temperatures increased slightly from start up. After $t = 1226$ s, T_{TL} and T_{TR} showed a bigger increase than T_{BR} and T_{BL} as more heat was added. At the bottom of the loop, water (cold) coming from the tank mixed with the warm water inside the loop affecting T_{BR} . This also affected T_{BL} as water from the tank at higher pressure than the pressure inside the loop forced his way in, thus increasing difference in temperature ($\Delta T_c = T_{TR} - T_{BR}$). The temperature difference was also greater than in test-run 1 because of a higher cooling water mass flow rate of 0.081 g/s, 0.08 g/s, 0.083 g/s, 0.084 g/s, 0.082 g/s 0.081 g/s and 0.083 g/s for HE1, HE2, HE3, HE4, HE5, HE6 and HE7 respectively. With this

cooling rate more heat was removed from the system than in test-run 1, as it can be seen in the Figure 5.3(b) with the highest peak temperature of 74.61 °C reached for T_{TL} less than in test-run 1.

The pressure difference profile in Figure 5.3(c) is similar to that shown for test run 1 in Figure 5.1(c). It however shows a dynamic or erratic pressure difference profile with more oscillations due to the sudden start up to full power. The driving force (or the difference in hydrostatic pressure between the left hand side and the right hand side of the loop) is more pronounced and the higher the rate of which the left hand side is heated; the higher the rate the higher the peak of the start-up transient

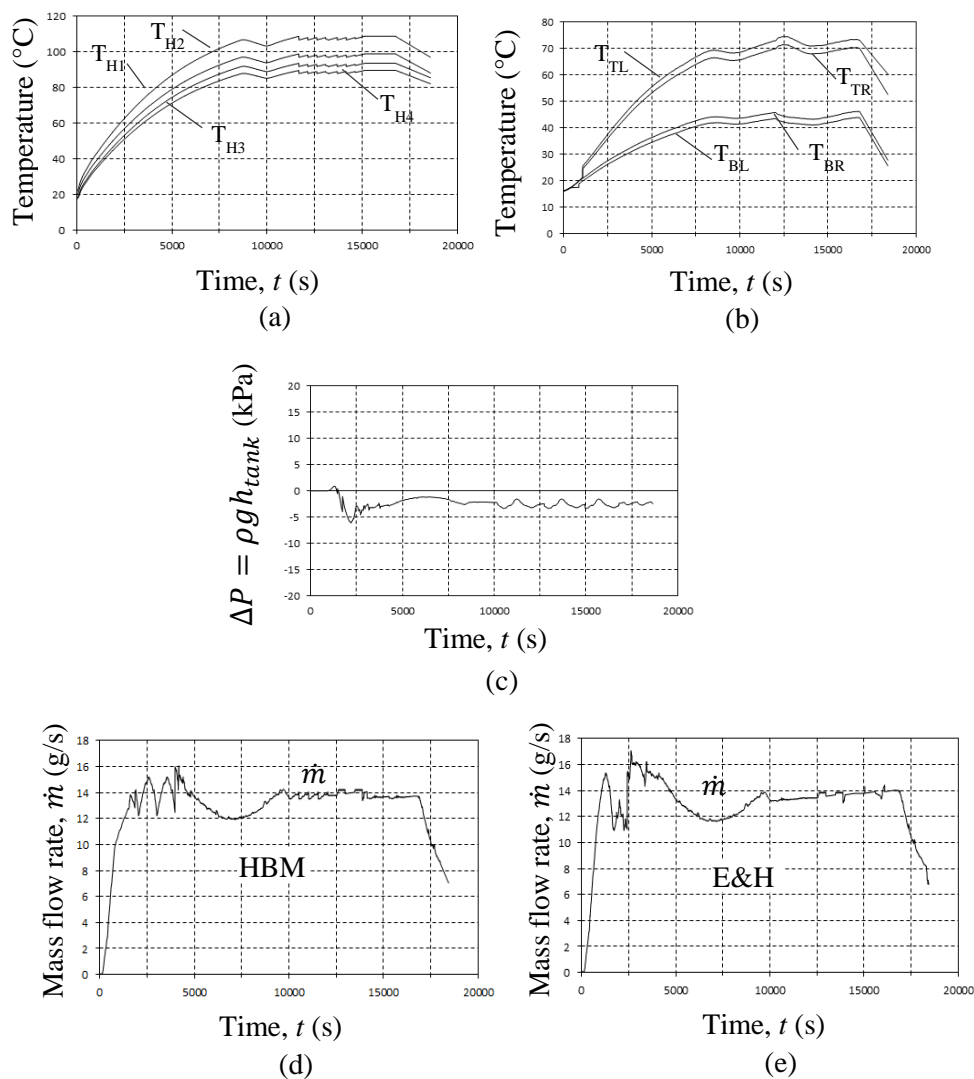


Figure 5-3 Experimental single phase operating mode at full power from start-up to switch-off (a) plate temperatures, (b) working fluid temperatures, (c) system pressure difference ΔP and (d) mass flow rate read with HBM and (e) mass flow rate read with E&H for test-run 2

The heat input for Figure 5.1(d) varied from 0 to 9.4 kW over a time period of about 3.2 hours, whereas in Figure 5.3 the full power of 9.4 kW was immediately input at start-up. Both Figures converged to a more or less steady mass flow rate of 14 g/s after the 3.2 hours. Both figures exhibit a typical start-up transient in which the mass flow rate increases suddenly and then drops down and repeat the cycle until more or less steady state is maintained. The mass flow rate as presented in Figure 5.3(d) increased for 1735 s to reach a peak of 14.22 g/s and oscillated for about 3000 s reaching the highest peak of 15.98 s before it decreased to 12 g/s and increased again to continue with a steady mass flow rate of more or less 14 g/s while in Figure 5.3(e) the mass flow rate increased for 1255 s to reach a peak of 15.26 g/s before it dropped to 11 g/s and increased again for about 900 s oscillating before stabilising at about 14 g/s.

5.1.2 Single to two-phase experimental operating mode

Single to two-phase operating mode tests were conducted and representable results for three tests (test-runs 3, 4 and 5) are given in Figures 5.4, 5.5 and 5.6 respectively as well as a comparison between test-runs 3 and 3a given in Figure 5.7 (test-run3b results are shown in Appendix D). Figures 5.4 and 5.5 show the temperature, pressure difference, power and mass flow rates for a low water cooling rate and a higher cooling rate. Figure 5.5 shows the single to two-phase operating mode at full power from start-up to switch off and with a relatively high cooling rate measured with the E&H pressure sensor.

Test-run 3

Results for test-run 3, as shown in Figure 5.4 shows that the heating plates' electrical powers were input, as in test-run 1, in steps of 30 to 100 per cent of full power as given in Table 5-4. The table shows that after 18000 s, the electrical power was switched off.

Table 5-4 Heating plate electrical power input for single to two-phase operating mode for test-run 3

Power (%)	Time (s)	Heating plate 1 (W)	Heating plate 2 (W)	Heating plate 3 (W)	Heating plate 4 (W)	Total (W)
30	0	451.16	451.16	243.04	140.24	1285.60
50	3180	1134.04	1080.00	1080.00	474.79	3768.83
70	8025	2098.29	1984.89	2079.18	960.26	7122.62
100	14904	2734.38	2734.38	2757.20	1173.06	9399.02
0	18000	0.00	0.00	0.00	0.00	0.00

Figure 5.4(a) shows four temperatures of the heating plates T_{H1} , T_{H2} , T_{H3} and T_{H4} that were measured along the plates at different positions (see Figure 4.1). Figure 5.4(b) shows temperatures (T_{TL} , T_{TR} , T_{BL} and T_{BR}) of the working fluid that was measured using thermocouples installed at the four corners of the loop as

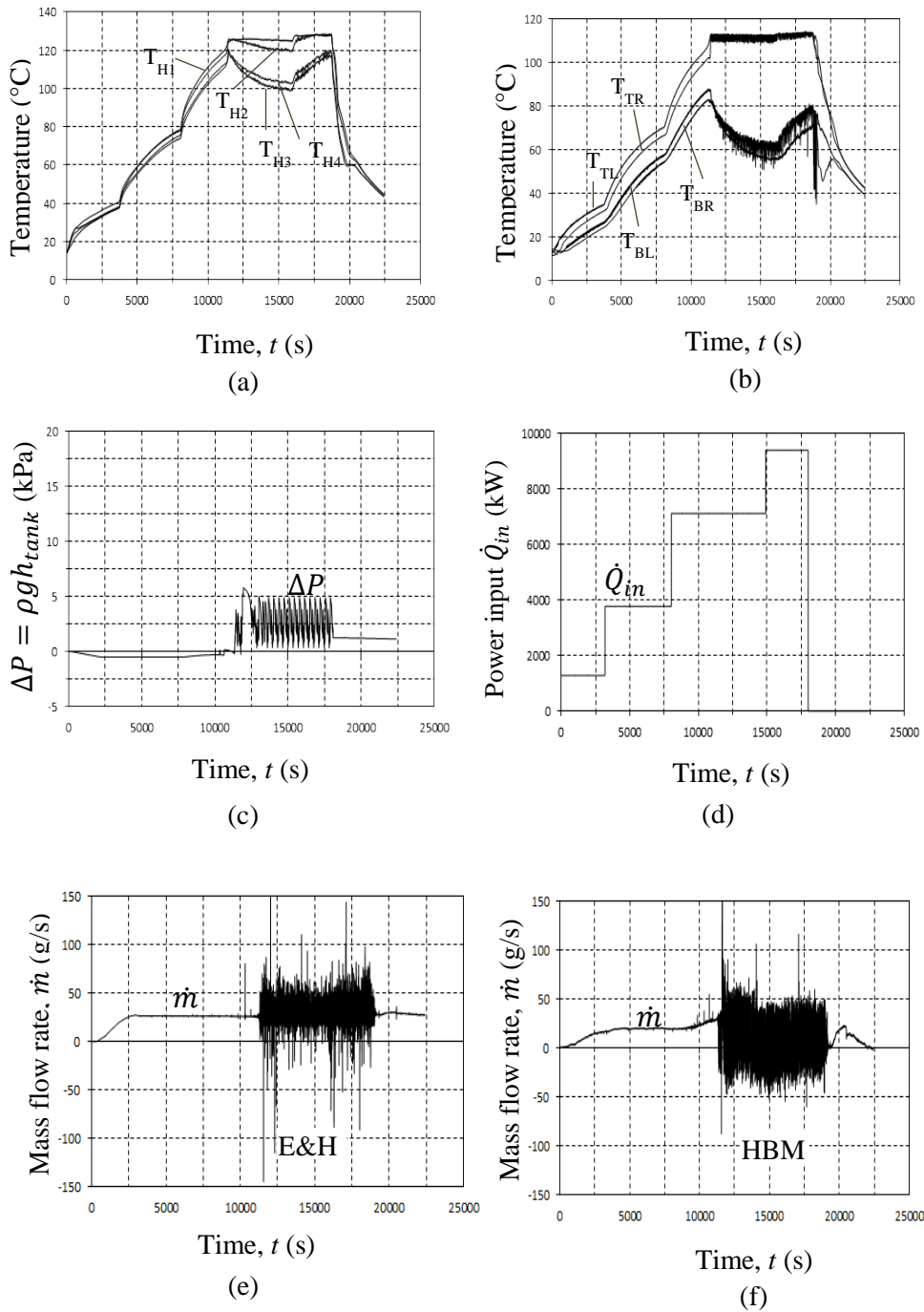


Figure 5-4 Experimental single to two-phase operating mode with power gradually input (a) fin temperatures, (b) working fluid temperatures, (c) system pressure difference ΔP (d) electrical power input, (e) mass flow rate \dot{m} measured with E&H pressure sensor and (f) mass flow rate \dot{m} measured with HBM pressure sensor for test-run 3

explained in test-run 1. From Figures 5.4(a) and 5.4(b) it can be seen that the increase in the heating plates temperatures correspond with the increase in the working fluid temperatures and the increase in power levels as shown in Figure 5.4(d). The temperatures in the top of the loop T_{TL} and T_{TR} are more or less the same at about 107 °C, whereas at the bottom of the loop both were more or less the same. The working fluid in top is boiling and both temperatures are about the same because the pressure is more or less constant.

Figure 5.4(b) shows that the saturation point (107.45 °C) at the working pressure (131.53 kPa) in the top section of the loop was reached and thus boiling occurred in the top pipe of the circulation loop. This is the reason why the temperature profiles show an oscillatory behaviour with frequencies of amplitudes of up to 5 °C for T_{TL} and T_{TR} . In the bottom section of the loop, no temperature reached the saturation point (120.24 °C with the working pressure at the bottom of the loop equal to 200.2 kPa) as heat was removed through the condenser, therefore boiling did not occur in that section. The thermocouple used to measure the temperature at the bottom the loop T_{BR} gave a more chaotic oscillatory behaviour than the other thermocouples with amplitudes up to 40°C. This is due to the interaction (mixing) of the light warm water inside the loop and the dense (cold) water coming from the expansion tank as a result of the characteristic oscillatory behaviour of boiling-condensing in a natural circulation loop; T_{BL} on the other was less erratic.

Figures 5.4(e) and 5.4(f) show that boiling occurred at 70 per cent. This is interpreted by the oscillatory behaviour of both the working fluid temperature and mass flow rate profiles. After 14904 s, power was increased to 100 per cent of the available electrical power, however this had very little effect on the top section temperatures (T_{TL} and T_{TR}) already at maximum (saturation) in two-phase mode. Small increases in temperatures were observed at the bottom section (for T_{BL} and T_{BR}) that was still in the single phase. The two figures show that as more heat was added, the working fluid mass flow rate response exhibited the typical transient behaviour associated with natural circulation especially in the two-phase region where more oscillations were observed. The mass flow rate increased to reach a peak of 15.26 g/s after 1255 s from start-up, dropped to 11 g/s after about 7300 s before stabilised at about 14 g/s after 16740 s. At 18000 s of the test, the power was switched off; the heating plates and the working fluid temperatures started decreasing until the test was stopped.

Figure 5.4(c) shows the pressure difference $\Delta P = \rho g h_{tank}$ where the change in fluid density due to the rise in temperature of both the heating plates and the working fluid temperatures was causing either the drop or gain in the pressure inside the loop. The pressure profile of test-run 3 shows that the pressure dropped proportional to heat added with time to 0.54 kPa after 2142 s and stayed constant due to thermal equilibrium. When power was increased to 70% of full power and boiling occurred, the pressure difference profile affected by dynamic instabilities (Vijayan & Nayak, 2010), started oscillating with amplitudes of up to 4.5 kPa.

This behaviour continued for about 800 s after the power was switched off, the pressure gradient stabilised at $\Delta p = 1.23$ kPa.

Test-run 3 was conducted at a relatively low cooling water mass flow rate of 0.032 g/s and only one heat exchanger (top heat exchanger; HE7) was used, this achieved the two-phase flow operating mode.

Test-run 4

Test-run 4 was conducted with heating plate electrical power inputs as shown in Table 5-5 and at a relatively higher cooling rate than for test run 3. The resulting temperature, pressure and mass flow rates response curves are shown in Figure 5.5. After 22250 s the power was switched off and the test stopped after 22500 seconds of experiment.

Table 5-5 Heating plate electrical power input for test run 4

Power (%)	Time (s)	Heating plate 1 (W)	Heating plate 2 (W)	Heating plate 3 (W)	Heating plate 4 (W)	Total (W)
30	0	462.89	451.16	243.04	140.24	1297.33
50	7350	1080.00	1134.04	1040.38	449.54	3703.96
70	14596	2079.18	2003.58	2079.18	960.26	7122.20
100	17285	2728.30	2704.70	2767.20	1173.06	9373.26
0	22250	0.00	0.00	0.00	0.00	0.00

Figure 5.5(a) shows the temperature profiles of the heating plates. The changes in the profile correspond to the change in power input as shown in Table 5.5. The working fluid temperatures depicted in Figure 5.5(b) shows that after 17910 s, the working fluid temperature reached the saturation and boiling occurred opening way to two-phase flow in the loop. Figure 5.5(c) shows the power input and Figure 5.5(d) gives the system difference in pressure gradient from the start of the test to the end.

Figures 5.5(e) and 5.5(f) show the working fluid flow rate as measured by the pressure drop over the orifice plate using the HBM pressure sensor and E&H pressure transducer respectively. The reading of the flow meters showed that the test ran for a long time before boiling started (about 17500 s). This was due to the fact that more heat was removed from the system through the heat exchanger in use at a higher cooling rate. Boiling started from subcooled to nucleate boiling as explained in the previous section. Figures 5.4(e) and 5.4(f) illustrate that the two flow meter readings showed that boiling started at the same time, however in the single phase stage, there were slight differences with the HBM increasing first then decreasing continuously until boiling started, while the E&H readings showed that in the single phase, the mass flow rate kept increasing.

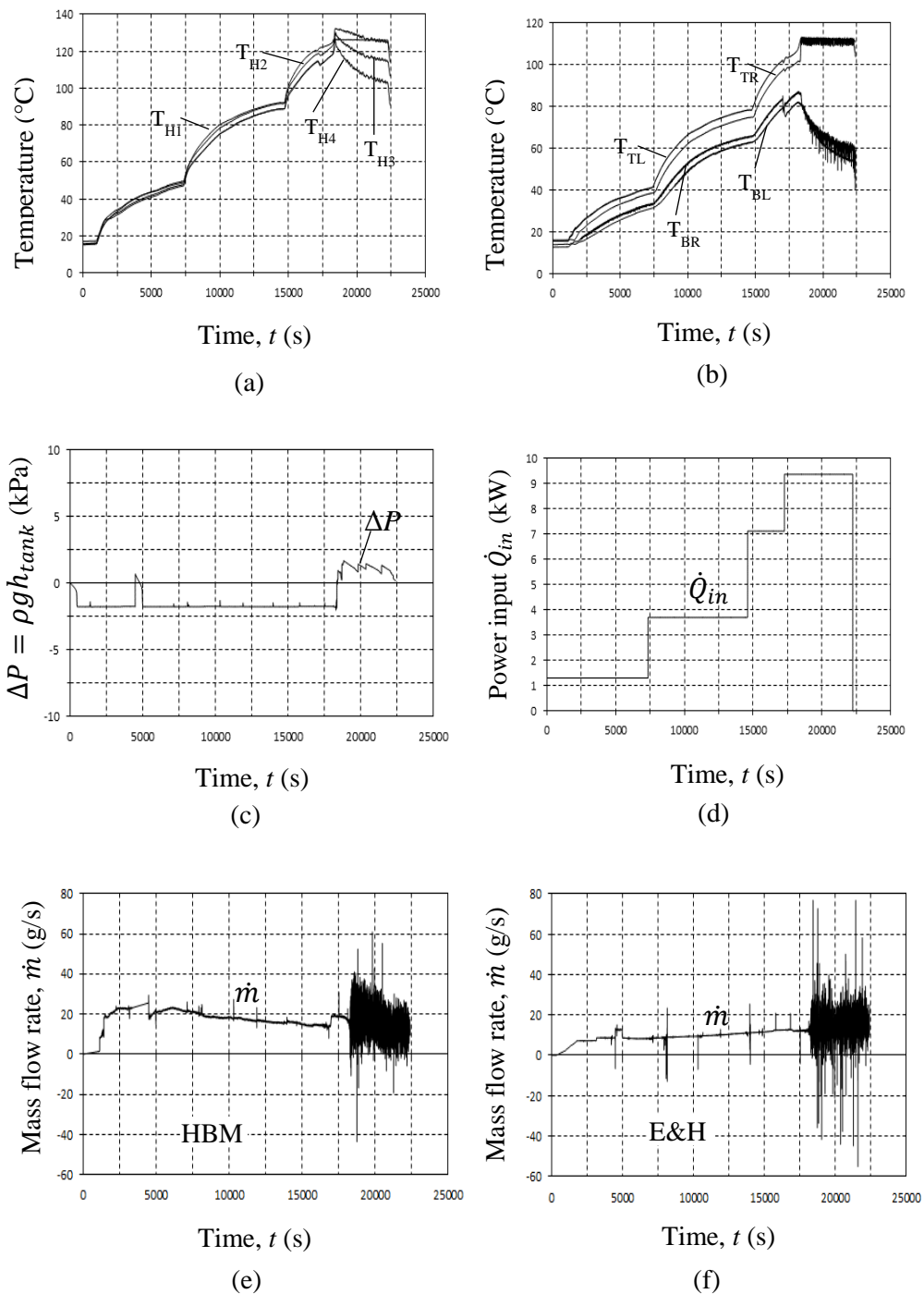


Figure 5-5 Experimental single to two-phase operating mode with increased cooling rate (a) Heating plate temperatures, (b) working fluid temperatures, (c) system pressure difference ΔP (d) power input, (e) mass flow rate \dot{m} measured with HBM pressure sensor and (f) mass flow rate \dot{m} measured with E&H pressure sensor.

Test-run 5

Test-run 5's results are shown in Figure 5.6. This was a typical single to two-phase circulation operating mode with full power input of 9.4 kW from start-up to switch off and at the same cooling rate as for test run 3. Figure 5.6(a) shows the temperatures of the heating plates. Figure 5.6(b) shows the temperature profiles of working fluid where in the top section T_{TL} and T_{TR} reached the saturation point, therefore boiling occurred and two-phase flow mode was observed. Figure 5.6 (c) shows the pressure difference ($\Delta P = \rho g h_{tank}$) and Figure 5.6(d) gives the working fluid mass flow rate response showing more chaotic oscillations from the single phase to the two-phase mode. The mass flow rate behaviour showed that for a start-up at higher power, there is more transient behaviour in the system as the thermal equilibrium that requires a step by step increase in power input, was not reached.

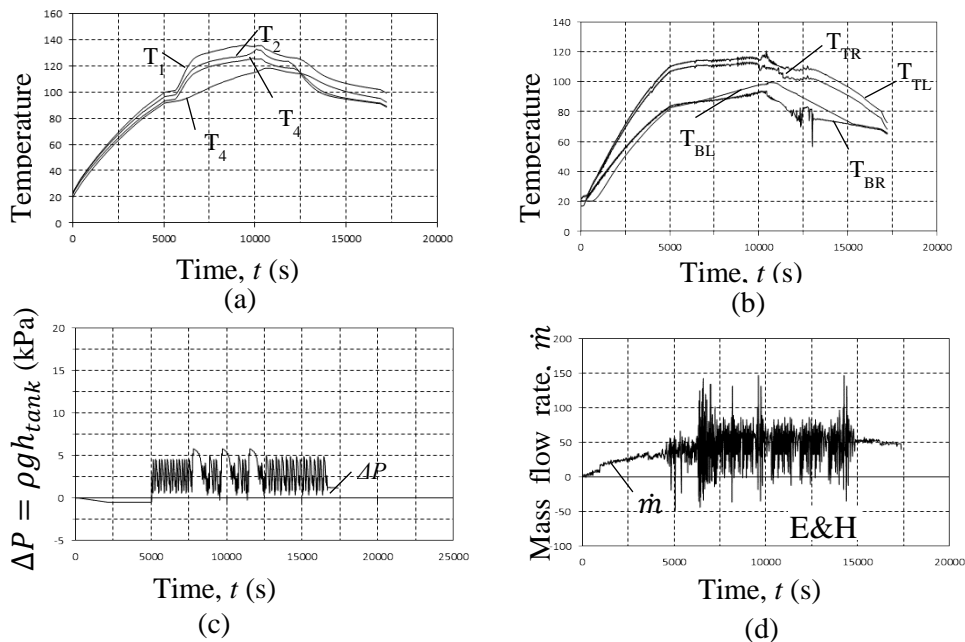


Figure 5-6 Experimental single to two-phase operating mode at full power (9400 W) (a) average fin temperatures, (b) working fluid temperatures, (c) system pressure difference ΔP and (d) mass flow rate \dot{m} (using the E&H)

The single to two-phase tests (test-run 3, test-run 4 and test-run 5) show that when boiling occurred, the two-phase patterns characteristic were observed. In test run 5 it is seen that, ostensibly due to the higher heat rate (100 per cent of available electrical power input from start), there are more of both the acoustic and the void instabilities (Vijayan & Nayak, 2010) observed through an oscillatory behaviour more intense than in test-runs 3 and 4.

Test-run 3a

As in test-run 1a, Figure 5.7 shows the mass flow rate comparison between test-run 3 and test-run 3a a repeat of test-run 3 with the same time step, power inputs and cooling water mass flow rate. The mass flow rate profiles for both test-runs are typically identical however they showed small deviation due to probable errors, ambient conditions and power ratings as shown in table 5.6.

Table 5-6 Heating plate electrical power input for test run 3a

Power (%)	Time (s)	Heating plate 1 (W)	Heating plate 2 (W)	Heating plate 3 (W)	Heating plate 4 (W)	Total (W)
30	0	451.12	451.12	243.04	140.20	1285.48
50	3180	1134.04	1080.01	1079.04	474.70	3767.79
70	8025	2098.27	1984.87	2079.15	960.26	7122.55
100	14904	2734.38	2734.36	2757.20	1173.06	9399.00
0	18000	0.00	0.00	0.00	0.00	0.00

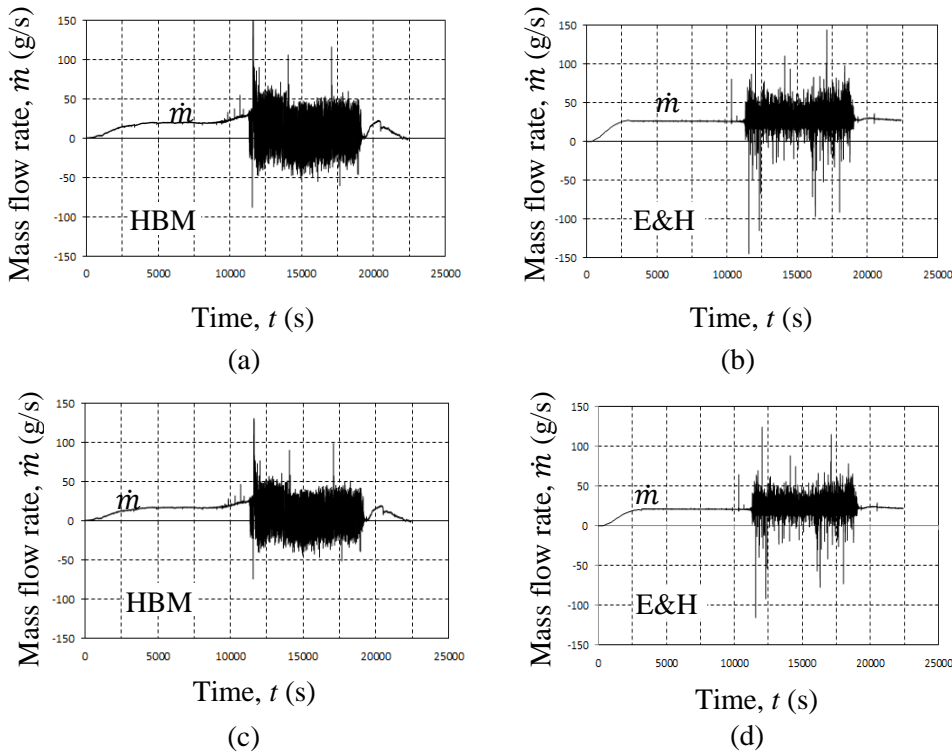


Figure 5-7 Two-phase working fluid mass flow rate repeatability comparison with power gradually input measured with (a) HBM test-run 3, (b) E&H test-run 3 (c) HBM test-run 3a and (d) E&H test-run 3a

Two-phase flow patterns

Figure 5.8 attempts to illustrate the flow pattern behaviour of the two-phase flow. At first, as illustrated in Figure 5.8(a), small isolated bubbles as found in the bubbly flow were seen throughout the liquid. After a period of time (200 seconds), slugs form where bubbles were dispersed toward the wall of the pipe by slugs of liquid, as shown in Figure 5.8(b). With Boiling continuing the slugs broke down and some big diameter bubbles went back-ward through the slugs of liquid, as it happens in a churn flow, and shown in Figure 5.8(c). In the two-phase region, during the single to two-phase test-runs, these three vapour-liquid flow patterns (bubbly, slugs and churn flow) were observed when boiling occurred through the sight glass pipes installed on the loop as depicted in Figure 4.1 and 4.2.

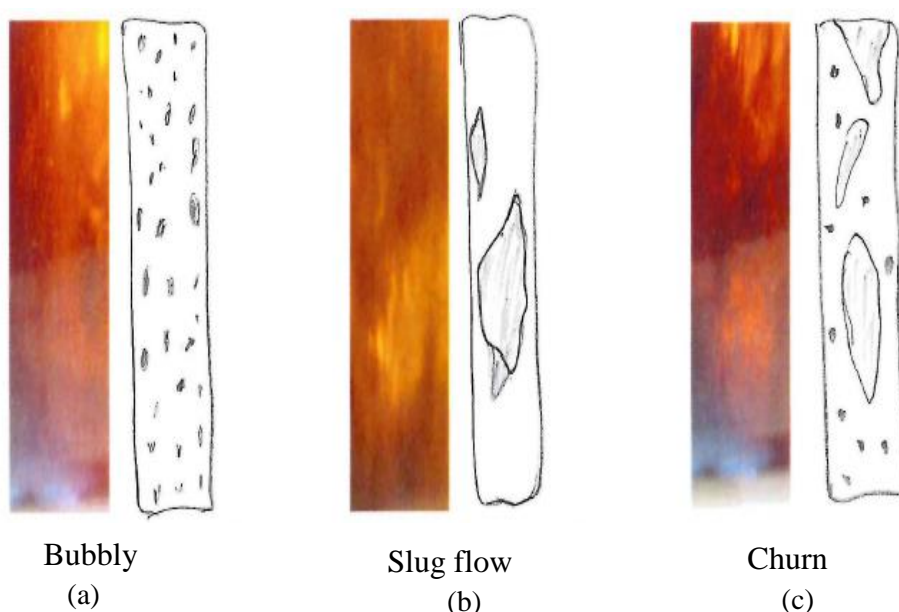


Figure 5-8 Hand drawing depictions of two-phase flow patterns adjacent to the photographic images of two-phase flow [poor photographic images due to semi-transparent observation windows]

5.2 Theoretical results

Theoretical results generated by the mathematical model described in Chapter 3 are given and discussed in this section. From literature, theoretical results are dependent on the type of correlations used. Results are shown for a single to two-phase operating mode.

The mathematical model was generated for the circulation loop as discretised in Figure 3.2. The model uses different correlations for the heat transfer and the

pressure drop in both the single phase and the two-phase flow modes. For single phase natural circulation, free convection takes place and there is slow moving fluids near surfaces, but is rarely significant in turbulent flow. Thus, it is necessary to check and compensate for free convection only in laminar flow problems using the Collier correlation (Collier & Thome, 1994) to calculate the heat transfer coefficient as given in equation 2.21. For two-phase flow, different correlations are applied based on the two-phase flow model used between the homogeneous and the separated two-phase flow models. For this project, a separated two-phase flow model was assumed with frictional multipliers and vapour-liquid void fraction correlations similar to those originally suggested by Martinelli.

Figure 5.9 shows the theoretical results for the single to two-phase natural circulation loop depicted in Figure 4.2 and discretised as illustrated in Figure 3.2. Figure 5.9(a) presents the temperature profiles of four control volumes located on the two top and two bottom corners. Figure 5.9(b) shows the system pressure difference and Figure 5.9(c) shows the mass flow rate related to the power input and power removed from the circulation loop.

Figure 5.9(a) shows that the temperature is dependent on the heat input. From the start-up, heat was input into the system as shown in Figure 5.9(c). The heat was added to the system for about 100 s, causing the temperatures to increase. At the time that heat is removed, the temperatures stay constant for about 15 minutes until the power is increased. Each time that input power is adjusted (increased or decreased), the temperatures also followed. Four temperatures are considered and calculated for the working fluid where T_{W1} represents the temperature of the control volume (N_1+N_2), T_{W2} of control volume ($N_1+N_2+N_3+1$), T_{W3} of control volume (2) and T_{W4} represents the temperature of control volume (N_1+1) as it can be seen in Figure 3.2.

From Figure 5.9(a) it is seen that T_{H1} reaches the saturation point after 12641 s and T_{H2} followed 262 s after. Boiling occurs causing two T_{W1} and T_{W2} to oscillate with amplitudes up to 3 °C. At the bottom of the loop T_{W3} and T_{W4} are both below saturation point as heat is being removed. They reached a maximum of 87 °C and oscillate due to two-phase transient behaviour in the top section of the loop.

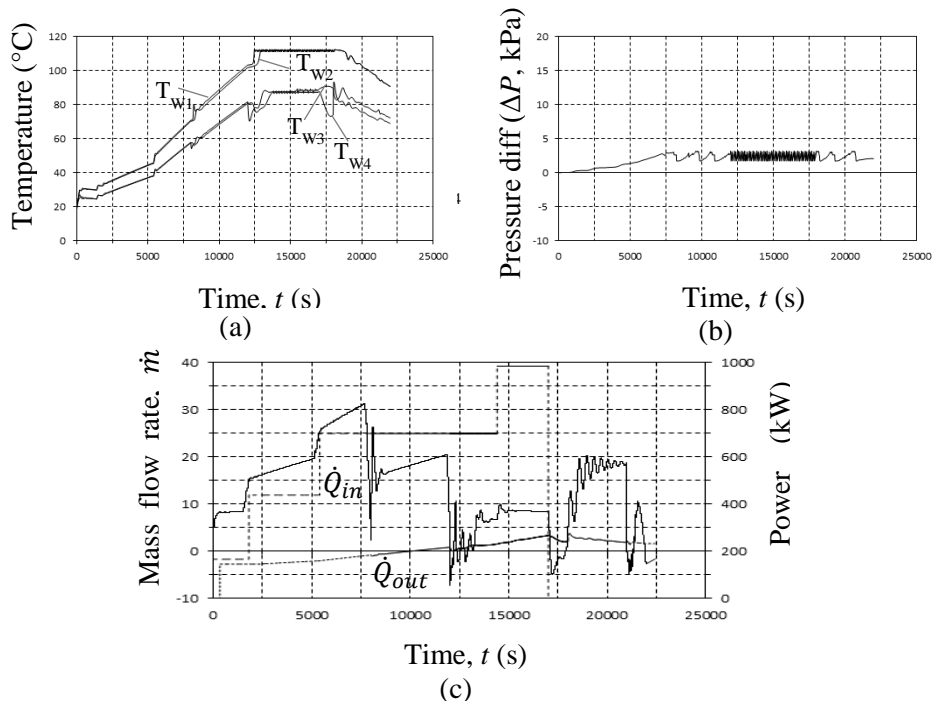


Figure 5-9 Theoretical temperature, pressure, mass flow rate and power as function of time, (a) working fluid temperatures, (b) system pressure difference and (c) mass flow rate, power input and power output

Figure 5.9(b) shows the system pressure difference (ΔP) from start-up to shut down. It displays that the pressure increases when the temperatures increase. During boiling, the pressure difference profile shows oscillations with constant frequencies of amplitudes of up to 2 kPa.

Figure 5.9(c) shows the heating and cooling process of the natural circulation loop and the calculated mass flow rate for the single to two-phase operating mode as a function of time. The mass flow rate is calculated in terms of the power input and the fluid properties at the inlet and the outlet of the heating and cooling sections. At start-up, the left hand side (evaporator) temperature was set at 20 °C and the right hand side (condenser) temperature at 19.5 °C. This is to allow circulation of the fluid in the loop due to the induced density difference of the fluid from the two sides. The mass flow rate reached a peak of 8.4 g/s after 300 s and stayed constant for 1500 s until the power input was increased. As the heat input increases (e.g. at 1800 s) the mass flow rate increases. When boiling occurs although the driving force is now greater the restraining friction force is more dominant. After about 7500 s the mass flow rate decreases, followed by a short oscillation of big amplitudes showing that two-phase has started with many bubbles filling up the loop. During boiling, the mass flow rate oscillates with time to time reaching negative values. The maximum flow rate reached during the process was 31.6 g/s.

After calculating the mass flow rate using the power in and power out as shown in Figure 5.9, it was decided to check what impact a low cooling water mass flow rate would have on the results, as presented in Figure 5.10. This figure gives the theoretical results for single to two-phase with a relatively low cooling water mass flow rate resulting in small power removed out of the system discretised as shown in Figure 3.2. Figure 5.10(a) shows the temperature profiles of the working fluid calculated from four points along the loop, Figure 5.10(b) shows the system pressure difference and Figure 5.10(c) shows the mass flow rate related to the power input and power removed from the circulation loop.

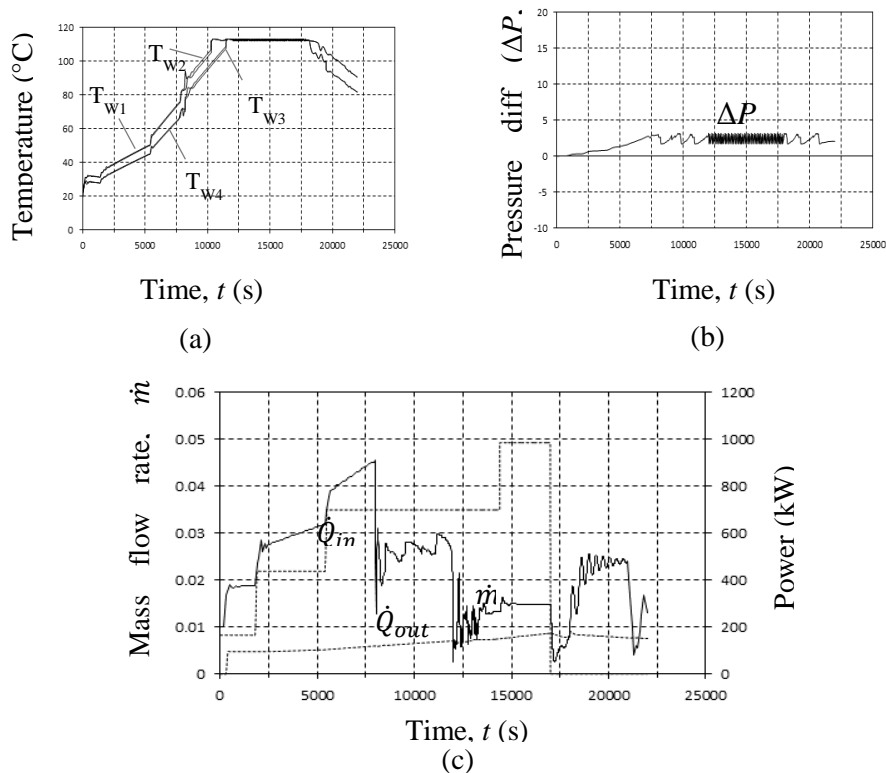


Figure 5-10 Theoretical single to two-phase operating mode with low cooling water mass flow rate (a) working fluid temperatures, (b) system pressure difference and (c) mass flow rate, with a cooling water mass flow rate of 0.024 g/s

Figure 5.10(a) shows that when boiling occurs (at about 10410 s from start-up), the two top temperatures (T_{W1} and T_{W2}) reached the saturation point of 113.25 °C and T_{W3} and T_{W4} were only slightly less than the top two. This indicates that there is a density difference between the heated and cooled vertical sides of the loop and that causes the flow that is now a mixture of liquid and vapour. At 18000 s the power input was switched off and from Figure 5.10(a) it can be seen that the bottom temperatures decrease faster than the top temperatures due to the heat removed from the condenser.

From Figure 5.10(b) it can be seen that the pressure difference profile is similar to the one given in Figure 5.10(b). The mass flow rate increases as the power input is increased. When boiling occurs the mass flow rate drops from a peak of 19.6 g/s to about 12.8 g/s due to the increased flow resistance characteristic of two-phase flow. The heat transfer rate however does not decrease but rather increases due to there now being more latent heat being transferred (as opposed to the sensible heat transferred of single phase flow). A note of interest is that the theory captures the transient oscillatory behaviour when sudden changes (in flow pattern) occur.

5.3 Comparison results

The experimental results for the single to two-phase operating mode shown in Figures 5.4(e) and 5.4(f) are combined with the theoretical results shown in Figure 5.9 and are presented as Figures 5.11, 5.12, 5.13 and 5.14.

From Figures 5.11 and 5.12, it can be seen that the experimentally measured mass flow rate as given in Figure 5.4(f) is more in line with the theoretical mass flow Figure 5.9(c) than the experimental measured mass flow rate in Figure 5.4(e). Both results show that when boiling occurs, their mass flow rate profiles present more oscillations, recording positive and negative values, with the experimental mass flow rate showing bigger amplitudes than the theoretical. This is due to the sensitivity of the measurement instruments. This indicates that due to boiling, although the average velocity is positive, both negative and positive oscillatory pressure pulses are detected by the pressure sensors. When still in the single phase mode, the mass flow rate increases proportional with the heat input and time in both the experimental and theoretical tests, as it is shown in Figure 5.11 and Figure 5.12.

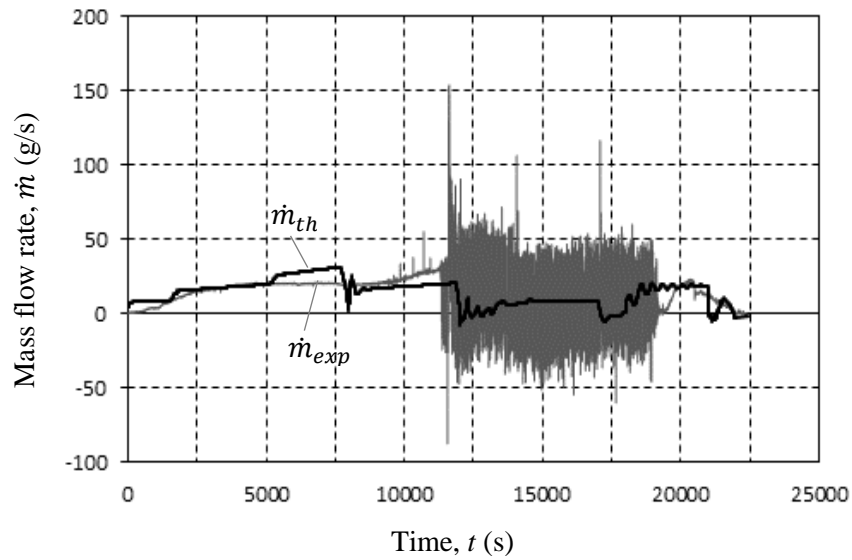


Figure 5-11 Experimental mass flow rate \dot{m}_{exp} as given in figure 5.4(f) vs theoretical mass flow rate \dot{m}_{th} as given in figure 5.6(c) function of time.

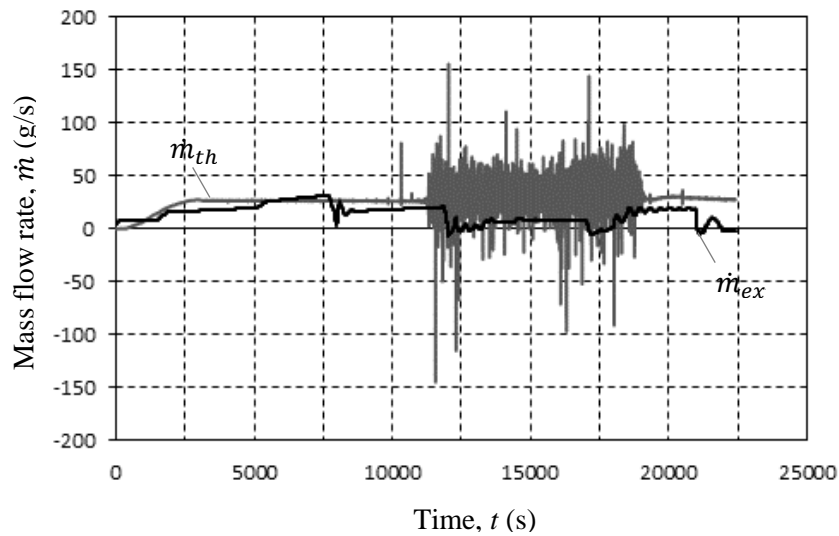


Figure 5-12 Experimental mass flow rate \dot{m}_{exp} measured with E&H pressure sensor vs theoretical mass flow rate \dot{m}_{th} , as a function of time

Figure 5.13 shows the theoretical (Figure 5.4(c)) and experimental (Figure 5.9) working fluid pressure difference between the level of liquid in the expansion tank and the bottom of the loop. The experimental results show a drop in pressure from start-up as the working fluid density decreases when heat is added to the evaporator section. It then stabilised for some time before it increases while the working fluid gets close to two-phase mode and then oscillates due to boiling.

After power is switched off, oscillations stop and the pressure profile stopped oscillating and stayed constant at a relatively higher pressure than the initial pressure at the beginning of the test-run. The theoretical results show that the pressure increases from start-up then moves up and down and as the working fluid reaches the two-phase mode oscillatory behaviour starts and amplifies with time due to boiling. After switching off the power, the pressure difference profile goes back to moving up and down until the end of the process. It is seen that the experimental pressure drops first before it increases and then starts oscillating due to boiling while the theoretical result shows that the pressure does not decrease, however it increases and then oscillates also because of boiling.

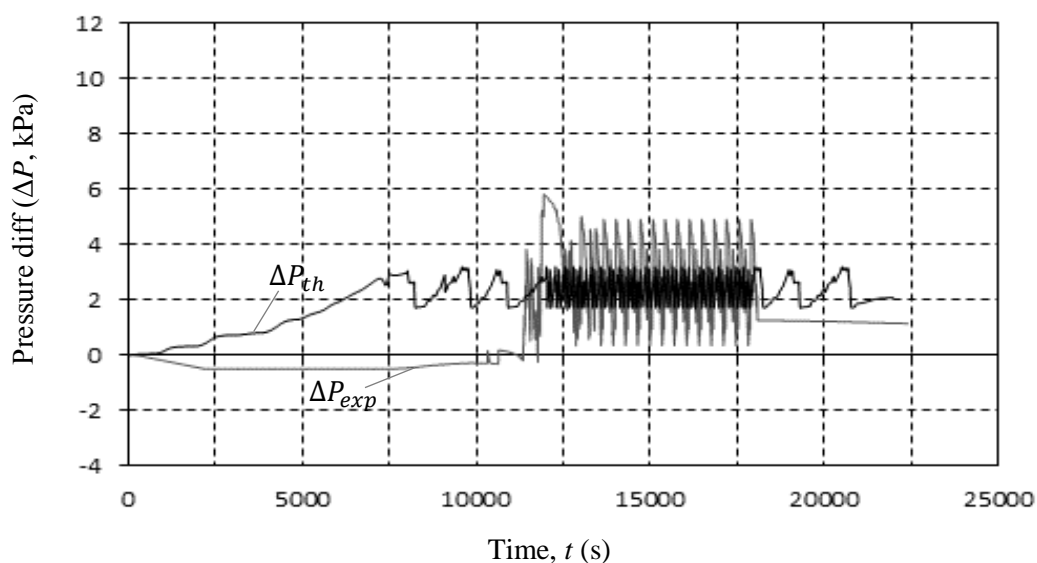


Figure 5-13 Experimental (test-run 3) vs theoretical pressure difference, as a function of time

Figure 5.14 presents a comparison between the experimental and theoretical working fluid temperature, as given in Figure 5.4(a) and Figure 5.9(a), from start-up to finish of the test. Figure 5.14(a) gives the experimental temperatures and Figure 5.14(b) shows the theoretical temperatures as function of time. All results show that at each change in heat input, the working fluid temperatures increase with time, however the change in heat input has no effect on the fluid temperatures after they have reached their saturation point where boiling starts. During boiling, more oscillations with bigger amplitudes are observed in the experimental temperature results than in the theoretical results due to the sensitivity of the measurement instruments.

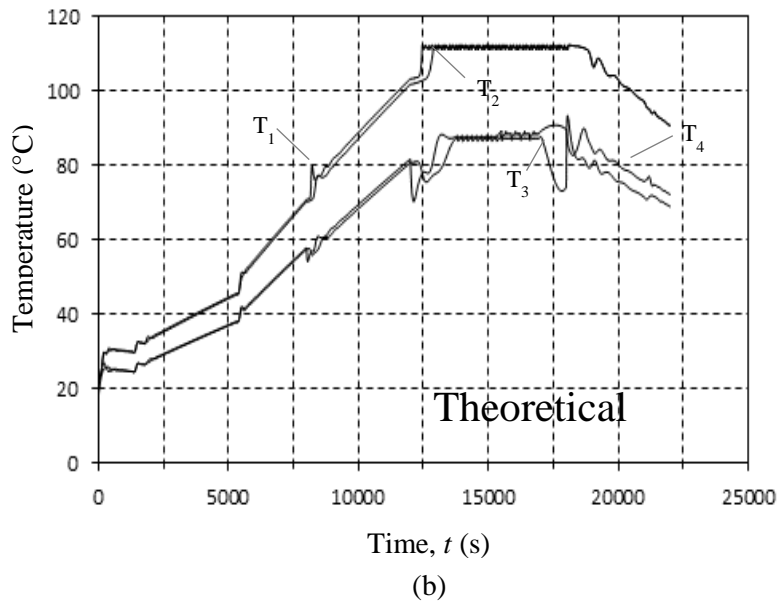
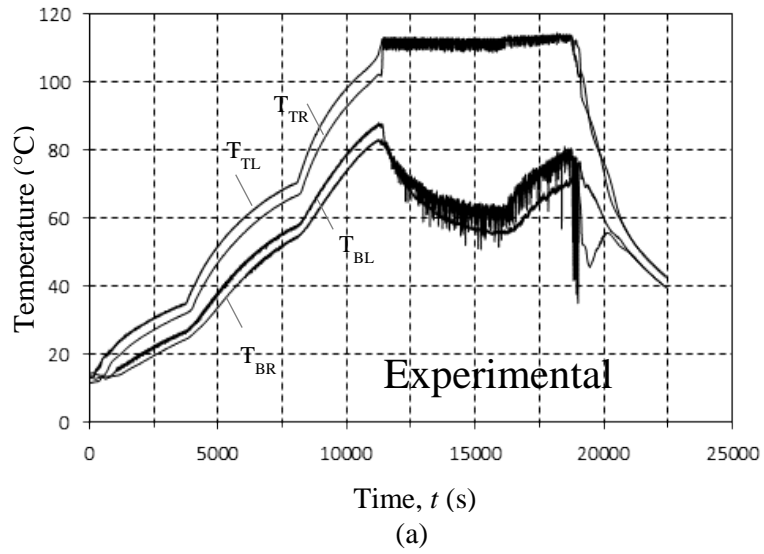


Figure 5-14 Working fluid temperatures as function of time for (a) experimental working fluid temperatures, (b) theoretical working fluid temperatures

6 DISCUSSION AND CONCLUSION

This Chapter discusses and draws conclusions based on the objectives and findings of the project.

The first objective of this project was to do a literature survey to collect enough theory in order to analyse the transient behaviour and study the flow pattern of a two-phase flow natural circulation using the later technique which is based on the separated flow model. There is a relatively large amount of published literature on natural circulation modeling and both single and two-phase flows have been widely investigated and assumptions made (Dobson, 1993; Grief, 1988). The amount of information collected from the literature review provided enough material to support the theory used in the elaboration and simulation of the theoretical model of the loop.

In order to study the transient behaviour and analyse the flow patterns of the two-phase flow in natural circulation, the literature survey shows that there are various methods of dealing with the two-phase flow. However this thesis considered only the homogeneous and separated flow models. In the homogeneous two-phase flow model, the two-phase flow is replaced by a special single-phase incompressible fluid with both phase considered being well mixed and travelling at the same velocities $u_g = u_l = u$ and with a homogeneous density ρ_h and void fraction α_h . In the separated two-phase flow model, which is the focus of this project, gas and liquid flow are considered separately.

Information collected through the literature review shows that the basic approach in theoretically simulating the single and two-phase flow in the separated model is to discretize the loop into a series of parallel one-dimensional axially symmetrical control volumes, in which the two-phases are treated as two separate fluids. The loop was thus discretised and conservation equations of mass, momentum and energy were applied that also show the difference in correlations used for the homogeneous two-phase flow and the separated two-phase flow.

The literature survey also provides sufficient material and information on flow patterns. This has allowed investigating into the flow pattern characterization and the difference in pressure due to the change in temperature. The flow pattern varies as the temperature rises and bubbles appear. It is shown that the rising velocity of the bubble is dependent on the Morton number, the Bond number and the Reynolds number. The pressure drops in natural circulation systems is a key element in their steady state, transient and stability performance. The uncertainty and complexity encountered with two-phase flow patterns in tubes is revealed to be very difficult to predict and therefore accurate prediction is empirical and limited in a range of applicability (Mills & Ganesan, 2015).

Empirical prediction depends on the type of correlations used and the literature review gives available heat transfer coefficient correlations. The prediction of the heat coefficient still difficult as no comprehensive theory exists in determining or using them in natural convection. The conclusion is that heat transfer coefficient correlations for natural circulation are a debatable matter and are specifically dependent on the experimental conditions such as the type of flow whether it is laminar or turbulent, but most heat transfer coefficients are only valid in a specific mass flow rate range.

The theory provided by the literature review appears to be acceptable as the calculated theoretical results using the separated two-phase flow model are in accordance with the experimentally determined results.

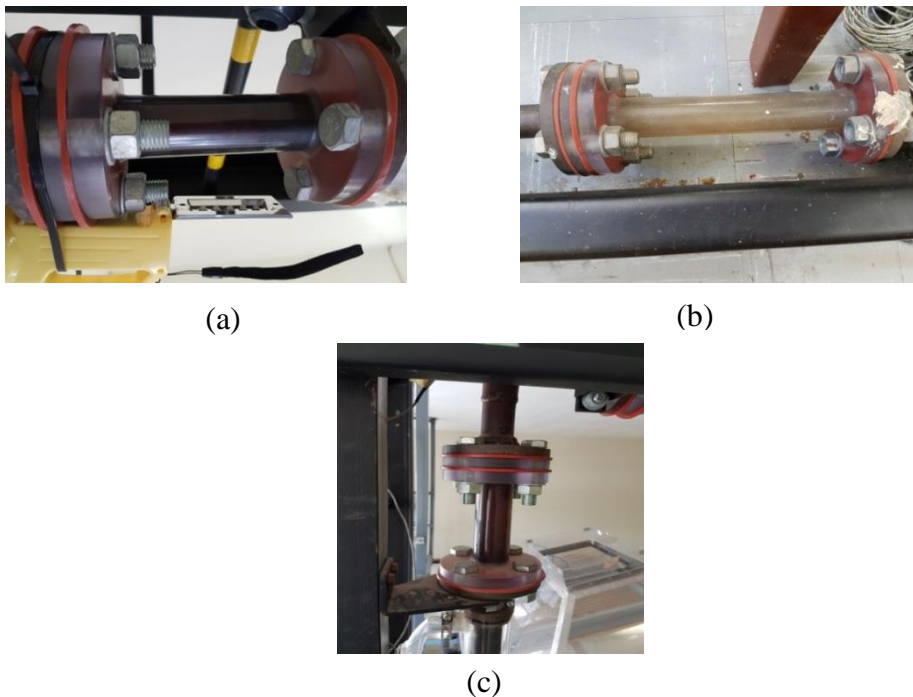


Figure 6-1 Polycarbonate sight glass located on the (a) top of the evaporator section, (b) bottom pipe and (c) top of condenser

The second objective of this project was to theoretically model and simulate the thermal-hydraulic behaviour of the natural circulation loop of the medium scale model of the RCCS available in the laboratory and built by Sittmann in 2010. The RCCS was designed with copper piping in order to eliminate material and surface property uncertainties, which affected the accuracy of theoretical models, identified during previous RCCS experimental tests. Four sight glasses were incorporated into the model in order to visualize and identify the two-phase flow patterns characteristics. However the flow patterns could not be clearly identified, as can be seen in Figure 5.8, due to the change in colour or copper colouring of

the sight glasses (see Figure 6.1). Figure 6.1 shows the sight glasses used to view the two-phase patterns. Figure 6.1(a) gives the sight glasses located in the top corner of the heating plates side, Figure 6.1(b) shows the one installed at the bottom pipe and Figure 6.1(c) gives the sight glass at the top right of the loop (condenser section).

The natural circulation thermosyphon loop was discretized as depicted in Figure 3.2 and modeled as a one-dimensional system before the conservation equations (mass, momentum and energy) to the i^{th} control volume were applied. Several simplifying assumptions were made: the thermo-fluid process is quasi-static; compressibility effects due to heating or cooling of the liquid and vapour phases are negligible; and the flow is one-dimensional. At any cross-section both the liquid and vapour phases are in thermodynamic equilibrium with each other. The separated two-phase flow model was used to determine the properties and behaviour of the control volume containing both the liquid and gas. The void fraction, the frictional multiplier and the Lockhart-Martinelli correlation were used as control parameters. The calculated results as shown in Figures 5.11 to 5.14 are in reasonable agreement with the experimentally determined results thus strengthening the case for using a separated flow model for future two-phase natural circulation simulations.

The third objective of the project was to develop a computer program to numerically simulate the theoretical model developed in Chapter 3 by writing a basic computer algorithm in QBASIC 64 language. This theoretical model was based on the separated two-phase flow model and the computer code was developed and simulated. A comparison of the theory and experiment for the computer code accuracy verification was successfully conducted through results comparison.

The fourth objective of this project was to re-commission and install new instruments to the loop built by Sittmann in 2010 and which had not been in use for the past eight years. Damaged and missing thermocouples were replaced and all twenty three thermocouples including twelve K-type and eleven cladded K-type were calibrated against a calibrated (Rapid Instrumentation cc certificate number RAP15738, 4 February 2013) Platinum Resistance Thermometer (PRT). The working fluid mass flow rate was measured using two pressure transducers; the HBM and the E&H in order to more confidently present the complex temperature and sound (acoustic) waves experimentally observed in boiling in natural circulation loops. The thermocouples and pressure transducers were calibrated in-situ to reduce possibilities of experimental errors and repeatability tests were used to check the accuracy of the readings. A data logger was used and set to collect data every 10 ms, however, averaged values were recorded every 1.445 s. Data collected were used in excel to draw graphs in order to study the transient behaviour and oscillations, however these were not adequately captured during two-phase flow.

The fifth objective of the project was to validate the theoretical simulation with the experimentally determined results. Ten experimental tests regrouped in single phase test and single to two-phase tests were conducted and results presented in Chapter 5 are discussed in this section.

Test-run 1

Test-run 1 presents the results of the single phase operating mode with low cooling water where the power was input into the heating element gradually. Figure 5.1 presents the behaviour of the average fin temperatures, working fluid temperatures read from the four corners representing the inlet and outlet of the evaporator and condenser sections, the system pressure difference and the working fluid mass flow rate. The mass flow rate increases rapidly for the first 3000 s from start-up and then decreases slightly due to static friction and increases again after a bout 500 s. For this test all four heaters and seven heat exchangers are operational. Even though the individual heat exchangers were operating at a relatively low water cooling mass flow rate, the heat removed from the system was revealed to be significant as this was affected by all heat removed by each heat exchanger. The highest working fluid temperature reached from the hottest point of the loop, located at the outlet of the evaporator and designated T_1 , was 91.72°C. This is far below the saturation temperature of 107.51°C at local pressure where boiling occurs, allowing only the single phase operating mode. Instabilities were also observed for a certain time as more heat was added into in the system before it then stabilizes. These instabilities are explained by the up and down behaviour of the difference in the pressure profile. If the system were used primarily for reactor cooling, the behaviour of both the pressure difference profile and the working fluid mass flow rate suggests that the nuclear reactor should be sequentially started up in order to minimize the intensity of the transients that occur when heat is added and/or removed to/from two-phase heat transfer loops. A repeat of this test was also conducted four days after to check on the accuracy of the reading devices. This test named *test-run 1a* increased confidence on the validity of the results obtained as it can be seen from their mass flow rate profiles that are similar, however a small deviation from the initial values was observed due to the ambient conditions on the day of the test, the power ratings and possible errors that may have occurred as shown in Figure 5.2.

Test-run 2

Test-run 2 also presents results for the single operating mode as in test-run 1: the difference is in the way heat is added to the system. For this test, the full available power is input into the heating elements from start-up to shut down. In comparison to test-run 1, it can be seen that in this case there are more instabilities reflected in the system pressure difference profile behaviour and the working fluid mass flow rate that shows more oscillations than in test-run 1. Even by using big cooling water mass flow rate, this can be seen from the working fluid temperature where the highest reached a peak of 74.61°C is below the peak temperature in test-run 1, it shows more instabilities with more oscillations. This also supports

the fact that power should be gradually added to the system to prevent the possibility of more instability, therefore the nuclear reactor should start sequentially. A repeat of this test was also done to check on the accuracy of the results at full power (see Appendix D).

Test-run 3

Test-run 3 shows results for the single to two-phase mode at low cooling water mass flow rate and where the power is gradually input into the system. From the results shown in Figure 5.4 it can be seen that the working fluid reaches two-phase flow mode and boiling occurs as shown by the behaviour of the working fluid temperature reaching the saturation point and the working fluid mass flow rate oscillations with big amplitudes read with both pressure transducers including the HBM and the E&H. They both show that when boiling occurs, the working fluid and pressure difference oscillate with big amplitudes. This shows that there is more instability in the two-phase flow than in the single phase flow operating mode. In order to get the two-phase mode and boiling, only one heat exchanger in the top of the condenser section was used, while all four heating elements were operational. This test was repeated five days later and results shown in table 5.7 allow justifying the use with confidence of both pressure sensors. A repeat of test-run 3 was also successfully conducted as shown in Figure 5.7 strengthening confidence in the validity of the results.

Test-run 4

Test-run 4 presents results for the same parameters as test-run 3, however the cooling water mass flow rate in test-run 4 is higher than in test-run 3. It shows that boiling also occurs in this case, but after a long period of time. At the point where boiling starts, results show that instabilities are present, as this is shown in Figure 5.5.

Test-run 5

This test shows results of a classic single to two-phase operating mode at full power from start-up to shut down. The mass flow rate measured only with the HBM pressure sensor shows more oscillation starting in the single phase due to the fact that there is more heat and frictional forces to overcome (The E&H pressure sensors was disconnected for this experiment due its default reading caused by the displacement of materials during the cleaning of the lab). The combination of the two factors then generates more oscillations in the working fluid.

Theoretical results were generated with the mathematical model of the natural circulation loop as described in Chapter 3. Theoretical calculations of the single to two-phase operating mode were performed in order to analyse the transient behaviour of the flow and evaluate the natural circulation loop were based on the separated two-phase model. Thermo-fluid characteristics of the working fluid were evaluated using experimentally used cooling water mass flow rate. In the

single phase the friction factor was used as a control parameter to calculate the working fluid mass flow rate and in the two-phase the viscosity and void fraction were used.

An important objective of the experimental work was to assist in determining the validity and accuracy of the theoretical model. Figures 5.12 and 5.13 show the theoretical results superimposed on the experimental results. They show that the theoretical results correspond reasonably with the experimental results where the mass flow rate kept increasing in the single phase until it reaches the two-phase mode. When boiling starts, both figures show oscillations occurring in both the theoretical and experimental mass flow rates. The pressure difference profiles correspond more relatively when the working fluid is boiling and prove that the two-phase flow is more unstable than the single-phase operating mode. Finally the theoretical working fluid temperature profile also corresponds to the experimental, however the thermocouples placed at the outlet of the condenser and closer to the pipe from the tank to the loop shows more oscillations, which is due to the fact that the valve is open and there is an exchange between the warm water from the loop and the cold water coming from the expansion tank.

In conclusion, the theoretical investigations provided the calculated thermo-fluid parameters of the natural circulation loop more accurately with respect to the experimental results although there are areas that required improvements. The theory shows that at sufficient cooling water mass flow rate, only the single phase operating mode will take place meaning heat is being removed from the system successfully. This makes a strong argument for the use of the thermosyphon loop as a RCCS.

7 RECOMMENDATIONS

The topics investigated in this project dealing with natural circulation and two-phase flow operating mode have many applications and still have a lot research avenues. For example, the experimental and theoretical investigations showed excellent results that support the use of natural circulation for energy transportation or for passive cooling as the RCCS. However, there is still much room for improvement that would enhance the theoretical and experimental results in future studies; the following are some of the recommendations.

7.1 Loop materials

Some of the materials used on the loop should either be renewed or replaced for better experimental investigations.

Sight glasses

The sight glasses used for the two-phase viewing should be replaced with clear ones, as they do not currently allow clear visual observation to be made. Neutron and proton photography could also be considered.

Temperature measurements

A careful study must be undertaken to determine the number of thermocouples that must be used along the loop, the length of the heat exchangers and the length of the heaters to more accurately describe the temperature profiles.

7.2 Mathematical model

The separated two-phase flow model using the Martinelli correlations predict reasonably accurately the thermo-fluid behaviour of the working fluid (as shown in Figures 5.11 to 5.14). Therefore this model can be confidently used in future two-phase flow studies.

8 REFERENCES

- Alagesan, V. & Sundaram, S., 2012. Two-phase experimental studies on a water-diesel system in a shell and tube heat exchanger. *Brazilian Journal of Chemical Engineering*, 29(2), pp. 275-283.
- Arneth, S. & Stichlmair, J., 2001. Characteristics of thermosiphon reboilers. *International Journal of Thermal Science*, Volume 40, pp. 385-391.
- Autee, A. & Giri, S., 2016. Experimental study on two-phase flow pressure drop in small diameter bends. *Perspectives in Science*, Volume 8, pp. 621-625.
- Basaran, T. & Kucuka, S., 2003. Flow through a rectangular thermosyphon at specified wall temperatures. *International Communications in Heat and Mass Transfer*, 30(7), pp. 1027-1039.
- Batty, J. & Folkman, S., Food engineering fundamentals. *John Wiley & Sons, Inc.* 1983.
- Bau, H. & Torrance, K., 1981. On the stability and flow reversal of an asymmetrically heated open convection loop. *Journal of FluidMechanics*, Volume 106, pp. 417-433.
- Beck, J., Blackwell, B. & Clair, C. R. S., 1985. *Inverse Heat Conduction. Ill-posed Problems*. New York, John Wiley & Sons.
- Bhattacharyya, S., 2012. Two-phase natural circulation loops: a review of the recent advances. *Heat Transfer Engineering*, Volume 4-5, pp. 461-482.
- Bieliński, H. & Mikielwicz, J., 2011. Natural circulation in single and two phase thermosyphon loop with conventional tubes and minichannels. *The Szewalski Institute of Fluid-Flow Machinery*, Volume 14, pp. 475-494.
- Bird, R., Stewart, W. & Lightfoot, E., 2000. Fundametal equations. In: *Transport phenomena*. Wisconsin: John Wiley & Sons, pp. 304-325.
- Boure, J., Bergles, A. & Tong, L., 1973. Review of two-phase flow instability. *Nuclear Engineering and Design*, Volume 25, pp. 165-192.
- Brennen, C., 2005. Homogeneous flows. In: C. U. Press, ed. *Fundamentals of Multiphase Flows*. Pasadena: California Institute of Technology, pp. 220 - 227.
- Bromet, E.J., 2014. Emotional consequences of nuclear power plant disasters. *Health physics*, Volume 106(2), pp. 206-210.

- BSI, 1981. Measurement of flow in closed conduits, *Part 1: Pressure Differential Devices.*, London: BS 1042.
- Burgazzi, L., 2012. Reliability of passive systems in nuclear power plants. In: W. Ahmed, ed. *Nuclear-Power practice aspects*. Rome: InTech, pp. 23-31.
- Buzz, P., 2009. Nuclear energy: Pros and Cons, Triple Pundit
- Carey, V., 1992. Liquid-vapor phase-Change phenomena, s.l.: Hemisphere.
- Cengel, Y. and Boles, M., 2014. Thermodynamics, An Engineering Approach 7th Edition. New York: McGraw Hill.
- Cengel, Y. & Cimbala, J., 2014. Thermodynamics, An Engineering Approach 3rd Edition. Singapore: McGraw Hill.
- Cheng, K., Marioka, I. & Sadler, G., 1982. Experimental study of a two phase thermosyphon system. *Alternative Energy Sources*, Volume 1, pp. 151-170.
- Chen, K., Tsai, S. & Yu, W., 1987. Experimental study of the heat transfer characteristics of a two-phase double-loop thermosyphon. *Experimental Heat Transfer*, Volume 4, pp. 171-188.
- Chexal, V. & Bergles, A., 1986. Two phase instabilities in a low pressure natural circulation loop. *AIChE Symposium Series*, Volume 69, pp. 37-45.
- Chisholm, D., 1983. *Two-Phase Flow in Pipelines and Heat Exchangers*. New York, Longman Inc..
- Chisholm, D., 1967. A theoretical basis for Lockhart-Martenilli correlation for two-phase flow. *International Journal of Heat and Mass Transfer*, Volume 10, pp. 1767-1778.
- Cioncolini, A. & Thome, J., 2017. Pressure drop prediction in annular two-phase flow in macroscale tubes and channels. *International Journal of Multiphase Flow*, Volume 89, pp. 321-330.
- Collier, J. & Thome, J., 1994. *Convective boiling and condensation*. Oxford, Clarendon press.
- Collier, J. & Thome, J., 1996. Basics equations of two-phase models. In: O. E. S. Series, ed. *Convective boiling and condensation*. Oxford: Clarendon Press, pp. 39-56; 67-70.
- Creveling, H., Paz, J., Baladi, J. & Schoenhals, R., 1975. Stability characteristics of a single-phase free convection loop. *Journal of Fluid Mechanics*, Volume 67, pp. 65-84.

- Damerell, P. & Schoenhals, R., 1979. Flow in a toroidal thermosyphon with angular displacement of heated and cooled sections. *ASME J. Heat Transfer*, Volume 101, pp. 672-676.
- Dobson, R., 1993. Transient response of a closed loop thermosyphon. *R&D Journal*, 9(1), pp. 32-38.
- Dobson, R., 2006. A Novel Closed Loop Thermosyphon Heat Modular Reactor, *8th Int. Heat Pipe Symp.*, Kumamoto, pp. 397-384.
- Pipe Reactor Cavity Cooling System for a Pebble Bed
- Dobson, R., 2015. *Advanced heat transfer class notes*, Stellenbosch: Stellenbosch University.
- Dobson, R. & Harms, T., 12-16 Sept 1999. *Lumped parameter analysis of closed and open oscillatory heat pipes*. Tokyo, International Heat Pipe Conference.
- DOE (Department of Energy), 2015. South Africa's energy situation, *Energy Advocacy*, Pretoria
- DTI (Department of Trade and Industry), 2014. The impact of electricity price increase on the competitiveness of selected mining sector and smelting value chains in South Africa, *Global Green Growth Institute, TIPS*, Pretoria (www.tips.org.za)
- Durig, B. & Shadday, M. J., 1986. Flow in a rectangular closed-loop thermosyphon with vertical heat transfer passages. *ASME, Winter Annual Meeting, Anaheim*, Volume 6, pp. 621-632.
- Eskom, 2004. *Eskom-pbmr*. [Online]
Available at:
http://www.eskom.co.za/nuclear_energy/pebble_bed/pebble_bed.html
[Accessed 6 February 2017].
- Faghri, A. & Zhang, Y., 2006. *Transport Phenomena in Multiphase Systems*, Elsevier, Burlington, MA.
- Fukuda, K. & Kobori, T., 1979. Classification of two-phase flow stability by density-wave oscillation model. *Nuclear Science and Technology*, Volume 16, pp. 95-108.
- Gebhart, B., Jaluria, Y. & Sammakia, R., 1988. Buoyancy-induced flows and transport. *Hemisphere Publishing Corporation*, Volume 221, pp. 689-695.
- Goldberg, S. & Rosner, R., 2011. Nuclear reactors: generation to generation. *The American Academy of Arts and Sciences*, Volume I, pp. 3-17.

- Grief, R., 1988. Natural circulation loops. *ASME J. Heat Transfer*, Volume 110, pp. 1243-1258.
- Grief, R., Zvirin, Y. & Mertol, A., 1979. The transient and stability behavior of a natural convection loop. *ASME J. Heat Transfer*, Volume 101, pp. 684-688.
- Guanghai, S., Dounan, J., Fukuda, K. & Yujun, G., 2002. Theoretical and experimental study on density wave oscillation of two-phase natural circulation of low equilibrium quality. *Nuclear Engineering and Design*, 215(3), pp. 187 - 198.
- Guo, X. et al., 2015. Numerical simulation of the transient behaviors in an open natural circulation system with large scale. *Annals of Nuclear Energy*, Volume 77, pp. 83-93.
- Haider, S., Joshi, Y. & Nakayama, W., 2002. A natural circulation model of the closed loop, two-phase thermosyphon for electronics cooling. *Journal of Heat transfer*, Volume 124, pp. 881 - 890.
- Hernandez-perez, V., Zangana, M., Kaji, R. & Azzopardi, B., 2010. *Effect of pipe diameter on pressure drop in vertical two-phase flow*. Tampa, International Conference on Multiphase Flow (ICMF).
- Hewitt, J., 1982. *Thermopedia*. [Online]
Available at: www.thermopedia.com/content/37
[Accessed 23 April 2017].
- Hsu, J., Ishii, M. & Hibiki, T., 1988. Experimental study on two-phase natural circulation and flow termination in a loop. *Nuclear Engineering and Design*, Volume 186, pp. 395-409.
- IAEA, 1991. *Safety related terms for advanced nuclear plants*, Vienna: IAEA-TECDOC-626.
- IAEA, 1993. *37th IAEA General conference; strengthening nuclear safety through the early conclusion of nuclear safety convention*. Vienna, IAEA.
- IAEA, 2000. *Heat Transport and afterheat removal for gas cooled reactors under accident conditions*, Vienna: TECDOC-1162, IAEA.
- IAEA, 2005. *Natural circulation in water cooled nuclear power point*, Vienna: IAEA-TECDOC-1162.
- IAEA, 2009. *Nuclear fuel cycle information system*, Vienna: IAEA-TECDOC-1613.
- IAEA, 2009. *Passive safety systems and natural circulation in water cooled nuclear power plants*, Vienna: TECDOC-1624, IAEA.
- IEE (Institution of Electrical Engineers), 2005. *Nuclear reactor types*, London: The Institution of Electrical Engineers.

- IWGAT (International Working Group on Advanced Technology), 1989. *Passive safety features in current and future water cooled reactors*. Moscow, IAEA.
- Kamal, M. A., 2012. An overview of passive cooling techniques in buildings: design concept and architectural interventions. *Acta Technica Napocensis: Civil Engineering & Architecture*, 55(1), pp. 85-87.
- Kays, W., 1955. Numerical solution for laminar flow-heat transfer in circular tubes. *Trans. ASME*, Volume 77, pp. 1265 - 1274.
- Kerswell, R., 2005. Recent progress in understanding the transition to turbulence in a pipe. *Nonlinearity*, Volume 18, pp. 17-44.
- Kew, P. & Cornwell, K., 1997. Correlations for the prediction of boiling heat transfer in small-diameter channels. *Applied Thermal Engineering*, 17(8-10), pp. 705-715.
- Khodabandeh, R. & Palm, B., 2002. Influence of system pressure on the boiling heat transfer coefficient in a closed two-phase thermosyphon loop. *International Journal of thermal sciences*, Volume 41, pp. 619-624.
- Knaai, A. & Zvirin, Y., 1990. Investigation of a two-phase natural circulation loop, Proc. *Int. Heat Transfer Conf.*, Jerusalem, Volume 1, pp. 395-400.
- Knaai, A., Zvirin, Y., 1993. Bifurcation phenomenon in two-phase natural circulation, *Int. J. Multiphase Flow*, 1993, Volume 19 (6), pp. 1129-1151.
- Kolev, N.I., 2011. Boiling of subcooled liquid, In: *Multiphase flow dynamic 3*, Springer, Berlin, pp. 195-205.
- Kroger, D., 1998. Heat Transfer in Ducts. In: S. University, ed. *Air-cooled heat exchangers and cooling towers*. Stellenbosch: Matieland, pp. 3.2.1 - 20.
- Kroger, D., 1998. Pressure drop in two phase flow. In: *Air-cooled heat exchangers and cooling towers*. Stellenbosch: University of Stellenbosch, pp. 2.7.13-15.
- Lee, S. & Rhi, S., 2000. *Lumped and sectorial (flow pattern) methods for computer simulation of a two-phase natural circulation loop*. Chiang Mai, Proceedings of the 6th International Heat Pipe symposium.
- Makhijani, A., 2001. The pebble bed modular reactor. *Science for Democratic Action*, 9(Energy & Security Issue #18), pp. 14-15.
- Manera, A., 2003. *Experimental and analytical investigations on flashing induced instabilities in natural circulation two-phase systems*, Deft: PhD Thesis, Deft University of Technology.

- Mills, A. & Ganesan, V., 2009. Convection fundamentals and correlations. In: *Heat Transfer, 2nd edition*. New Delhi: Pearson Education, pp. 250-255.
- Mills, A. & Ganesan, V., 2015. Forced-convection boiling and condensation; Pressure drop. In: *Heat Transfer*. Delhi, India: Pearson Education, pp. 616-632.
- Nayak, A. et al., 2003. Study on the flow-pattern-transition instability in a natural circulation heavy water moderated boiling light water cooled reactor. *Nuclear Engineering and Design*, 225(2-3), pp. 159-172.
- Nayak, A. et al., 1995. Mathematical modelling of the stability characteristics of a natural circulation loop. *Mathematical and Computer Modelling*, 22(9), pp. 77-87.
- Nayak, A. & Vijayan, P., 2008. Flow Instabilities in Boiling Two-Phase Natural Circulation Systems: A Review. *Science and Technology of Nuclear Installations* (<http://dx.doi.org/10.1155/2008/573192>)
- NEA (Nuclear Energy Agency), 2002. Advanced nuclear reactor safety issues and research needs. *Workshop Proceedings, Paris, France*, 18-20 February, pp. 14-16.
- NEI, 2015. *Nuclear Energy Institute*. [Online]
Available at: www.nei.org/Knowledge-Center/nuclear-Statistics/Workshop-Statistics
[Accessed 2017 April 2017].
- NuclearEnergy, O., 2004. *U.S. Department of Energy*. [Online]
Available at: <http://nuclear.energy.gov/genIV/neGenIV1.html>
[Accessed 6 February 2017].
- OECD, Nuclear Energy Agency, 2011. *world-nuclear*. [Online]
Available at: <http://www.world-nuclear.org/information-library/nuclear-fuel-cycle/nuclear-power-reactors/nuclear-power-reactors.aspx>
[Accessed 08 April 2017].
- PBMR, 2017. *Power generation*. [Online]
Available at: www.pbmr.co.za
[Accessed 10 April 2017].
- Petelin, S. & Bostjan, K., 1998. Prediction of void fraction in subcooled flow boiling. *Nuclear Energy in Central Europe*, Catez
- Pioro, I., Duffey, R., Kirillov, P. & Panchal, R., 2016. The safety of advanced reactors. In: I. L. Pioro, ed. *Handbook of Generation IV Nuclear Reactors*. Cambridge: Elsevier, pp. 1-30; 37-50.
- Premoli, A., Francesco, D. & Prina, A., 1970. An empirical correlation for evaluating two-phase mixture density under adiabatic conditions. *European Two-Phase Flow Group Meeting*

- Ravnik, M., 1991. *Nuclear safety parameters of mixed TRIGA cores*, s.l.: World Scientific.
- Royen, J., 2002. *Advanced reactors:safety issues and research needs*, Paris: NEA.
- Ruppersberg, J., 2008. *The reactor cavity cooling of a pebble bed modular reactor*, Stellenbosch University: Master of Science in Mechanical Engineering Thesis, Stellenbosch .
- Ruppersberg, J. & Dobson, R., 2007. Flow and heat transfer in a closed loop thermosyphon Part II - experimental simulation. *Journal of Energy in Southern Africa*, Volume 3, pp. 41 - 48.
- Ruppersberg, J. & Dobson, R., 2007. Flow and heat transfer in a closed loop thermosyphon - experimental and simulation. *Journal of Energy in Southern Africa*, 18(3), pp. 41 - 48.
- Sardeshpande, M. & Ranade, V., December 2013. Two-phase flow boiling in small channels: a brief review. *Sadhana*, Volume 38, Part 6, pp. 1083-1126.
- Schlunder, E., 1972. *Einführung in die Wärme*, Braunschweig: Vieweg.
- Senda, F., 2012. *Aspects of waste heat recovery and utilisation (WHR&U) in pebble bed modular Reactor (PBMR) Technology*, Stellenbosch: MSc Thesis, Stellenbosch University.
- Senru, Z., 1988. *Safety category and inherent safety for water-cooled reactor*. VÄSTERAS, IAEA, pp. 89-97.
- Shah, R., 1975. *Thermal entry length solutions for circular tube and parallel plates*. Bombay, Proc 3rd Natl. Heat Mass Transfer Conf., Indian Inst.
- Sha, W., Chien, T., Sun, J. & Chao, B., 2004. Analysis of large-scale tests for AP-600 passive containment cooling system. *Nuclear Engineering and Design*, Volume 232, pp. 197-216.
- Sherry, A., Howarth, P., Kearns, P. & Waterman, N., 2010. *A review of the UK's nuclear R&D capability*, London: Authority of the House of Lords.
- Shih, Y., 2009. Basic equation in integral form for a control volume. *Fluid mechanics*, Spring.
- Sinha, R. & Kakodkar, A., 2006. Design and development of the AHWR - the indian thorium fuelled innovative nuclear reactor. *Nuclear Engineering and Design*, Volume 236, pp. 683-700.
- Sittmann, I., 2010. *Inside-pipe heat transfer coefficient characterisation of a one third height scale model of a natural loop suitable for reactor cavity cooling system of the PMBR*, Stellenbosch: MSc Thesis, Stellenbosch University.

- Stenning, A., & Martin, C., 1968. An Analytical and Experimental Study of Air-Lift Pump Performance, *ASME J. Eng. Power*. Volume 90, pp. 106-110.
- Stephan, K. & Abdelsalam, M., 1980. Heat-transfer correlations for natural convection boiling. *International Journal of Heat and Mass Transfer*, 23(1), pp. 73-87.
- Sutharshan, B., Mutyala, M., Vijuk, R. & Mishra, A., 2011. The AP1000TM reactor passive safety and modular design. *Energy Procedia*, Volume 7, pp. 293-302.
- Taylor, J., 1997. An Introduction to Error Analysis: The Study of Uncertainties in Physical Measurements, 2d Edition, University Science Books.
- Thome, J., 2011. Fundamentals of void fraction in two-phase flows. *Ecole Polytechnique de Lausanne*,
- Torrance, K., 1979. Open-loop thermosyphons with geological application. *ASME J. Heat Transfer*, Volume 101, pp. 677-683.
- Tsukahara, T., Seki, Y., Kawamura, H. & Tochio, D., 2014. DNS of turbulent channel flow at very low Reynolds numbers, *arXiv*, Tokyo
- Tuma, PE., 2006. Evaporator/boiler design for thermosyphons utilising segregated hydrofluoroether working fluids, IEEE semi-therm symposium.
- US-DOE United States Department of Energy, 2011. *www.energy.gov*. [Online] Available at: <https://energy.gov/node/28891/genIV/neGenIV1.html> [Accessed 10 April 2017].
- Van Staden, M., 2001. *Analysis of effectiveness of the PBMR cavity cooling system*, Potchefstroom: South Africa: PBMR Ltd(Pty).
- Vijayan, P., Sharma, M. & Pilkwal, D., 2013. *Steady state and stability characteristics of a supercritical pressure natural circulation loop (SPNCL) with CO₂*, Mumbai: Bhabha Atomic Research Center Report BARC/2013/003.
- Vijayan, P. & Nayak, A., 2010. *Introduction to instabilities in natural circulation systems*, Trieste: In: IAEA Training Course on Natural Circulation Phenomena and Passive Safety Systems in Advanced Water-cooled Reactors, ICTP.
- Vijayan, P., Kamble, M., Nayak, A., Vaze, K. & Sinha, R., 2013. Safety features in nuclear power plants to eliminate the need of emergency planning in public domain, *Indian Academy of Science*, Sadhana, Volume 38, pp. 925-943.
- Vincent, C. & Kok, J., 1992. Investigation of the overall transient performance of the industrial two-phase closed loop thermosyphon. *International Journal of Heat and Mass Transfer*, 36(6), pp. 1419-1426.

- Welander, P., 1967. On the oscillatory instability of a differentially heated loop. *Journal of Fluid Mechanics*, 20(1), pp. 17-30.
- Whalley, P., 1987. *Boiling, condensation and gas-liquid flow*, Oxford: Clarendon Press..
- White, F. (2006). *Viscous Fluid Flow* 3rd Edition. McGraw-Hill.
- William, K., Crawford, M. & Weigand, B., 2005. *Convective heat and mass transfer*, 4th edition, Singapore, McGraw-hill international edition
- WNO (World Nuclear Association, 2017). *Small nuclear power reactors*, Toronto: World Nuclear Association (<http://www.worl-nuclear.org>).
- Yadigaroglu, G. & Lahey, J. R., 1975. *A Lagrangian analysis of two-phase hydrodynamic and nuclear-coupled density wave oscillations*. Tokyo, Fifth International Heat transfer Conference.
- Yeo, J., Yamashita, S., Hayashida, M. & Koyama, S., A loop thermosyphon type cooling system for high heat flux, *Journal of Electronics Cooling and Thermal control*, Volume 4, pp. 128-137.
- Yang, R., Liu, R., Zhong, Y. & Liu, T., 2006. Experimental study on convective heat transfer of water flow in a heated tube under natural circulation. *Nuclear Engineering and Design*, Volume 236, pp. 1902 - 1908.
- Yilmaz, T., 1991. Computer simulation of two-phase flow thermosyphon solar water heating system. *Energy Conversion and Management*, 32(2), pp. 133 - 144.
- Zhang, W., Hibiki, T. & Mishima, K., 2010. Correlations of two-phase frictional pressure drop and void fraction in mini-channel. *International Journal of Heat and Mass Transfer*, Volume 53, pp. 453-465.

APPENDIX A THERMOPHYSICAL PROPERTIES OF MATERIALS

A.1 Properties of water

Thermophysical properties of saturated water vapor and water liquid from 273.15K to 380K, Kröger (1998)

Water

, vapor pressure:

$$P_v = 10^z \text{ N/m}^2 \quad (\text{A.1})$$

$$z = 10.795861(1 - 273.17/T) + 5.02808 \log_{10}(273.16/T) \\ + 1.50474x10^{-4}[1 - 10^{-8.29692\{(T/273.16)-1\}}] \\ + 4.2873x10^{-4}[10^{4.76955(1-273.16/T)} - 1] + 2.786118312$$

Water vapor specific heat:

$$c_{p,v} = 1.3605x10^3 + 2.31334T \\ - 2.46784x10^{-10}T^5 + 5.91332x10^{-16}T^6 \quad (\text{A.2})$$

Water vapor dynamic viscosity:

$$\mu_v = 2.562435x10^{-6} + 1.816683x10^{-8}T + 2.579066x10^{-11}T^2 \\ - 1.067299x10^{-14}T^3 \quad (\text{A.3})$$

Water vapor thermal conductivity:

$$k_v = 1.3046x10^{-2} - 3.756191x10^{-5}T + 2.217964x10^{-7}T^2 \\ - 1.111562x10^{-10}T^3 \quad (\text{A.4})$$

Water vapor density:

$$\rho_v = -4.062329056 + 0.10277044T - 9.76300388x10^{-4}T^2 \\ + 4.47520795x10^{-6}T^3 - 1.004596894x10^{-8}T^4 \\ + 8.9154895x10^{-12}T^5 \quad (\text{A.5})$$

Water vapor temperature:

$$T = 164.630366 + 1.832295x10^{-3}p_v + 4.27215x10^{-10}p_v^2 \\ + 3.738954x10^3p_v^{-1} - 7.01204x10^5p_v^{-2} + 16.161488 \ln p_v$$

$$-1.437169 \times 10^{-4} p_v \ln p_v \quad (\text{A.6})$$

Water liquid density:

$$\rho_l = \left(\frac{1.49343 \times 10^{-3} - 3.7164 \times 10^{-6} T + 7.09782 \times 10^{-9} T^2}{-1.90321 \times 10^{-20} T^6} \right)^{-1} \quad (\text{A.7})$$

Water liquid specific heat:

$$c_{p,l} = 8.15599 \times 10^3 - 2.80627 \times 10 T + 5.11283 \times 10^{-2} T^2 - 2.17582 \times 10^{-13} T^6 \quad (\text{A.8})$$

Water liquid dynamic viscosity:

$$\mu_l = 2.414 \times 10^{247.8/(T-140)} \quad (\text{A.9})$$

Water liquid thermal conductivity:

$$k_l = -6.14255 \times 10^{-1} + 6.9962 \times 10^{-3} T - 1.01075 \times 10^{-5} T^2 + 4.74737 \times 10^{-12} T^4 \quad (\text{A.10})$$

A.2 Properties of loop's structure materials

- Heating elements

Two sizes of heating elements are used (Sittmann, 2010)

- Three 60.025 x 1.9 m heating elements are installed of 35Ω resistance and 1.5 kW rated power capability each
- One 225 x 850 mm heating element is installed with 105Ω resistance and 500 W rated power capability

- Copper pipes

At 300 K values for pure copper are (Mills, 2009):

- Density: 8933 kg/m³
- Specific heat: 0.385 KJ/kg.K
- Thermal conductivity: 401 W/mK

- Insulation material

Values for density, thermal conductivity and specific heat capacity of the B64-25 Ceramic Fibre were provided by the manufacturer, Thermal Ceramics UK Ltd, through a South African distributor, Cape Refractory Industries. Emissivity values for insulation material are found in Mills (1999), (Sittmann, 2010)

- Density: 64 kg/m^3
- Specific heat: 1.13 KJ/kg.K
- Thermal conductivity: 0.07 W/mK

- Glass

At 300 K values for pure copper are (Mills, 2009):

- Density: 2220 kg/m^3
- Specific heat: 0.745 KJ/kg.K
- Thermal conductivity: 1.38 W/mK

- Clear Polycarbonate (Cengel & Boles, 2014)

- Density: 64 kg/m^3
- Specific heat: 1.13 KJ/kg.K
- Thermal conductivity: 0.07 W/mK

A.3 Property functions

Table A-1 Saturated liquid specific internal energy u_f as a function of pressure

	$u_f = c_0 + c_1P + c_2P^2 + c_3P^3 + c_4P^4 + c_5P^5 + c_6P^6$ u_f in kJ/kg if P in kpa		
	$0.061 < P < 16.53$	$16.53 \leq P \leq 327.11$	$327.11 < P \leq 4111.97$
c_0	-51.1226157751	46.844529833265000	146.8445298333
c_1	102.0209601818	6.532811633588440	6.5328116336
c_2	-27.1553689066	0.076063530916023	-0.0760635309
c_3	4.4293810645	0.000570032965924	0.0005700330
c_4	-0.3975462815	-0.000002404987948	-0.0000024050
c_5	0.0181153216	0.000000005227374	0.0000000052
c_6	-0.0003266039	0.000000000004543	-0.0000000000

Table A-2 Saturated vapour specific internal energy u_g as a function of pressure

$u_g = c_0 + c_1P + c_2P^2 + c_3P^3 + c_4P^4 + c_5P^5 + c_6P^6$ u_g in kJ/kg if P in kpa			
	$0.5061 < P < 163$	$16.53 \leq P \leq 327.11$	$327.11 < P \leq 4111.97$
c_0	2358.1579797960	-0.0000000000014806505	2504.272669486530000000
c_1	33.4363477297	2.0623656318928900000	0.1717752935832960000
c_2	-8.9147174687	-0.0246750292382747000	-0.0001545079243937680
c_3	1.4531404289	0.0001854320539063890	0.0000000834158796614
c_4	-0.1303615077	-0.0000007831768285205	-0.0000000000259833654
c_5	0.0059384234	0.0000000017032285964	0.00000000000000042435
c_6	-0.0001070414	-0.0000000000014806505	-0.00000000000000000003

Table A-3 Saturated liquid density ρ_f as function of pressure

$\rho_f = c_0 + c_1P + c_2P^2 + c_3P^3 + c_4P^4 + c_5P^5 + c_6P^6$ ρ_f in kg/m ³ if P in kpa		
	$0.061 < P < 83.637$	$83.637 < P \leq 4111.97$
c_0	1.001232757E+03	9.7462483233E+02
c_1	-1.4934139621E+00	-1.8563005257E-01
c_2	4.5101215471E-02	1.8155246915E-04
c_3	1.0291970864E-03	1.1891680937E-07
c_4	1.385131118E-05	4.2788169665E-11
c_5	-9.8267145797E-08	-7.7879043171E-15
c_6	2.8281383615E-10	5.5972407274E-19

Table A-4 Saturated vapour density ρ_g as function of pressure

$\rho_g = c_0 + c_1P + c_2P^2 + c_3P^3 + c_4P^4 + c_5P^5 + c_6P^6 + c_7P^7 + c_8P^8 + c_9P^9 + c_{10}P^{10} + c_{11}P^{11} + c_{12}P^{12} + c_{13}P^{13} + c_{14}P^{14} + c_{15}P^{15} + c_{16}P^{16}$ ρ_g in kg/m ³ if P in kpa		
	$0.061 < P < 4111.97$	
c_0	0.00257852	
c_1	0.006536332	
c_2	-1.03322E-05	
c_3	5.27676E-08	
c_4	-1.80680E-10	
c_5	4.13859E-13	
c_6	-6.55818E-16	
c_7	7.40924E-19	
c_8	-6.09745E-22	
c_9	3.70293E-25	
c_{10}	-1.66754E-28	
c_{11}	5.54789E-32	
c_{12}	-1.34454E-35	

c_{13}	2.30584E-39	
c_{14}	-2.64995E-43	
c_{15}	1.82982E-47	
c_{16}	-5.73680E-52	

Table A-5 Saturated temperature T_{sat} as a function of pressure

$u_f = c_0 + c_1P + c_2P^2 + c_3P^3 + c_4P^4 + c_5P^5 + c_6P^6$ u_f in kJ/kg if P in kpa			
	$0.061 < P < 16.53$	$16.53 \leq P \leq 327.11$	$327.11 < P \leq 4111.97$
c_0	-1.2133791931E+01	3.5056654728E+01	9.5805436011E+01
c_1	2.4219031307E+01	1.56324542296E+00	+1.5957346907E-01
c_2	-6.4228657264E+00	-1.8237112219E-02	-1.2408184883E-04
c_3	1.0458389499E+00	1.3667691171E-04	1.367691171E-04
c_4	-9.3775141201E-02	-5.7663295221E-07	-2.04389571188E-11
c_5	4.27005211636E-03	1.2533171143E-09	3.3262325892E-15
c_6	-7.6962116033E-05	-1.0891455981E-12	2.1950298662E-19

Table A-6 Subcooled liquid density ρ as function of specific internal energy and pressure

$\rho = c_1 + c_2u + c_3u^2 + c_4P + c_4P^2 + c_5P^2 + c_6uP + c_7u^2P + c_8uP^2 + c_9u^2P^2$ ρ in kg/m ³ if u in kJ/kg and P in kpa		
	$0.061 < P < 4111.97$ kPa and $29.43 < u < 1090.27$ kJ/kg	
c_1	0.006536332	
c_2	-1.03322E-05	
c_3	5.27676E-08	
c_4	-1.800680E-10	
c_5	4.13859E-13	
c_6	-6.55818E-19	
c_7	7.40924E-19	
c_8	-6.09745E-22	
c_9	3.70293E-25	

Table A-7 Subcooled temperature T as a function of specific internal energy and pressure

$T = c_1 + c_2u + c_3u^2 + c_4P + c_4P^2 + c_5P^2 + c_6uP + c_7u^2P + c_8uP^2 + c_9u^2P^2$ T in °C if u in kJ/kg and P in kpa		
	$0.061 < P < 4111.97$ kPa and $29.43 < u < 1090.27$ kJ/kg	
c_1	0.006536332	
c_2	-1.03322E-08	
c_3	5.27676E-08	
c_4	-1.80680E-10	
c_5	4.13859E-13	
c_6	-6.55818E-16	
c_7	7.40924E-19	

c_8	-6.09745E-22	
c_9	3.70293E-25	

Table A-0-8 Superheated temperature T as a function of specific internal energy and pressure

$T = c_1 + c_2u + c_3u^2 + c_4P + c_4P^2 + c_5P^2 + c_6uP + c_7u^2P + c_8uP^2 + c_9u^2P^2$ T in °C if u in kJ/kg and P in kpa		
0.061 < P < 4111.97 kPa and 29.43 < u < 1090.27 kJ/kg		
c_1	0.006536332	
c_2	-1.03322E-05	
c_3	5.27676E-08	
c_4	-1.80680E-10	
c_5	4.13859E-13	
c_6	-6.55818E-16	
c_7	7.40924E-19	
c_8	-6.09745E-22	
c_9	3.70293E-25	

Table A-0-9 Liquid viscosity μ_l as function of temperature

$\mu_f = c_0 + c_1T + c_2T^2 + c_3T^3 + c_4T^4 + c_5T^5 + c_6T^6$ μ_f in kg/ms if T in °C		
c_0	1.7699E-03	
c_1	-5.2826E-05	
c_2	9.0025E-07	
c_3	-8.8006E-09	
c_4	4.7856E-11	
c_5	-1.3362E-13	
c_6	1.4878E-16	

Table A-0-10 Vapour dynamic viscosity μ_v as a function of temperature

$\mu_f = c_0 + c_1T + c_2T^2$ μ_v in kg/ms if T in °C		
c_0	9.1242E-06	
c_1	2.9931E-08	
c_2	1.4879E-11	

Table A-11 Saturated pressure P_{sat} as a function of temperature

$P_{sat} = c_0 + c_1T + c_2T^2 + c_3T^3 + c_4T^4 + c_5T^5 + c_6T^6 + c_7T^7 + c_8T^8 + c_9T^9$ $+ c_{10}T^{10} + c_{11}T^{11} + c_{12}T^{12} + c_{13}T^{13} + c_{14}T^{14} + c_{15}T^{15}$ $+ c_{16}T^{16}$ P in kpa if T in °C		
0.01 < T < 252		
c_0	0.611212951	
c_1	0.044418033	

c_2	0.001430598	
c_3	2.64902E-05	
c_4	3.022592E-07	
c_5	2.08279E-09	
c_6	6.51325E-12	
c_7	-9.96032E-15	
c_8	-1.17130E-16	
c_9	-3.89616E-19	
c_{10}	8.90392E-21	
c_{11}	-4.83077E-23	
c_{12}	1.38120E-25	
c_{13}	-2.13181E-28	
c_{14}	1.15491E-31	
c_{15}	1.20129E-34	
c_{16}	-1.53740E-37	

Table A-12 Saturated temperature T_{sat} as a function of saturated specific internal energy

$T_{sat} = c_0 + c_1u_f + c_2u_f^2 + c_3u_f^3 + c_4u_f^4 + c_5u_f^5 + c_6u_f^6 + c_7u_f^7 + c_8u_f^8 + c_9u_f^9$ $+ c_{10}u_f^{10} + c_{11}u_f^{11} + c_{12}u_f^{12} + c_{13}u_f^{13} + c_{14}u_f^{14} + c_{15}u_f^{15}$ $+ c_{16}u_f^{16} \quad T_{sat} \text{ in } ^\circ\text{C if } u_f \text{ in kJ/kg}$		
$0.0 < u_f < 1090.27$		
c_0	0.019752569	
c_1	0.23589048	
c_2	6.66166E-05	
c_3	-1.02046E-06	
c_4	1.11601E-08	
c_5	-8.40511E-11	
c_6	4.44253E-13	
c_7	-1.69203E-15	
c_8	4.73321E-18	
c_9	-9.83571E-21	
c_{10}	1.52395E-23	
c_{11}	-1.752395E-23	
c_{12}	1.47413E-29	
c_{13}	-8.80502E-33	
c_{14}	3.53546E-36	
c_{15}	-8.55373E-40	
c_{16}	9.42042E-44	

Table A-13 Surface tension σ as a function of temperature

$\sigma = c_0 + c_1T + c_2T^2$ σ in N/m if T in $^{\circ}\text{C}$ [$R^2 = 1.0000$]		
c_0	7.573636E-02	
c_1	-1.458939E-04	
c_2	-2.234848E-11	

APPENDIX B CONSERVATION OF THERMAL ENERGY EQUATION

The conservation of energy as applied to a stationary control volume through which a fluid is moving may take on a number of equally applicable forms (Bird, Stewart and Lightfoot, 2000). In this appendix it is shown how the one-dimensional conservation of energy equation is derived in terms of the internal energy from the more commonly used total energy equation.

The total energy equation is given, using vector and tensor notation (Bird, Stewart and Lightfoot, 2000) as

$$\frac{\partial}{\partial t}(\rho(u + v^2/2)) + [\nabla \cdot \rho v(u + v^2/2)] = \dot{Q}_{ht}''' + \rho(\mathbf{v} \cdot \mathbf{g}) - (\nabla \cdot p\mathbf{v}) - (\nabla \cdot [\boldsymbol{\tau} \cdot \mathbf{v}]) \quad [\text{N/m}^3] \quad (\text{B.1})$$

Note that the potential energy term is included not in the left hand terms but as a term of its own on the right hand side. Another form of the energy equation, the so-called mechanical energy equation, is obtained by taking the momentum equation given as

$$\frac{\partial}{\partial t}(\rho\mathbf{v}) + [\nabla \cdot \rho\mathbf{v}\mathbf{v}] = -\nabla p + \rho\mathbf{g} - (\nabla \cdot p) - [\nabla \cdot \boldsymbol{\tau}] \quad [\text{N/m}^3] \quad (\text{B.3})$$

and forming the scalar product of equation B.3 and the velocity vector \mathbf{v} , that is

$$\frac{\partial}{\partial t}(\rho\mathbf{v}) \cdot \mathbf{v} + [\nabla \cdot \rho\mathbf{v}\mathbf{v}] \cdot \mathbf{v} = -\nabla p \cdot \mathbf{v} + \rho\mathbf{g} \cdot \mathbf{v} - (\nabla \cdot p) \cdot \mathbf{v} - [\nabla \cdot \boldsymbol{\tau}] \cdot \mathbf{v} \quad [\text{W/m}^3] \quad (\text{B.4})$$

After rearranging and making use of the continuity equation

$$\frac{\partial \rho}{\partial t} = -\nabla \cdot (\rho\mathbf{v}) \quad [\text{kg/sm}^3] \quad (\text{B.5})$$

and the identities

$$(\nabla \cdot p) \cdot \mathbf{v} = (\nabla \cdot p\mathbf{v}) - p(\nabla \cdot \mathbf{v})$$

$$[\nabla \cdot \boldsymbol{\tau}] \cdot \mathbf{v} = \nabla \cdot [\boldsymbol{\tau} \cdot \mathbf{v}] - (\boldsymbol{\tau} : \nabla \mathbf{v})$$

$$\frac{\partial}{\partial t}(\rho\mathbf{v}) \cdot \mathbf{v} = \frac{\partial}{\partial t} \left(\frac{1}{2} \rho v^2 \right), \text{ and}$$

$$[\nabla \cdot \rho\mathbf{v}\mathbf{v}] \cdot \mathbf{v} = (\nabla \cdot \frac{1}{2} \rho v^2 \mathbf{v})$$

equation B4 may be written as equation B.6, the so-called *mechanical energy equation*, as

$$\begin{aligned} \frac{\partial}{\partial t} \left(\frac{1}{2} \rho v^2 \right) = & - \left(\nabla \cdot \frac{1}{2} \rho v^2 \mathbf{v} \right) - \nabla(p \cdot \mathbf{v}) + \rho(\mathbf{v} \cdot \mathbf{g}) - p(-\nabla \cdot \mathbf{v}) \\ & - (\nabla \cdot [\boldsymbol{\tau} \cdot \mathbf{v}]) - (-\boldsymbol{\tau} : \nabla \mathbf{v}) \quad [\text{W/m}^3] \end{aligned} \quad (\text{B.6})$$

Now, subtracting the mechanical energy equation, equation B.6 from the total energy equation, equation B.1 yields the so-called equation for *internal energy* or the *thermal energy equation* [that is that internal energy may be expressed as a function, more-or-less proportional, to the temperature.] as

$$\frac{\partial}{\partial t} (\rho \mathbf{u}) = -\nabla \cdot \rho u \mathbf{v} + \dot{Q}_{ht}''' - p(-\nabla \cdot \mathbf{v}) - (\boldsymbol{\tau} : \nabla \mathbf{v}) \quad [\text{W/m}^3] \quad (\text{B.7})$$

or, for one dimensional flow

$$\frac{\partial}{\partial t} (\rho \mathbf{u}) = -\frac{\partial}{\partial z} (\rho u v) + \dot{Q}_{ht}''' - p \frac{\partial v}{\partial z} - \tau_{rz} \frac{\partial v_z}{\partial r} \quad [\text{W/m}^3] \quad (\text{B.8})$$

The term $[-\nabla \cdot \rho u \mathbf{v}]$ is the net addition of internal energy by convective transport, per unit volume. By addition is meant that internal energy carried into the control volume increases its internal energy and is taken as positive and internal energy carried out decreases its internal energy and hence is taken as negative. The term $+\dot{Q}_{ht}'''$ is the net rate of increase in internal energy by conduction from the adjacent control volumes and conduction and convective heat transfer from the boundary into the fluid in the control volume, per unit volume. The heat transfer is necessarily driven from a higher to lower temperature; the heat transfer is thus positive when it flows, so to speak, into the control volume and negative if it flows out of the control volume. The term $[-p(-\nabla \cdot \mathbf{v})]$ is the so-called *irreversible* rate at which the internal energy of a Newtonian fluid is increased due to viscous dissipation (another word for the work done against friction) and hence is necessarily always positive and always increases the internal energy and thus always manifests itself as an increase in temperature of the fluid in control volume, all else being equal.

Equation B.8 for a finite sized one-dimensional control volume of constant cross-sectional area A , radius R and length Δz

$$\frac{\Delta}{\Delta t} (m \mathbf{u}) = -\Delta(\dot{m} u) + \dot{Q}_{ht} - p A_x \nabla v - \bar{\tau}_w A_z \bar{v} \quad [\text{W}] \quad (\text{B.9})$$

Where $A = \pi R^2$, $A_z = \wp \Delta z$, and the perimeter $\wp = 2\pi R$ and $\tau_{rz@r=R} = \bar{\tau}_w$ the so-called wall stress and \bar{v} is the average velocity long its length Δz .

APPENDIX C NUMERICAL SIMULATION ALGORITHM

The numerical simulation to solve the natural circulation loop of this project is given step-wise as follow:

Step 1 Referring to figure 3.2 define the geometry of the loop consisting of a series of cylindrical control volumes

Defining dimensions

$$L_1 = 8 : L_2 = 7 : L_3 = L_1 : L_2 = L_4$$

$$OD = 0.035 : ID = 0.032$$

$$h_{tank} = 12$$

Control volume numbers

$$N_1 = 2 : N_2 = 10 : N_3 = 2 : N_4 = 3$$

$$N_{11} = N_1 : N_{12} = N_1 + N_2 : N_{13} = N_1 + N_2 + N_3 : N_{tot} = N_{14} = N_1 + N_2 + N_3 + N_4$$

Control volume lengths

$$\Delta L_1 = L_1/N_1 : \Delta L_2 = L_2/N_2 : \Delta L_3 = L_3/N_3 : \Delta L_4 = L_4/N_4$$

Step 2 Define the initial values and heat pipe parameters

$$T_{amb} = 20 : T_{beginRHS} = 19.5 : T_{beginLHS} = 20$$

$$x_{begin} = 0 : ALPHA_{begin} = 0 : MDOT (\dot{m}) = 0 : QDOT (\dot{Q}) = 0$$

Heat pipe heat exchanger

$$U_{hp} = 250 : T_{hpc} = 20$$

Step 3 Define the problem-specific constants and stability criteria

$$\Delta Time = 0.1 : SF = 250 : GIPPOF1 = 1 : GIPPOF2 = 1 : GIPPOF3 = 1 :$$

$$GippoHOMOff = 2.5$$

1 Start the time-step loop

$$t = t + \Delta t \tag{C.1}$$

$$u_{i=0} = u_{i=N_{tot}} : u_{N_{tot}+1} = u_{i=1} \tag{C.2}$$

if $\dot{m}^t \geq 0$ then

Estimate the new mass and pressure

$$\begin{aligned} \text{For } i = 1 \text{ to } N_{tot} : m_i^{t+\Delta t} &= m_i^t + \Delta t \left(\frac{\Delta m}{\Delta t} \right)_i^{t-\Delta t/2} : P_i^{t+\Delta t} = \\ P_i^t + \Delta t \left(\frac{\Delta P}{\Delta t} \right)_i^{t-\Delta t/2} : &\text{next } i \end{aligned} \quad (\text{C.3})$$

The new mass can also be determine using $m_i^{t+\Delta t} = m_i^t + \Delta t(\dot{m}_{in} - \dot{m}_{out})_i^t$

Calculate the total heat

The total heat is evaluated based by the total reactor heat input minus the total heat removal or losses from the environment and heat removed by the pipe in pipe heat exchangers.

Heat losses to the environment

Calculate the heat transfer coefficients for control volumes 1 to N_{tot}

For $i = 1$ to N_{tot}

$$h_i = 5 : R_i = 1/h_i A Z_i$$

$$k_w = 18 : t_w = R_{wo} - R_{wi} : A Z_w = (A Z_{wi} + A Z_{wo})/2 : R_w = t_w/k_w A Z_w$$

$$k_{ins} = 0.5 : t_{ins} = R_{inso} - R_{insi} : A Z_{ins} = (A Z_{insi} + A Z_{inso})/2 : R_{ins} = \frac{t_{ins}}{k_{ins} A Z_{ins}}$$

$$h_0 = 5 : R_i = \frac{1}{h_0 A Z_0}$$

Calculate thermal resistances

$$R_i = R_i + R_w + R_{ins} + R_0 \quad (\text{C.4})$$

Calculate the heat losses

$$\dot{Q}_{loss,i} = (T_i - T_a)/R_i \quad (\text{C.5})$$

Next i

Heat removal by Heat exchanger

$$\dot{Q}_{hp} = (T_{in} - T_{out})/R_{hp} : \dot{Q}_{loss,1} = \dot{Q}_{loss,1} + \dot{Q}_{hp} \quad (\text{C.6})$$

Heat transfer rates for each control volume

For $i = 1 : \dot{Q}_i = -\dot{Q}_{loss,i}$

Change in internal energy due to convection

$$(-\Delta\dot{m}u)_i^t = -\dot{m}^t(u_i - u_{i-1})_i^t$$

Reversible work rate terms

$$\rho_{h,i}^t = ((x/\rho_v + (1-x)/\rho_l)_i^t)^{-1}$$

$$\rho_{h,i-1}^t = ((x/\rho_v + (1-x)/\rho_l)_{i-1}^t)^{-1}$$

$$\left(\frac{P}{\rho_h}\right)_{i,out}^t = \frac{P_{i+1/2}^t}{\rho_{h,i}^t}$$

$$\left(\frac{P}{\rho_h}\right)_{i,in}^t = \frac{P_{i-1/2}^t}{\rho_{h,i-1}^t}$$

$$(-\Delta PAV)_i^t = -\dot{m} \left(\left(\frac{P}{\rho_h}\right)_{i,out}^t - \left(\frac{P}{\rho_h}\right)_{i,in}^t \right) \quad (C.7)$$

Irreversible work rate terms $\tau A_z v$

$$-\tau_{w,i}^t = -(\tau_{lo}\phi_{lo}^2)_i^t$$

$$\tau_{lo,i}^t = \left(C_{f,lo}\rho_l \left(\frac{\dot{m}}{\rho_l A}\right)^2 / 2 \right)_i^t$$

$$(\phi_{lo}^2)_i^t = f(X) \quad (C.8)$$

$$\rho_i^t = (\alpha\rho_v + (1-\alpha)\rho_l)_i^t$$

$$v_i^t = \frac{\dot{m}^t}{\rho_i^t A_i}$$

$$F_i^t = (\tau_{lo,i}\phi_{lo,i}^2\phi_i(\Delta Z_i + Z_{i,minor}))^t,$$

$$(Fv)_i^t = F_i^t v_i^t$$

Calculate the sum of the thermal energy terms

$$\sum \dot{E}_i^t = (-\Delta\dot{m}u)_i^t + \sum \dot{Q}_i^t + (-\Delta PAV)_i^t + (Fv)_i^t \quad (C.9)$$

Calculate the internal energy

$$u_i^{t+\Delta t} = [(mu)_i^t + \Delta t \sum \dot{E}_i^t] / m_i^{t+\Delta t} \quad (C.10)$$

Calculate the saturated liquid and vapour internal energies at the estimated new pressure

$$u_{f,i}^{t+\Delta t} = f(P_i^{t+\Delta t})$$

$$u_{g,i}^{t+\Delta t} = f(P_i^{t+\Delta t})$$

$$\text{If } u_i^{t+\Delta t} \leq u_{f,i}^{t+\Delta t} \text{ then } x_i^{t+\Delta t} = 0 : \alpha_i^{t+\Delta t} = 0 : T_i^{t+\Delta t} = f(u_i^{t+\Delta t}, P_i^{t+\Delta t}) : \\ \rho_i^{t+\Delta t} = (u_i^{t+\Delta t}, P_i^{t+\Delta t})$$

$$\text{If } u_i^{t+\Delta t} > u_{f,i}^{t+\Delta t} \text{ and } u_i^{t+\Delta t} \leq u_{g,i}^{t+\Delta t} \text{ then}$$

$$x_i^{t+\Delta t} = (u_i^{t+\Delta t} - u_{f,i}^{t+\Delta t}) / (u_{g,i}^{t+\Delta t} - u_{f,i}^{t+\Delta t})$$

$$T_i^{t+\Delta t} = f(P_{sat,i}^{t+\Delta t}) : \rho_{f,i}^{t+\Delta t} = f((P_{sat,i}^{t+\Delta t})) \text{ and } \rho_{g,i}^{t+\Delta t} = f(P_{sat,i}^{t+\Delta t})$$

$$SF = f(Re, Fr, We, d)$$

$$\alpha_i^{t+\Delta t} = \left(1 + SF \frac{\rho_{g,i}^{t+\Delta t}}{\rho_{f,i}^{t+\Delta t}} \frac{1-x_i^{t+\Delta t}}{x_i^{t+\Delta t}} \right)^{-1}$$

$$\rho_i^{t+\Delta t} = \alpha_i^{t+\Delta t} \rho_{g,i}^{t+\Delta t} + (1 - \alpha_i^{t+\Delta t}) \rho_{f,i}^{t+\Delta t}$$

$$m_i^{t+\Delta t} = \rho_i^{t+\Delta t} V_i$$

$$\left(\frac{\Delta m}{\Delta t} \right)_i^{t+\Delta t/2} = \frac{m_i^{t+\Delta t} - m_i^t}{\Delta t} \quad (C.11)$$

end if

$$\text{If } u_i^{t+\Delta t} > u_{g,i}^{t+\Delta t} : T_i^{t+\Delta t} = f(u_i^{t+\Delta t}, P_i^{t+\Delta t}) : \rho_i^{t+\Delta t} = (u_i^{t+\Delta t}, P_i^{t+\Delta t}) : x_i^{t+\Delta t} = \\ 1 \text{ and } \alpha_i^{t+\Delta t} = 1$$

Calculate the new mass flow rate $\dot{m}^{t+\Delta t}$

To evaluate the new mass the momentum equation for i^{th} control volume expressed in terms of the mass and void fractions is considered as given by equation 3.35. The mass flow rate at $t + \Delta t$ is obtained by summing all the control volumes around the loop. Using an explicit finite difference numerical solution method and the so-called *upwind differencing*, and noticing that the pressure terms all cancel out, required mass is given by

$$\dot{m}^{t+\Delta t} = [\dot{m}^t \sum M_i^t + \Delta t (\dot{m}^2 \sum MF + \sum G - \sum F)_i^t] / \sum M_i^{t+\Delta t} \quad (C.12)$$

Where

If the control volume is subcooled or superheated

$$M_i^{t+\Delta t} = \frac{(m/\rho)_i^{t+\Delta t}}{A_i^2}, M_i^t = \frac{(m/\rho)_i^t}{A_i^2} \text{ and } MF = \frac{1}{A_i} \left(\frac{1}{(A\rho)_j} - \frac{1}{(A\rho)_i} \right)^t \quad (C.13)$$

And for a two-phase liquid and vapour control volume

$$M_i^{t+\Delta t} = \frac{m_i^{t+\Delta t}}{A_i^2} \left(\frac{x^2}{\alpha \rho_g} + \frac{(1-x)^2}{(1-\alpha)\rho_f} \right)_i^{t+\Delta t}, M_i^t = \frac{m_i^t}{A_i^2} \left(\frac{x^2}{\alpha \rho_g} + \frac{(1-x)^2}{(1-\alpha)\rho_f} \right)_i^t \text{ and}$$

$$MF = \frac{1}{A_i} \left[\left(\frac{x^2}{\alpha \rho_v} + \frac{(1-x)^2}{(1-\alpha)\rho_l} \right)_j - \left(\frac{x^2}{\alpha \rho_v} + \frac{(1-x)^2}{(1-\alpha)\rho_l} \right)_i \right]^t, \text{ where } j = i - 1 \text{ if } \dot{m} \geq 0 \text{ or } j = i + 1 \text{ if } \dot{m} < 0 \quad (\text{C.14})$$

$$G = \rho_i^t \Delta z_i g \sin \theta_i \quad (\text{C.15})$$

Where $\rho = \alpha \rho_v + (1 - \alpha)\rho_l$, $\theta = \pi/2$ for the vertical LHS of the loop, that is the reactor side, $\theta = -\pi/2$ for the vertical RHS of the loop, that is the cooling side and $\theta = 0$ for the horizontally oriented portions of the circulation loop.

$$F = \wp \tau_i^t (\Delta z + z_{minor})_i / A_i \quad (\text{C.16})$$

where $\tau_i^t = \tau_{lo} \phi_{lo}^2$, $\tau_{lo} = \frac{1}{2} C_{f_{lo}} \rho_l \left(\frac{\dot{m}}{\rho_l A} \right)^2 = \frac{C_{f_{lo}}}{2 \rho_l A^2} \dot{m}^2$, and to ensure that the friction always acts against the flow \dot{m}^2 is replaced by $\dot{m}|\dot{m}$,

$$\phi_{lo}^2 = f(X), \wp = \pi d, X = \left(\frac{\rho_v}{\rho_l} \right)^{0.5} \left(\frac{\mu_l}{\mu_v} \right)^{0.5} \left(\frac{1-x}{x} \right)^{0.875} \text{ and}$$

if $Re < SS_1$ then $C_{f_{lo}} = 16/SS_1$

if $Re \geq SS_1$ and $Re \leq SS_2$ then $C_{f_{lo}} = 16/Re$

if $Re > SS_2$ then $C_{f_{lo}} = 0.079Re^{-0.25}$

Where $Re = \frac{\dot{m}^t |d_h}{\mu A}$, $\mu = f(T^t)$ and SS_1 is a correlating coefficient that attempts to identify the transition point between static and dynamic friction (viscosity) or the so-called concept of slip-stick, and SS_2 is a correlating coefficient that attempts to define the transition between laminar and turbulent flow conditions. They may be taken arbitrarily as 1 and 1181, respectively where 1181 is the Reynolds number corresponding to the intersection of the smooth wall Blasius type coefficient of friction $C_{f_{lo}} = 0.079Re^{-0.25}$ and the laminar coefficient of friction given as $C_{f_{lo}} = 16/Re$.

Calculate the new pressures $P_i^{t+\Delta t}$

The pressure at the bottom of the loop is the highest and is given by

$$P_{bottom} = \rho g h_{tank}$$

And the pressure at each control volume will then be

$$P_i = P_{i-1} + \rho g \Delta L_i$$

Having the new mass flow rate and the pressure at one end of the control volume, the pressure at other can be calculated using equation 3.43. Equation 3.43 can also be simplified as below

$$P_{out,i}^{t+\Delta t} = P_{in,i}^{t+\Delta t} + (MF)_i^{t+\Delta t} - G_i^{t+\Delta t} - F_i^{t+\Delta t} - \left(\frac{\Delta M}{\Delta t}\right)_i^{t-\Delta t/2}$$

$$\text{Where } P_{in,i}^{t+\Delta t} = P_{out,i-1}^{t+\Delta t}$$

If control volume is subcooled or superheated

$$M_i^{t+\Delta t} = \frac{(m\dot{m}/\rho)_i^{t+\Delta t}}{A_i^2}, M_i^t = \frac{(m\dot{m}/\rho)_i^t}{A_i^2} \text{ and } \left(\frac{\Delta M}{\Delta t}\right)_i^{t-\Delta t/2} = (M_i^{t+\Delta t} - M_i^t)/\Delta t$$

$$MF_i^{t+\Delta t} = \frac{(\dot{m}^{t+\Delta t})^2}{A_i} \left(\frac{1}{(A\rho)_j} - \frac{1}{(A\rho)_i} \right)^{t+\Delta t} \text{ where } j = i - 1 \text{ if } \dot{m} \geq 0 \text{ or } j = i + 1 \text{ if } \dot{m} < 0$$

If the control volume is a two-phase (liquid and vapour) control volume

$$M_i^t = \frac{(m)_i^t \dot{m}^t}{A_i^2} \left(\frac{x^2}{\alpha\rho_g} + \frac{(1-x)^2}{(1-\alpha)\rho_f} \right)_i^t \text{ and } M_i^{t+\Delta t} = \frac{(m)_i^{t+\Delta t} \dot{m}^{t+\Delta t}}{A_i^2} \left(\frac{x^2}{\alpha\rho_g} + \frac{(1-x)^2}{(1-\alpha)\rho_f} \right)_i^{t+\Delta t}$$

$$MF_i^{t+\Delta t} = \frac{(\dot{m}^{t+\Delta t})^2}{A_i} \sum \left[\left(\frac{x^2}{\alpha A \rho_g} + \frac{(1-x)^2}{(1-\alpha) A \rho_f} \right)_j - \left(\frac{x^2}{\alpha A \rho_g} + \frac{(1-x)^2}{(1-\alpha) A \rho_f} \right)_i \right]^t, \text{ where } j = i - 1 \text{ if } \dot{m} \geq 0 \text{ or } j = i + 1 \text{ if } \dot{m} < 0$$

$$G_i^{t+\Delta t} = \rho_i^{t+\Delta t} \Delta z_i g \sin \theta_i$$

Where $\rho = \alpha\rho_g + (1-\alpha)\rho_f$, $\theta = \pi/2$ for the vertical LHS of the loop, that is the reactor side, $\theta = -\pi/2$ for the vertical RHS of the loop, that is the cooling side and $\theta = 0$ for the horizontally oriented portions of the circulation loop.

$$F_i^{t+\Delta t} = \wp \tau_i^{t+\Delta t} (\Delta z + z_{minor})_i / A_i$$

where $\tau_i^{t+\Delta t} = (\tau_{lo} \Phi_{lo}^2)_i^{t+\Delta t}$, $\tau_{lo} = \frac{1}{2} C_{flo} \rho_l \left(\frac{\dot{m}}{\rho_l A} \right)^2 = \frac{C_{flo}}{2 \rho_l A^2} \dot{m} |\dot{m}|$, where to ensure that the friction always acts against the flow \dot{m}^2 is replaced by $\dot{m} |\dot{m}|$, $\Phi_{lo}^2 = f(X)$ and \wp = perimeter of the control volume, and

$$\text{if } Re < SS_1 \text{ then } C_{flo} = 16/SS_1$$

$$\text{if } Re \geq SS_1 \text{ and } Re \leq SS_2 \text{ then } C_{flo} = 16/Re$$

$$\text{if } Re > SS_2 \text{ then } C_{flo} = Re$$

$$\text{Where } Re = \frac{|\dot{m}^t| d_h}{\mu A} \text{ and } \mu = f(T^t)$$

The pressure of the control volume is then given as

$$P_i^{t+\Delta t} = (P_{in,i}^{t+\Delta t} + P_{out,i}^{t+\Delta t})/2$$

Replace the old values by the new values and go to “1”

APPENDIX D CALIBRATION OF EXPERIMENTAL MEASURING INSTRUMENTS AND ERROR ANALYSIS

D.1 Calibration of thermocouples

The accuracy of the thermocouples used in the experiments was verified by comparison with the calibrated sub-standard thermometer made of platinum (platinum resistance thermometer; PRT). The PRT model number 935-14-72 was manufactured by ISOTECH South Africa with serial number 191069 calibrated on the 4th February 2013 by Rapid Instrumentation cc with certificate number RAP15738 (See Figure D-6) and is used with an oil bath. Table D.1 shows the comparison for the 4 K-type thermocouple probes used to measure the temperatures of the working fluid Table D.2 shows the comparison for the nine K-type thermocouples used to measure the temperatures of the heater plate. Table D.3 shows the comparison for the eleven K-type thermocouples used to measure the cooling fluid in the pipe-in-pipe heat exchangers. The standard deviation for the K-type thermocouples at each of the measured points lies between 0.041 and 0.63 with a maximum error of 1.85 %.

Table D-1 Working fluid K-type thermocouples calibration

Reference	Temperature [°C]				SD	%error			
	TBL	TBR	TTL	TTR		TBL	TBR	TTL	TTR
20.152	20.23	20.41	20.30	20.3	0.095805	0.4118	1.290	0.7393	0.7393
30.203	30.6	30.60	30.3	30.3	0.188720	1.3144	1.344	0.3211	0.3211
40.126	40.2	40.2	40.1	40.2	0.050489	0.1844	0.184	0.0647	0.2093
48.231	48.4	48.6	48.54	48.6	0.158613	0.3503	0.765	0.6406	0.7650
53.265	53.68	53.34	53.5	53.4	0.15862	0.7791	0.150	0.4411	0.3510
60.213	60.5	60.5	60.5	60.4	0.126411	0.4766	0.476	0.4766	0.4434
66.501	66.1	66.3	66.23	66.4	0.163163	0.6029	0.302	0.4075	0.0766
74.357	74.56	74.6	74.52	74.2	0.151742	0.2730	0.326	0.2192	0.1573
80.85	81.23	81	80.9	80.7	0.179916	0.4700	0.185	0.0618	0.1113
85.61	86	86	85.97	86	0.171551	0.4555	0.455	0.4205	0.4555
90.234	89.94	89.95	89.9	89.7	0.190801	0.3258	0.314	0.3701	0.5917

Table D-2 Heating plates K-type thermocouples calibration

Reference	Temperature [°C]								
PRT	T1(A)	T1(B)	T1(C)	T2(A)	T2(B)	T2(C)	T3(A)	T3(B)	T3(C)
25.24	25.22	25.2	25.26	25.36	25.26	25.3	25.22	25.23	25.32
30.354	30.5	30.5	30.4	30.41	30.5	30.56	30.421	30.56	30.54
42.56	42.71	42.71	42.71	42.68	42.65	42.54	42.57	42.6	42.6
50.12	50.3	50.3	50.31	50.32	50.3	50.3	50.1	50.23	50.2
55.31	55.48	55.5	55.5	55.5	55.41	55.3	55.28	55.41	55.41
60.28	60.35	60.3	60.3	60.3	60.3	60.31	60.31	60.5	60.5
66.501	66.55	66.62	66.57	66.54	66.5	66.5	66.53	66.5	66.51
75.015	74.85	74.9	74.9	75.1	74.86	74.86	74.86	74.9	74.9
81.22	81.23	81.23	81.2	80.98	81.2	81.2	81.2	81.12	81.3
85.4	85.5	85.3	85.4	85.5	85.5	85.53	85.45	85.45	85.4
90.5	90.3	90.4	90.4	90.4	90.45	90.6	90.41	90.3	90.3

Temperature [°C]		SD	%error			
T4(A)	T4(B)		T1(A)	T1(B)	T1(C)	T2(A)
25.32	25.301	0.0500493	0.0792393	0.1584786	0.0792393	0.4754358
30.3	30.3	0.0947268	0.480991	0.480991	0.1515451	0.1844897
42.7	42.7	0.0659832	0.3524436	0.3524436	0.3524436	0.2819549
50.2	50.14	0.0812963	0.3591381	0.3591381	0.3790902	0.3990423
55.5	55.2	0.1040979	0.3073585	0.3435184	0.3435184	0.3435184
60.5	60.22	0.0964954	0.1161248	0.0331785	0.0331785	0.0331785
66.48	66.48	0.0411438	0.0736831	0.1789447	0.1037578	0.0586457
75.1	75.1	0.1025905	0.219956	0.1533027	0.1533027	0.1133107
81.2	81.12	0.0798104	0.0123122	0.0123122	0.0246245	0.2954937
85.38	85.52	0.0696039	0.117096	0.117096	0	0.117096
90.45	90.4	0.087434	0.2209945	0.1104972	0.1104972	0.1104972

%error						
T2(B)	T2(C)	T3(A)	T3(B)	T3(C)	T4(A)	T4(B)
0.0792393	0.2377179	0.0792393	0.0396197	0.3169572	0.3169572	0.2416799
0.480991	0.6786585	0.2207287	0.6786585	0.6127693	0.1779008	0.1779008
0.2114662	0.0469925	0.0234962	0.093985	0.093985	0.3289474	0.3289474
0.3591381	0.3591381	0.0399042	0.2194733	0.1596169	0.1596169	0.0399042
0.1807991	0.0180799	0.0542397	0.1807991	0.1807991	0.3435184	0.198879
0.0331785	0.0497678	0.0497678	0.3649635	0.3649635	0.3649635	0.0995355
0.0015037	0.0015037	0.0436084	0.0015037	0.0135336	0.0315785	0.0315785
0.2066253	0.2066253	0.2066253	0.1533027	0.1533027	0.1133107	0.1133107
0.0246245	0.0246245	0.0246245	0.1231224	0.0984979	0.0246245	0.1231224

0.117096	0.1522248	0.058548	0.058548	0	0.0234192	0.1405152
0.0552486	0.1104972	0.0994475	0.2209945	0.2209945	0.0552486	0.1104972

Table D-3 Cooling fluid K-type thermocouples calibration

Reference	Temperature [°C]								
	THE1 (in)	THE1 (out)	THE2 (out)	THE3 (in)	THE3 (out)	THE4 (out)	THE1 (in)	THE5 (out)	THE6 (out)
20.15	20.23	20.23	20.30	20.30	20.23	20.23	20.30	20.22	20.22
30.20	30.5	30.5	30.23	30.6	30.23	30.23	30.3	30.5	30.5
40.12	40.2	40.2	40.1	40.1	40.2	40.2	40.1	40.2	40.2
48.23	48.32	48.4	48.4	48.5	48.4	48.5	48.41	48.5	48.5
53.26	53.6	53.45	53.45	53.45	53.68	53.34	53.5	53.34	53.34
60.21	60.5	60.5	60.5	60.5	60.5	60.5	60.5	60.5	60.5
66.50	66.1	66.3	66.3	66.2	66.1	66.3	66.23	66.3	66.3
74.35	74.56	74.6	74.52	74.52	74.56	74.6	74.52	74.6	74.6
80.85	81.1	81	80.9	80.9	81.1	81	80.9	81	81
85.61	85.7	85.7	85.6	85.6	85.72	85.6	85.7	85.6	85.6
90.23	89.97	89.97	89.91	89.97	89.91	89.95	89.9	89.95	89.97

Temperature [°C]		SD	%error			
THE7(in)	THE7(out)		T1(A)	T1(B)	T1(C)	T2(A)
20.301	20.301	0.0478586	0.4118698	0.4118698	0.7393807	0.7393807
30.3	30.4	0.1406656	0.983346	0.983346	0.0893951	1.314439
40.1	40.2	0.0493162	0.1844191	0.1844191	0.0647959	0.0647959
48.43	48.52	0.086498	0.1845286	0.350397	0.350397	0.5577326
53.5	53.345	0.1196293	0.6289308	0.34732	0.34732	0.34732
60.5	60.5	0.0828498	0.4766413	0.4766413	0.4766413	0.4766413
66.23	66.3	0.1062334	0.6029985	0.3022511	0.3022511	0.4526248
74.52	74.6	0.0696713	0.2730072	0.3268018	0.2192127	0.2192127
80.9	81	0.0810677	0.3092146	0.1855288	0.0618429	0.0618429
85.97	85.6	0.1079001	0.1051279	0.1051279	0.0116809	0.0116809
89.9	89.97	0.0891312	0.2925726	0.2925726	0.3590664	0.2925726

%error						
T2(B)	T2(C)	T3(A)	T3(B)	T3(C)	T4(A)	T4(B)
0.4118698	0.4118698	0.7393807	0.3374355	0.3374355	0.7393807	0.7393807
0.0893951	0.0893951	0.3211601	0.983346	0.983346	0.3211601	0.6522531
0.1844191	0.1844191	0.0647959	0.1844191	0.1844191	0.0647959	0.1844191
0.350397	0.5577326	0.3711306	0.5577326	0.5577326	0.4125977	0.5991997

0.7791233	0.1501924	0.4411903	0.1501924	0.1501924	0.4411903	0.1501924
0.4766413	0.4766413	0.4766413	0.4766413	0.4766413	0.4766413	0.4766413
0.6029985	0.3022511	0.4075127	0.3022511	0.3022511	0.4075127	0.3022511
0.2730072	0.3268018	0.2192127	0.3268018	0.3268018	0.2192127	0.3268018
0.3092146	0.1855288	0.0618429	0.1855288	0.1855288	0.0618429	0.1855288
0.1284897	0.0116809	0.1051279	0.0116809	0.0116809	0.4205116	0.0116809
0.3590664	0.3147372	0.3701487	0.3147372	0.2925726	0.3701487	0.2925726

D.2 Orifice plate calibration

The orifice plate was calibrated in situ. The flow rate of the water through the pipe was measured by means of a measuring cylinder and stopwatch. Calibration data were obtained using the Endress and Hauser differential pressure transducer (serial number A8069B0109D) capable of measuring 0-500 mbar pressure differences in both the forward and reverse directions read in mili-volt Direct Current (mVDC) and mili-amp DC (mADC) with the data logger.

Calibration curves were fitted through the data in order to approximate the mass flow rate from the measured voltage for the HBM pressure transducer for positive and reverse flow respectively given in Figures D.1 and D.2 and the measured current for E&H pressure transducer, positive flow given in Figure D.3.

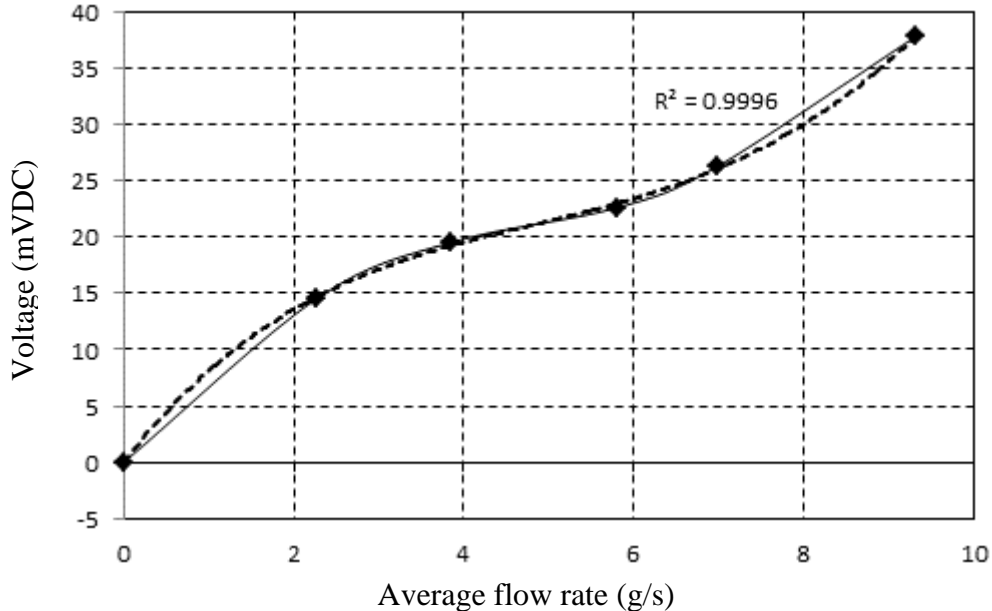


Figure D-0-1 HBM Pressure transducer calibration positive

Figure D.1 shows that the coefficient of determination described by the curve is 99.96% and that the calibrated HBM positive flow is approximate by a polynomial equation as

$$y = -0.0021x^4 + 0.1412x^3 - 1.744x^2 + 9.7312x - 0.0192 \quad (\text{D-1})$$

where

$$y = V \text{ (mVDC)}$$

$$x = \dot{m} \text{ (g/s)}$$

Figure D.2 shows the calibrated reverse flow for the HBM pressure sensor. The calibration has a proportion of variance $R^2 = 0.997$. This calibration is approximated by a polynomial equation given as

$$y = -0.0021x^4 + 0.1412x^3 - 1.744x^2 + 9.7312x - 0.0192 \quad (\text{D-2})$$

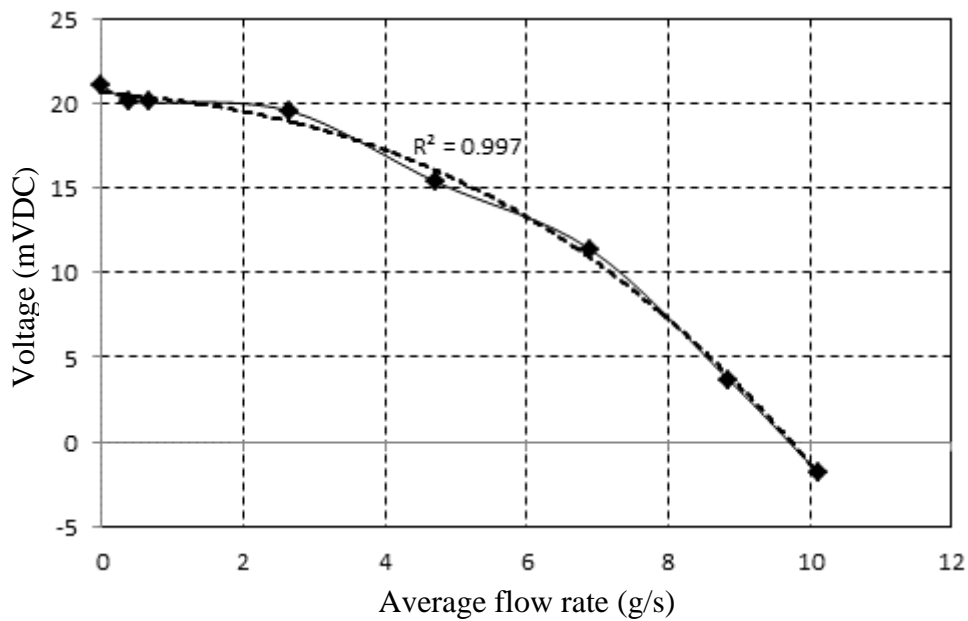


Figure D-0-2 HBM Pressure transducer calibration reverse flow

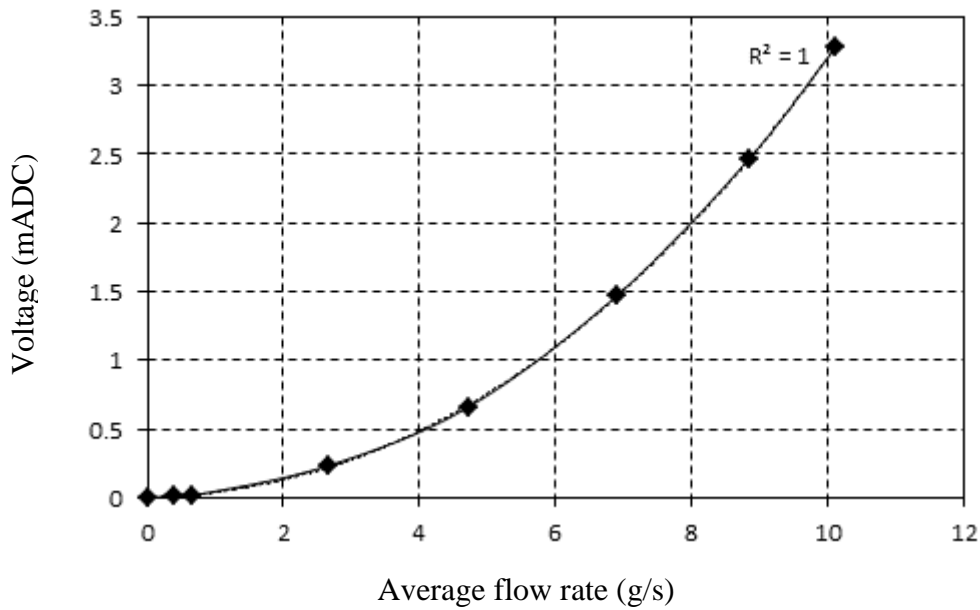


Figure D-0-3 E&H Pressure transducer calibration positive flow

Figure D.3 shows the calibrated E&H positive flow. It has $R^2 = 1$ and is approximated by equation D.3

$$y = 0.0006x^3 + 0.025x^2 + 0.0118x + 0.0005 \quad (\text{D-3})$$

D.3 Calibration of Endress and Hauser pressure sensor

The calibration for the pressure transducer for pressure reading was done by connecting both the micrometre and the CU1B2ED1A pressure transducer in parallel to a single tube. Air was used to compare results with Betz micrometre reading. Figure D.4 shows the calibrated results with $R^2 = 0.9997$ and the fitted polynomial equation given by equation D-4

$$y = 5E - 09x^3 - 3E - 06x^2 + 0.0083x + 12.971 \quad (\text{D-4})$$

where

y = current, mA

x = Pressure, Pa

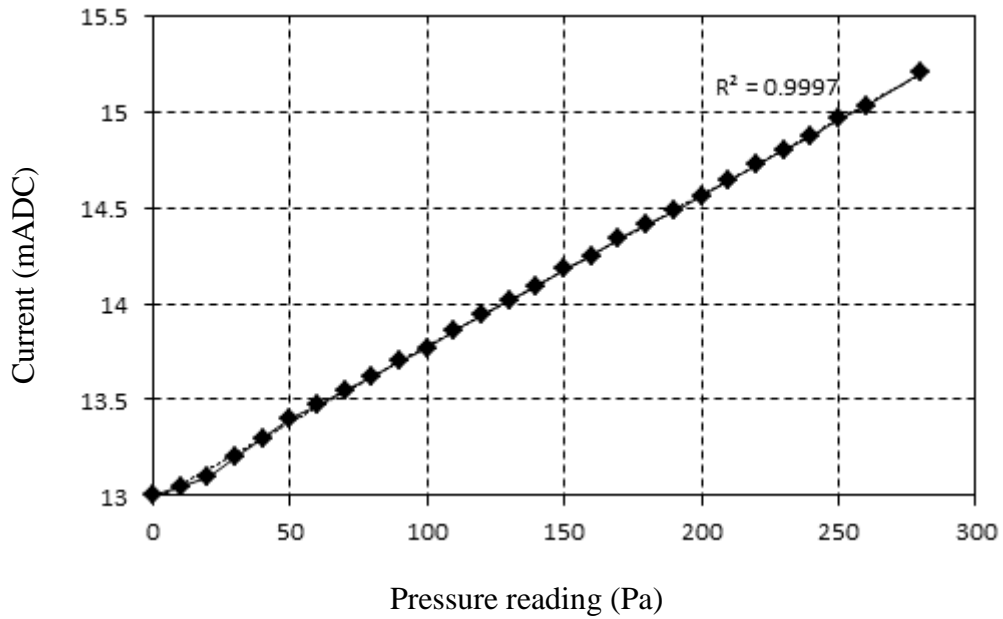


Figure D-4 E&H pressure transducer calibration

D.4 Test-runs 1c and 3b results sample

Figure D-5 shows results of the two test-runs not discussed in the thesis including one single phase (test-run 1c) and one two-phase (test-run 3b). These results include the mass flow rate measured with the E&H pressure sensor for single phase given in Figure D-5(a) and two-phase (Figure D-5(b)). They also present their respective working fluid temperature profiles.

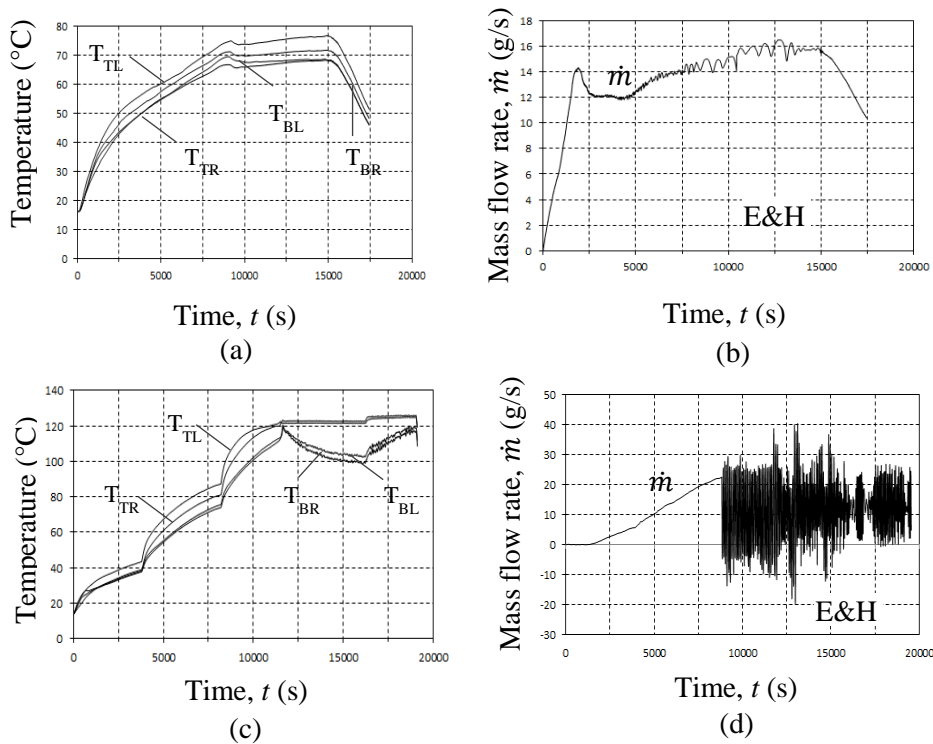


Figure D-5 Experimental single and two phase operating (a) working fluid temperatures test-run 1c, (b) working fluid mass flow rate test-run 1c, (c) working fluid temperatures test-run 2b, (b) working fluid mass flow rate test-run 2b

D.5 Error analysis

Errors always occur during experimental tests. Different types of errors can be identified including systematic errors that happened during calibration, random errors that may happened due to measurement conditions and lack of precision, and absolute or relative errors. This section presents the systematic errors due to calibration deviating the actual measurement consistently either too high or too low.

D.5.1 Temperature errors

On the temperature systematic errors are determined for the cooling water, heating plate and working fluid. This error is represented by the average percentage error calculated by the average error of the average error of each thermocouple used to measure the temperature for all the different sections.

$$\text{Average percentage error} = \frac{\sum_{i=0}^n \text{Average \% error}_i}{n} \quad (\text{D-5})$$

The actual temperature will be equal to the reading value plus minus the error.

For the cooling water

$$= (0.41 + 0.36 + 0.28 + 0.41 + 0.36 + 0.27 + 0.33 + 0.35 + 0.35 + 0.36 + 0.36)/11$$

$$= 0.35\%$$

$$T_{actual} = T_{reading} \pm \frac{0.35}{100} T_{reading} \quad (D-6)$$

For the heating plate

$$= (0.21 + 0.21 + 0.16 + 0.22 + 0.16 + 0.17 + 0.08 + 0.19 + 0.20 + 0.18 + 0.15)/11$$

$$= 0.18\%$$

$$T_{actual} = T_{reading} \pm \frac{0.18}{100} T_{reading} \quad (D-7)$$

For the working fluid

$$= (0.51 + 0.53 + 0.38 + 0.38)/4$$

$$= 0.45\%$$

$$T_{actual} = T_{reading} \pm \frac{0.45}{100} T_{reading} \quad (D-8)$$

D.5.2 Pressure sensor errors

From the Endress & Hauser pressure sensor final inspection report at standard temperature, pressure and humidity the maximum permissible error is specified as $\pm 0.2\%$ of full scale reading.

D.5.3 Calibration certificate

The calibration certificate of the PRT is given in Figure D-6

RAPID INSTRUMENTATION CC

38, 1st Avenue, Boston,
Bellville, 7530
R.S.A.

Tel: (021) 948-0413
Fax: (021) 948-0435
Cell: 083 458 2497

P O Box 1050
Oakdale
7535

Reg. No. 2000/021703/23

CERTIFICATE OF CALIBRATION

South African National Accreditation System
Accredited Laboratory Number 366



Calibration of a : PLATINUM RESISTANCE THERMOMETER
 Manufacturer : ISOTECH
 Model Number : 935-14-72
 Serial Number : 191069
 Factory Number : N/A

Calibrated for : UNIVERSITY OF STELLENBOSCH
 Address : Department of Mechanical Engineering
 Stellenbosch

Temperature : 0 °C; + 50 °C; + 100 °C; + 180 °C; + 300 °C

Technical Signatory : M P ACKHURST

Calibrated by : M P ACKHURST

Checked by : S R ACKHURST

Date of Calibration : 4 February 2013

Certificate Number : **RAP15738**

Issue Number : 2

The South African National Accreditation System (SANAS) is a member of the International Laboratory Accreditation Co-Operation (ILAC) Mutual Recognition Arrangement (MRA). The MRA allows for the mutual recognition of technical test and calibration data by member accreditation bodies worldwide. For more information on the MRA please refer to www.ilac.org.

245, +648047

RAPID INSTRUMENTATION CC
SANAS CALIBRATION LABORATORY 366

57, 259

SUMMARY OF RESULTS				
Actual Temperature °C	UUT Reading Ω	UUT Reading °C	Correction °C	Uncertainty U °C
+ 0.097	100.0297	+ 0.076	+ 0.022	± 0.70
+ 50.020	119.4191	+ 50.057	- 0.037	± 0.70
+ 99.985	138.5377	+ 100.085	- 0.100	± 0.70
+ 179.823	168.4702	+ 179.978	- 0.154	± 0.70
+ 300.004	212.1331	+ 300.229	- 0.225	± 0.70

IMMERSION DEPTH: 150mm

LABORATORY STANDARDS AND EQUIPMENT USED FOR MEASUREMENTS		
Standards of Equipment	Serial Number	Certificate Number
ASL F250 Digital Thermometer	1344029856	THDG-6460
Pt100 Probe	PT100 1-20	THDG-6460
Calibrator	RAP01G	

PROCEDURE/S UTILISED	
1016	Determination of Uncertainties
2001	Ice Point
2003	Calibration of RTD / PT100

METHOD
 The UUT was calibrated according to laboratory standards, the results of which were traceable to National Measuring Standards for Temperature.

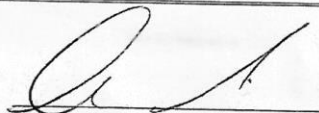
The reported expanded uncertainty is based on a standard uncertainty multiplied by a coverage factor $k = 2$ providing a level of confidence of approximately 95%, the uncertainty of measurement has been estimated in accordance with the principles defined in the GUM, Guide to Uncertainty of Measurement, ISO, Geneva, 1993.

The accuracy of the equipment used during calibration is traceable to the National Measuring Standards as maintained in the Republic of South Africa or International Measuring Standards.

The measurement results recorded in this certificate were correct at the time of calibration. The subsequent accuracy will depend on factors such as care, handling and frequency of use. It is recommended that recalibration be undertaken at an interval that will ensure that the instrument remains within the desired limits.

This certificate may not be reproduced other than in full, except with prior written approval of RAPID INSTRUMENTATION CC.

Signed:



M P ACKHURST
 Technical Signatory

Certificate No: **RAP15738**

Figure D-6: Certificate of calibration

APPENDIX E SAFETY PROCEDURES

E.1 Background

Prior to experiment on a natural circulation experiments it is compulsory to read and understand the potential health and safety risks and accompanying prevention procedures and corrective actions if required.

E.2 Safety Instructions

A closed loop thermosyphon is a method of transferring thermal energy from a heat source to a sink via thermally induced density gradients; it is capital that safety instructions are read and potential health and safety risks and accompanying preventions procedures understood. These procedures were initially prepared by Sittmann (2010):

Table E-1 Safety procedure instructions for closed loop thermosyphon (Sittmann, 2010).

Risk	Design Impact	Operating Instructions
High temperatures	<ul style="list-style-type: none"> • Screen and prevent people from accidentally accessing the warm area. • Conduct warm gases to an area where it can mix safely with cold gases. • Provide stopping mechanisms such as thermostats to prevent temperatures exceeding the maximum limits. • Provide transparent plastic piping and make use of the glass pipe heat exchanger • Provide ventilation 	<ul style="list-style-type: none"> • Ensure screens are in position before use. • Ensure insulations and plastic covers are used to avoid contact with people or other material. • Ensure that the coolant is flowing during experiments • Ensure all electrical components and sensors are working as they will help to detect temperature and stop the heating during experiments. • Avoid getting in touch of the heating copper pipe or if there is leaking with hot water. • Enough ventilation in the workshop or around the workplace where the experiments are done is required as this can help to avoid accidents.
Structural failure	<ul style="list-style-type: none"> • A structure that can fail can cause heavy objects to fall • Consider with big 	<ul style="list-style-type: none"> • Always wear safety shoes • Respect all colour coding in the lab • Remove all loose elements and

	importance the stability of all parts of the structure	equipments from the walkway
Electric shock	<ul style="list-style-type: none"> • Provide emergency stop. • Use fuses and circuit breaker • Visual feedback that power is switched on (e.g. LEDs). • Insulate live wires. 	<ul style="list-style-type: none"> • Ensure that emergency stops are easily accessible. • Ensure that the screens are in position. • Ensure that there is no leak to avoid any contact between water and electrical components, including wiring, sensors, circuit breaker, DB etc. • Ensure that all electrical work are done according to standard by a qualified electrician
People working on Scaffoldings from where they can fall	<ul style="list-style-type: none"> • Provide safety ladders and handrails. 	<ul style="list-style-type: none"> • Use safety harness.
High pressure gas or liquids	<ul style="list-style-type: none"> • Provide pressure regulators and pressure relief valves. • Screen piping to ensure that leaks cannot cause damage/injuries. 	<ul style="list-style-type: none"> • Ensure that pressure relief valves are working properly. • Ensure that couplings are firmly connected. • Examine pipes for external damage.
Safety and Hazards	<ul style="list-style-type: none"> • Provide fire extinguishers • Provide safety procedures • Provide user guide 	<ul style="list-style-type: none"> • In case of fire in the lab, open the electrical box with key provided and discharge fire extinguisher into electrical box. • Read and understand all instructions and follow them carefully.
Personal safeguarding	<ul style="list-style-type: none"> • Protect the body • Protect Hands • Protect Eyes • Protect Feet 	<ul style="list-style-type: none"> • A protective jacket can be worn when working with hot water or other liquids at higher temperature • Hands are constantly at risk when handling hot, leather gloves should be worn • Safety glasses must be worn when working with hot water to protect eyes • Closed shoes should be worn to protect feet from any unfortunate accidents

Housekeeping	<ul style="list-style-type: none"> • Safe house keeping 	<ul style="list-style-type: none"> • Keep the floors; passageways and the space around the structure clear of small objects and accessories. • Work inside the marked boundaries of the passageways. • Make sure that there is a place for each machine tool; accessory or attachments that you use so that you can store them after you use them. • Make sure that your work piece is properly secured before you switch the system on. • Do not leave the lab unattended while it is operating.
--------------	--	--

E.3 User guide

E.3.1 Normal operating conditions

In order to ensure that the experiment is executed in a safe manner, the operator is required to read, understand and follow the two procedures (start-up and shut down) available in the laboratory.

E.3.2 Accident and malfunction conditions

The accident and malfunction conditions can be grouped in three categories based on the main element involved in the malfunction condition.

- Loss of Coolant
- Temperature measurement
- Element malfunction